AUG 15 1988

070
Hof
Sta
M.S.

Statistical and geodetic approach to mon
AC .H3 no.H88 15343

Hoffmann, John P.
SOEST Library

A STATISTICAL AND GEODETIC APPROACH TO MONITORING THE FORMATION AND EVOLUTION OF THE SHALLOW PLUMBING SYSTEM AT PUU OO, KILAUEA HAWAII

RETURN TO
HAWAII INSTITUTE OF GEOPHYSICS
LIBRARY ROOM

A THESIS SUBMITTED TO THE GRADUATE DIVISION OF THE
UNIVERSITY OF HAWAII IN PARTIAL FULFILLMENT
OF THE REQUIRMENTS FOR THE DEGREE OF

MASTER OF SCIENCE

IN GEOLOGY AND GEOPHYSICS

AUGUST 1988

by

John P. Hoffmann

Thesis committee:

Lionel Wilson, Chairman
William T. Coulbourn
Michael O. Garcia
George P. L. Walker

We certify that we have read this thesis and that, in our opinion, it is satisfactory in scope and quality as a thesis for the degree of Master of Science in Geology and Geophysiscs.

THESIS COMMITTEE

Chairman

ACKNOWLEDGEMENTS

I would like to thank my thesis committee for their helpful comments relating to my thesis. It has been a pleasure to work with each of them. In particular, I thank Dr. Garcia for initially encouraging me to enroll at the University of Hawaii, many thoughtful Puu Oo discussions and for financial and computer support. Thanks also goes out to Dr. Coulbourn, whose "statistical" enthusiasm helped me through the statistics chapter. Dr. Walker provided many insightful suggestions and he as well as Dr. Garcia often acted as my advisor in Dr. Wilson's absence. Dr. Wilson's advice and suggestions were invaluable for the preparation of this document and I am grateful to him. He also provided all the computer time needed for the ground deformation section.

A sincere mahalo goes out to my fellow graduate students with whom I've shared this experience with. Special thanks go to Scott Rowland and Dan Johnson.

Most of all, I'd like to thank the Hawaiian Volcano Observatory. The data for this thesis was collected by the staff of HVO who unselfishly provided it for my use. HVO's dedication to collecting quality data made their reduction and analysis a relatively simple task. This paper benefits from discussions with HVO staffers including Christina Heliker, John Dvorak, Arnold Okamura, Paul Delaney, Paul Greenland, George Ulrich, Ed Wolfe and Tom Wright. Special thanks go to George Ulrich who spent many many of hours with me at the eruption site collecting data and in discussions in the early stages of my thesis preparation.

Finally, I'd like to thank Dr. William I. Rose and Dr. Theodore Bornhorst of Michigan Technological University. Their interest and enthusiam for volcanolgy was very contagious and spread to me when I was an undergraduate at MTU.

ABSTRACT

A series of multivariate statistical techniques were applied to the Puu Oo eruption data set. The data set consists of nine system parameters for 47 eruptive episodes. The statistical techniques demonstrated both qualatatively and quantitatively the rapid evolution and stabilization of the magmatic plumbing system.

Cluster analysis grouped the 47 episodes into 4 groups of episodes with similar eruption characteristics. Discriminant and factor analysis of the data set quantitatively defined fountain heights, deflation rates, eruption rates and length of eruptions as being the important parameters in describing and discriminating the data set. Factor analysis of the Puu Oo system parameters illustrates a temporal variation within the data set, and indicates relatively large-scale dynamic changes early in the series of eruptions. By episode 10 the system had nearly stabilized after which only small but continuous changes occurred.

A detatiled examination of the discriminating variables suggests that eruption site activity (timing and dynamics) preceded summit behavior. This time lag between eruption site and summit activity is interpreted, in part, as resulting from a near-vent controlling phenomenon. A near-vent reservoir is suggested as the controlling phenomenon.

Ground deformation analysis at the eruption site was successful in modeling the near-vent reservoir as a near vertical dike. Modeled dimensions of the local reservoir gave the dike a horizontal length of about 1.6 km, a vertical length of about 2.5 km, a depth to the top of 400 m, a dip of 87 degrees and a strike of N65E. The dike is centered about 800 m uprift of Puu Oo.

TABLE OF CONTENTS

Page

ACKNOWLEDGEMENTS..... iii

ABSTRACT..... v

LIST OF TABLES..... ix

LIST OF FIGURES..... x

LIST OF SYMBOLS.....xiii

Chapter

I. INTRODUCTION..... 1

Recent Kilauea Activity..... 1

Recent Kilauea Studies..... 3

II. STATISTICAL ANALYSES..... 5

Overview of Statistical Methods..... 5

Discussion of Statistical Methods Used..... 9

Cluster Analysis..... 9

R-Mode Analysis..... 11

Q-Mode Analysis..... 13

Discriminant Analysis..... 15

Factor Analysis..... 21

Stepwise Multiple Regression..... 29

Episode and Sequence Day Predicted..... 30

Repose Predicted..... 30

Volume Predicted..... 36

TABLE OF CONTENTS (Continued) Page

Numerical Recursion..... 39

Discusion: Geologic Interpretation of Statistical Results 45

Petrologic Evidence Supporting Interpretation..... 48

III. FOUNTAIN HEIGHTS AND SUMMIT SUBSIDENCE RATES..... 50

Fountain Height Data..... 52

Summit Deflation as a Measure of Eruption Rate..... 53

Fountain Heights as a Measure of Eruption Rate..... 55

Discussion..... 66

IV. EAST RIFT ZONE DEFORMATION..... 73

Geologic Setting..... 73

Previous Ground Deformation Studies..... 73

Description of Hawaiian Rift Zones..... 74

The Jan. 1, 1983 ERZ Dike Intrusion and the Events

Leading up to the Intrusion..... 75

Network Descriptions..... 77

KMM Instrument sites..... 77

Mauna Ulu Instrument Site..... 83

Instrumentation..... 83

Results of EDM Measurements..... 84

Error Considerations..... 84

The DIS3D Program..... 88

Model Constraints, Sensitivity and Discussion of Results. 93

Pressures.....112

TABLE OF CONTENTS (Continued) Page

Mauna Ulu Trends.....120

Conclusions.....125

REFERENCES.....129

LIST OF TABLES

Table		Page
1	Publications related to Puu Oo	3
2	Data set used in statistical routines	8
3	Centroids for each cluster	15
4	Variables used in discriminant function	16
5	Discriminating variables and their weightings	18
6	Variables used in discriminant function	20
7	Discriminating variables and their weightings	21
8	Varimax factor loadings	22
9	Varimax factor scores	23
10	Regression equations	30
11	Tested models for input/output recursion	43
12	Cluster number and volume per deflation	48
13	Digitized fountain areas	59
14	Instrument stations, locations, dates used	82
15	Calculated parameters (from DIS3D)	97
16	Calculated dike pressures, summit pressures, site-volume, lava volumes and line-length changes	119

LIST OF FIGURES

Figure		Page
1	Location map of Kilauea volcano	2
2	Dendogram from R-mode cluster analysis	12
3	Dendogram from Q-mode cluster analysis	14
4	Plot resulting from discriminating function	17
5	Plot resulting from discriminating function	19
6	Factor loadings	25
7	Ternary diagram of the 3 factors	26
8	Predicted episode number	31
9	Predicted sequence day	32
10	Residuals for predicted episode	33
11	Residuals for predicted sequence date	33
12	Predicted repose length	34
13	Predicted volume	35
14	Residuals for repose length	37
15	Residuals for volume	37
16	Raw input/output data used by microcaptain	41
17	Predicted microcaptain function and observed data	41
18	Lava volume versus summit deflation	54
19	Typical fountain heights and deflation rates	56
20	Volume of lava versus digitized fountain area	57
21	Deflation versus digitized fountain area	58

LIST OF FIGURES (Continued)

Figure		Page
22	Average fountain height versus ave. eruption rate..	61
23	Maximum fountain height vs. maximum deflation rate.	62
24	Deflation rate and fountain height for episode 29..	63
25	Deflation rate and fountain height for episode 23..	63
26	Deflation rate and fountain height for episode 25..	64
27	Deflation rate and fountain height for episode 13..	64
28	Deflation rate and fountain height for episode 19..	65
29	Conduit system connecting summit to Puu Oo.....	69
30	Segmented horizontal deformation lines.....	78
31	Near-vent segmented deformation lines.....	80
32	Line-length changes from far ends of line for episodes 22 to 35.....	85
33	Line-length changes from far ends of line for episodes 36-42.....	86
34	Horizontal strain profiles for near-vent line.....	89
35	Idealized half-space assumed in DIS3D.....	92
36	Line-length changes for Mauna Ulu.....	95
37	Calculated displacement profiles with observed.....	99
38	Calculated parameters from DIS3D for each episode..	111
39a	Change in site volume versus episode number.....	114
39b	Change in site volume versus volume erupted.....	115
39c	Line-length change versus volume of lava.....	116
39d	Site pressure versus summit pressure.....	117

LIST OF FIGURES (Continued)

40 Line-length changes for Mauna Ulu line.....121

41 Line-length changes for KMM lines.....124

42 Plan view of modeled dike.....126

43 Cross-section of east rift zone.....128

LIST OF SYMBOLS

$E(y)$ = dependent variable

$x_1 \ldots x_n$ = independent variables

y_k = output at the kth sampling instant

$\bar{y}$ = mean value of y

u_k = input measured at kth sampling instant

$u_{k-\delta}$ = input measured at δ sampling instants previously

z^{-1} = backward shif operator

δ = size of time delay

P_{ij} = covariance matrix

$\hat{x}_k$ = deterministic output modeled as being causally related to u_k

E_k = noise term for stochastic disturbances

$\hat{E}_k$ = estimated value of noise

R_T^2 = coefficient of determination

EVN = error variance

f = fanning friction factor

rho = magma density

U = magma velocity (m/s)

mu = magma viscosity (Pa s)

D = average dike thickness (m)

Re = Rynolds number

H = fountain height (m)

g = gravitational constant

H = dike half-length (km)

LIST OF SYMBOLS (Continued)

ϕ = strike of dike

θ = dip of the dike

DU = distance down-dip to the upper edge of the dike (km)

DL = distance down-dip to the lower edge of the dike (km)

op = amount of opening across the dike (mm)

t = thickness at the center of the dike (m)

P = pressure (Pa)

a = half height of the dike (km)

v = Poisson's ratio

u = shear modulus

delp = change in pressure (Pa)

delsite-vol = change in stored volume at the near-vent reservoir (m^3)

note: abbreviations of variables and places are defined in the text.

CHAPTER I

INTRODUCTION

Volcanoes are subject to complex physical and chemical processes. Yet, however complex these processes are, there are logical reasons for volcanic systems. To understand these reasons and processes is the fundamental reason for studying volcanoes. Recognition of eruption patterns can help constrain models of how volcanoes work and aid in forecasting future eruptions. Certainly, repetition of the magmatic processes acting on the Kilauea system modify the dynamic conditions. The Hawaiian Volcano Observatory (HVO), located at the summit of Kilauea volcano, has had the unique advantage of being perched on the rim of one of the world's most active and easily-monitored volcanoes. The knowledge gained at Kilauea (and in Hawaii in general) has been applied to research done on other volcanoes world-wide.

RECENT KILAUEA ACTIVTY

The geologic monitoring program at HVO has recently been focused on the Kilauea east rift zone (ERZ) eruption that began in January 1983 (Figure 1). Since June 1983, the activity had been localized at the Puu Oo vent. Kilauea's Puu Oo eruption, located about 18 kilometers downrift from the summit, consists of a series of 48 episodic eruptions spanning over three years; from January

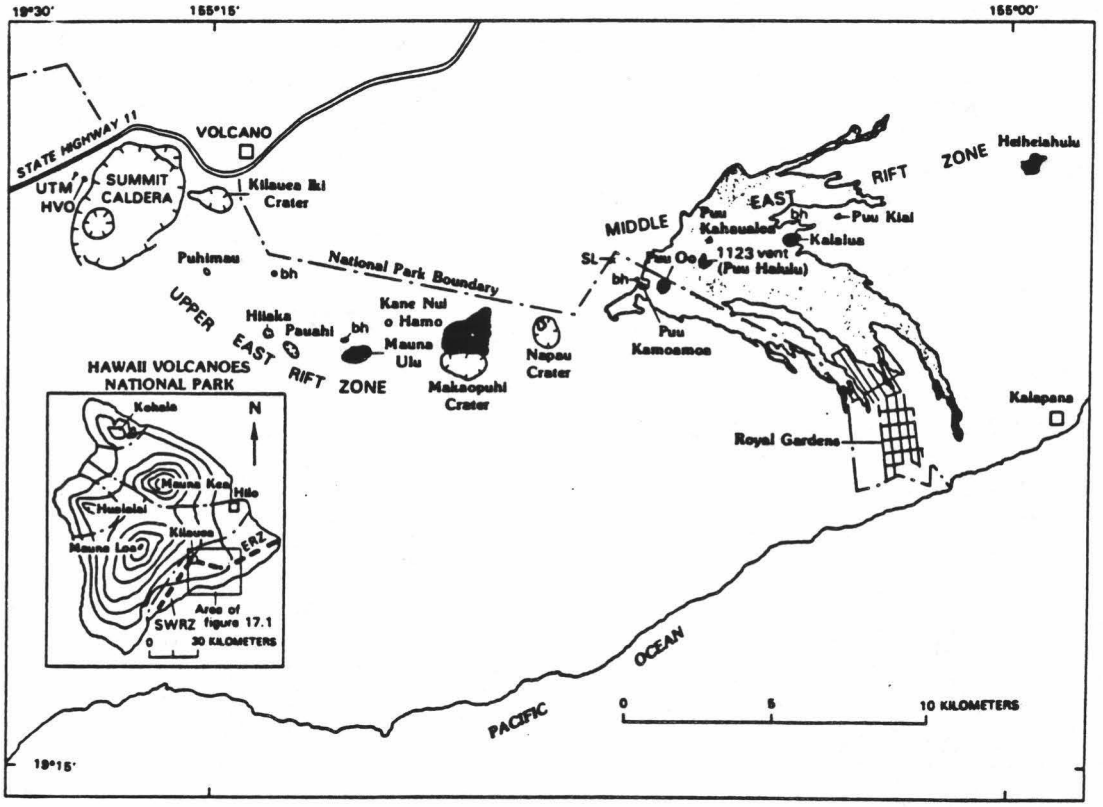

Figure 1. Map of Kilauea Volcano showing summit caldera, east rift zone, locations of the Hawaiian Volcano Observatory (HVO) and the Puu Oo eruption site (1983-present) are shown. Modified from Wolfe et al., (1987, Fig. 17.1).

1983 through July 1986. The active vent moved 3 kilometers downrift of Puu Oo and a continuous sustained steady-state eruption developed in July 1986 and continues to the day of this writing.

The Puu Oo eruption has been under the scrutiny of many and varied scientists, technicians, and laymen for the past four years. The variety of eruptive behavior, persistence of events, and the availability of state-of-the-art volcano monitoring equipment has provided a wealth of information and has led to an improved understanding of Kilauea's geologic structure and magmatic plumbing system.

RECENT KILAUEA STUDIES

An array of papers pertaining to, or related to, the recent series of episodic eruptions have been written. Table 1 that follows is a list of authors with publications dealing with the various aspects of the 1983-1986 Puu O'o eruption.

Table 1. Summary list of publications (non-abstract)related to the Puu Oo ERZ eruption.

Topic	Authors
Dynamics	Greenland, et al., (in press b);Wilson et al.,(in press a); Wilson, et al., (in press b).
General Summary	Wolfe, et al., 1987; Wolfe, et al., (in press.)
Geoelectrical	Jackson, et al., (in press).
Gravity	Johnson, 1987.
Ground Deformation	Dvorak, et al., 1985; Dvorak, et al., 1986; Okamura, et al., (in press).
Lava Chemistry	Garcia and Wolfe, (in press); Neal, et al., (in press).
Seismicity	Koyanagi, et al., 1987; Koyanagi, et al., (in press).
Volcanic Gas	Casadevall, et al., 1987; Greenland, et al., 1985; Greenland, et al., (in press a).

Table 1 indicates a number of topical studies have resulted from the recent Puu Oo eruption. These papers draw from many diverse disciplines, including petrology, geochemistry, geophysics, geodetics and classical geology. However, the search for meaningful patterns of eruptive activity at Puu Oo has not been seriously undertaken.

This thesis is divided into three sections: in the first section I apply various types of multivariate statistical methods to examine the pattern of eruption dynamics over the entire series of eruptions and use this to predict future events. The statistics section defines quantitatively the rate of evolution of the Puu Oo system and considers which variables are most important in distinguishing individual episodes. A univariate technique of numerical recursion is also examined in this chapter.

The next section of the thesis examines more closely three of the most important distinguishing system variables as determined in the discriminant and factor analysis of the statistics chapter. In this section fountain heights, especially their behavior, are compared with deflation rates and eruption rates.

The final section of the thesis examines the ground deformation patterns near the Puu Oo eruption site. Geodetic studies are imperative for successful forecasting of impending activity at Hawaii's volcanoes as the buildup of strain is manifested at the surface as horizontal and vertical displacement. Geodetic measurements are also used to evaluate the nature and geometry of the magma plumbing system.

CHAPTER II

STATISTICAL ANALYSES

OVERVIEW OF STATISTICAL METHODS

One objective of closely monitoring the active eruption is to ascertain the temporal variations of a number of system parameters during the eruptive sequence in order to predict future events successfully. Variations in eruption dynamics such as fountain heights and eruption rates within a sequence of eruptions can reveal aspects of the overall rate of evolution of the subterranean conduit system involved. To quantify the temporal variations of successive eruptions, first it is important to classify eruptions into groups with similar characteristic variables.

The following is a list of statistical methods used to identify and quantify variations within the episodic series of eruptions at Puu Oo.

1) Cluster analysis: uses the routine CLUST.FORT (Davis, 1976, modified by Coulbourn, 1985).

2) Discriminant analysis: uses BMDP 7M (Jennrich and Sampson, 1985).

3) Factor analysis: uses CABFAC.FORT (Klovan and Imbrie 1971).

4) Multiple linear regression: uses BMDP 2R (Dixon and Jennrich, 1985).

5) Numerical recursion: uses MCAPT (described in Young, 1984).

This chapter summarizes results of the series of statistical analyses applied to a data set with 47 samples and 9 variables (Table 2). The 47 samples refer to 47 episodes of eruptive activity at or near the Puu Oo, vent (episodes 2-48). The nine variables are as follows:

DEFL = Duration of deflation, measured at summit, associated with each eruptive episode (in hours).

LENG = Eruption duration (in hours).

AVDR = Average deflation rate (in microradians per hour X 100, measured at the summit).

MXDF = Maximum deflation rate (in microradians per hour X 100, measured at the summit).

MXFT = Maximum fountain height during an eruption (in meters, from time-lapse photography).

INFL = Summit inflation prior to episode (in microradians).

DEFT = Total deflation at the summit due to an eruption (in microradians).

RATE = Average eruption rate (in cubic meters per hour X 1000).

VOLU = Volume of erupted lava (million cubic meters).

Cluster analysis was used to classify eruptions into groups (clusters) with similar characteristics and provides, quantitatively, the correlation level at which eruptions are grouped. To determine how well the clusters are chosen, or how distinctive each cluster of eruptions is, stepwise discriminant analysis was applied. Discriminant analysis was performed on the

cluster-based data set and the variables with the greatest differences between groups were identified. Furthermore, these variables were ranked in heirarchial order according to their importance in distinguishing between clusters. Q-mode factor analysis, like cluster analysis, was useful in identifying eruptions with similar characteristics and also in indentifying the variables that account for most of the variance in the data set. Factor anaylsis minimizes the covariance caused by the interrelationships between variables and was used to identify and measure relationships of patterns in the data set. Using the data set listed in Table 2, a stepwise linear regression was performed as a predictive tool for volumes erupted, sequence day of eruption, episode number and repose lengths, for Puu Oo eruptions between February 1983 and July 1986. Finally, a recursion method was used to analyze stochastically a relationship between fountain heights and deflation rates.

Table 2. Data set used in all statistical routines. Variable definitions are described in text.

EPISODE	DEFL	LENG	AVDR	MXDF	MXFT	RATE	INFL	DEFT	VOLU
2	168.0	174.0	6.0	20.0	120.0	80.0	7.61	10.87	14.0
3	336.0	290.0	8.0	20.0	280.0	131.0	12.21	28.01	38.0
4	137.0	100.0	8.0	22.0	60.0	110.0	27.20	11.23	11.0
5	105.0	90.0	12.0	27.0	60.0	144.0	7.63	11.90	13.0
6	75.0	73.0	22.0	60.0	130.0	123.0	12.61	16.26	9.0
7	57.0	56.0	29.0	49.0	90.0	250.0	18.11	16.67	14.0
8	30.0	24.0	35.0	66.0	160.0	333.0	15.11	10.59	8.0
9	60.0	52.0	25.0	47.0	200.0	154.0	5.89	15.02	8.0
10	61.5	64.0	23.0	47.0	237.0	219.0	15.43	14.13	14.0
11	42.5	43.0	41.0	80.0	58.0	279.0	16.32	17.50	12.0
12	41.0	35.0	34.0	63.0	65.0	229.0	6.30	13.82	8.0
13	43.0	42.0	26.0	45.0	116.0	238.0	16.62	11.10	10.0
14	24.0	19.0	41.0	66.0	195.0	316.0	6.16	9.91	6.0
15	25.0	19.0	45.0	67.0	350.0	421.0	6.76	11.31	8.0
16	33.0	32.0	45.0	78.0	390.0	375.0	10.47	14.77	12.0
17	24.0	23.0	43.0	70.0	180.0	435.0	9.30	10.27	10.0
18	67.5	60.0	29.0	73.0	220.0	400.0	14.56	19.44	24.0
19	51.0	44.0	11.0	31.0	130.0	45.0	12.67	5.70	2.0
20	29.0	9.0	36.0	111.0	330.0	444.0	9.20	10.32	4.0
21	39.0	8.0	24.0	90.0	320.0	713.0	7.41	9.20	5.7
22	27.0	15.0	48.0	110.0	320.0*	513.0	5.89	13.07	7.7
23	22.5	18.0	57.0	85.0	320.0	528.0	12.67	12.93	9.5
24	22.0	20.0	65.0	99.0	410.0	580.0	10.51	14.28	11.6
25	20.0	13.5	75.0	135.0	470.0	822.0	16.50	14.90	11.1
26	16.0	5.0	47.0	109.0	394.0	1320.0	16.72	7.55	6.6
27	15.5	10.0	79.0	114.0	410.0*	840.0	7.75	12.27	8.4
28	19.0	14.5	84.0	130.0	420.0	855.0	9.66	15.91	12.5
29	21.0	16.0	76.0	126.0	460.0	813.0	18.56	15.92	12.9
30	22.0	21.0	100.0	175.0	445.0	671.0	14.31	22.00	14.1
31	23.0	21.5	89.0	231.0	310.0	843.0	18.59	20.38	19.4
32	17.0	17.5	100.0	210.0	390.0	906.0	17.15	17.01	16.3
33	15.0	6.0	47.0	125.0	400.0*	1317.0	8.71	7.00	7.9
34	18.0	14.0	67.0	129.0	410.0	757.0	5.99	12.03	10.5
35	12.0	7.0	101.0	163.0	425.0*	1029.0	9.07	12.09	7.2
36	14.0	9.5	84.0	191.0	440.0	1211.0	12.93	11.69	11.5
37	14.0	12.0	94.0	194.0	350.0	1225.0	11.96	13.18	14.7
38	20.0	8.5	65.0	240.0	390.0*	1762.0	13.03	12.96	14.8
39	13.0	10.0	107.0	190.0	440.0	1398.0	12.96	13.90	13.7
40	18.5	13.5	77.0	150.0	260.0	859.0	15.70	14.30	11.6
41	16.5	11.5	100.0	200.0	270.0*	1190.0	9.50	16.50	13.7'
42	20.5	13.1	70.0	170.0	390.0	925.0	16.40	14.80	12.1'
43	19.0	11.4	67.0	195.0	270.0	905.0	12.88	12.82	10.3'
44	45.0	11.0	30.0	190.0	310.0	925.0	15.22	13.66	11.5'
45	26.0	12.4	45.0	140.0	260.0	760.0	12.40	11.75	9.4'
46	16.0	10.9	42.0	140.0	225.0	900.0	12.75	12.17	9.8'
47	32.0	12.3	35.0	130.0	225.0	715.0	11.72	11.07	8.8'
48	16.5	21.6	114.0	260.0	30.0	330.0	15.17	18.79	7.2'
AVE	42.6	34.1	53.4	116.2	278.0	645.5	12.4	13.7	11.4
ST DEV	53.2	48.0	29.6	63.5	127.9	408.8	4.3	3.9	5.4
MINIMUM	12.0	5.0	7.0	20.0	30.0	45.0	5.9	5.7	2.0
MAXIMUM	336.0	290.0	114.0	260.0	470.0	1762.0	27.2	28.0	38.0

* Poor visibility, fountain heights estimated.

' Volumes estimated from DEFT, therefore not independent data.

DISCUSSION OF STATISTICAL METHODS USED

1. CLUSTER ANALYSIS

Given a large data set composed of a number of samples and variables, cluster analysis is a statistical method designed for grouping these into a relatively small number of classes such that the objects (samples or variables) within each class are similar and the unlike objects group into other classes. Most analysts use this approach to explore relationships within their data and it may serve as a basis for predictions of other external variables. The method was formalized for problems related to numerical taxonomy (Sokal and Sneath, 1963) and is now widely applied in psychology, sociology, zoology, biology, botany and geology (primarily in paleontology).

There is no analytical solution to cluster analyses; however, there are alternative classification procedures (Sneath and Sokal, 1973) and these may be grouped into four general types: partitioning methods, arbitrary origin methods, mutual similarity and hierarchical clustering. The reader is refered to Davis (1986) for a discussion of the first three types. The hierarchical clustering method will be employed in this analysis.

The hierarchical technique is the most common clustering technique. A data table containing n samples each described by m variables, forms an n by m matrix. A measure of similarity is chosen (a correlation matrix in this case). In a Q-mode analysis, computation of the correlation between all possible pairs of samples results in an n by n symmetric matrix. In an R-mode analysis

comparisons are made between all pairs of variables and results in an m by m symmetric matrix. Any coefficient c_{ij} in the matrix gives the correlation between samples (or variables) i and j. After a measure of similarity is chosen and computed for every possible pair, an appropriate linkage method is chosen. Linkage methods control the manner in which the numbers in the correlation matrix are condensed into a dendogram. A weighted pair group average (WPGA) method was used in this analysis. Using a WPGA method in a Q-mode analysis, samples are arranged into a hierarchy so that the pair of samples with the highest mutual similarity is linked first. Next, the correlation matrix is recomputed treating the grouped or clustered samples as a single element. New correlations between clustered and unclustered samples are recalculated by simple arithmetic averaging. This process iterates until the matrix is reduced to a dimension of 2 by 2. The levels of similarity at which samples are merged is used to construct a dendogram. The dendogram constructed has a branching shape, like a tree diagram.

Extensive discussions of hierarchical techniques are contained in books by Tyron and Bailey (1970), Bijnen (1973), Jardine and Sibson (1971), Clifford and Stephenson (1973), Sneath and Sokal (1973), Anderberg (1973), and Hartigan (1975).

The advantages of the clustering method are its highly visual diagramatic outcome and the fact that the computer routines needed to perform an analysis are generally easy to use and relatively inexpensive. The routine CLUST.FORT (Davis 1976, modified by Coulbourn 1985, for IBM-3081 application) is used here. The program

can perform a cluster analysis on the variables (an R-mode analysis) and/or on the samples (a Q-mode analysis).

R-MODE RESULTS

The R-mode cluster analysis performed on the data in Table 2 identifies two clusters of variables at a correlation level of about 0.55 (Figure 2). The highest correlated pair is between summit deflation length (DEFL) and eruption length (LENG) at 0.98 and is found in cluster A. This result implies an efficient link between the summit reservoir and the eruption site nearly 20 kilometers away. Cluster A also identifies a relationship between summit deflation (DEFT) and volume of lava erupted (VOLU) at a correlation of 0.78.

In cluster B, maximum and average deflation rates (MXDR and AVDR) are linked at 0.84, which is expected as they are intrinsically related. Maximum fountain heights (MXFT) are clustered with eruption rate (RATE) at about 0.70, implying that fountain heights are a partial measure of eruption rate, i.e., one of the variables controlling fountain heights is the rate at which magma is supplied to the local Puu Oo conduit. The variable INFL, the amount of inflation prior to an eruption, is correlated at a very low level to cluster A, and clusters A and B are negatively correlated at -0.1.

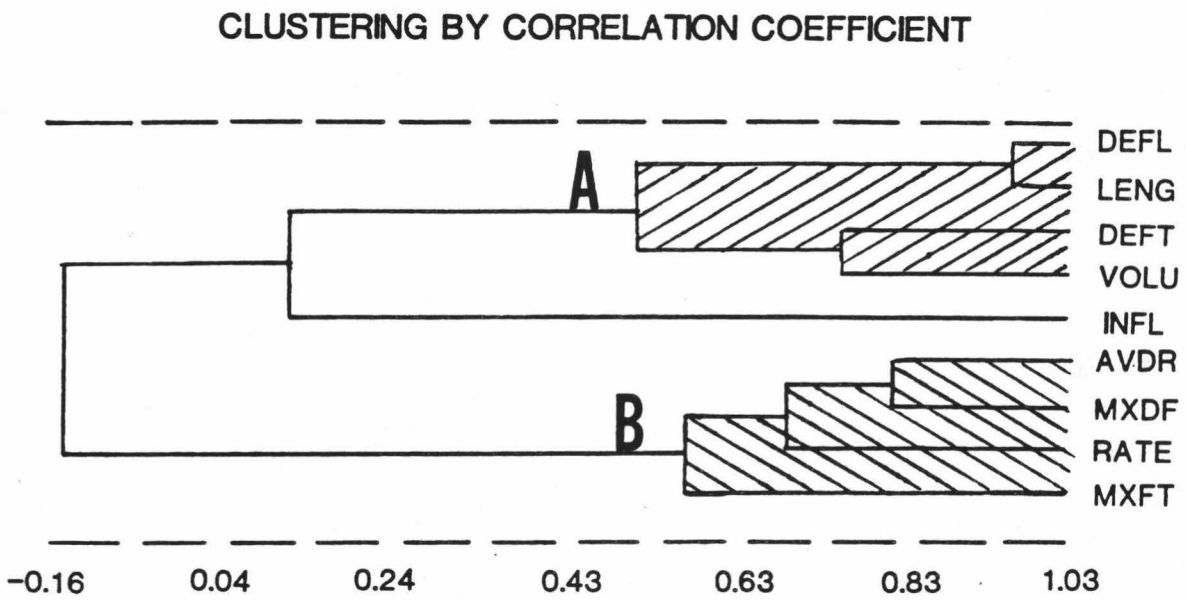

Figure 2. Dendogram produced from R-mode cluster analysis of data in Table 2.

Q-MODE RESULTS

The Q-mode cluster analysis of the data grouped the 47 eruptions into 5 groups; 3 groups cluster at a correlation near or greater than 0.80 and an isolated branch (only one episode included) is correlated to the four tightly clustered groups at 0.23, (Figure 3).

The following is a general description of the 5 clusters. Factor and discriminant analyses that follow will further expand on this discussion and quantitatively differentiate the clusters with respect to the nine characteristic variables.

Cluster 1 is composed of episodes 2-5. These were characteristically long eruptions, with low deflation rates, low fountain heights and high volumes. (see Table 3). Unlike later episodes, most of the episodes in this cluster erupted from several vents on the linear fissure system. All subsequent episodes were localized at what is now the Puu Oo vent.

Cluster 2 consists of episodes 6 and 19. This very small cluster is similar to cluster 1, however, the length of eruption and deflation is shorter and the amount of lava erupted, on the average, is less.

All the remaining episodes (except one) are divided between clusters 3 and 4. Cluster 3 includes later eruptions with higher deflation and discharge rates and shorter eruption durations than clusters 1 and 2 (see Table 3). Fountain heights are generally the greatest in this group. Cluster 4 generally includes still later episodes in the series of eruptions. This group of eruptions is characteristically very similar to cluster 3 yet the summit

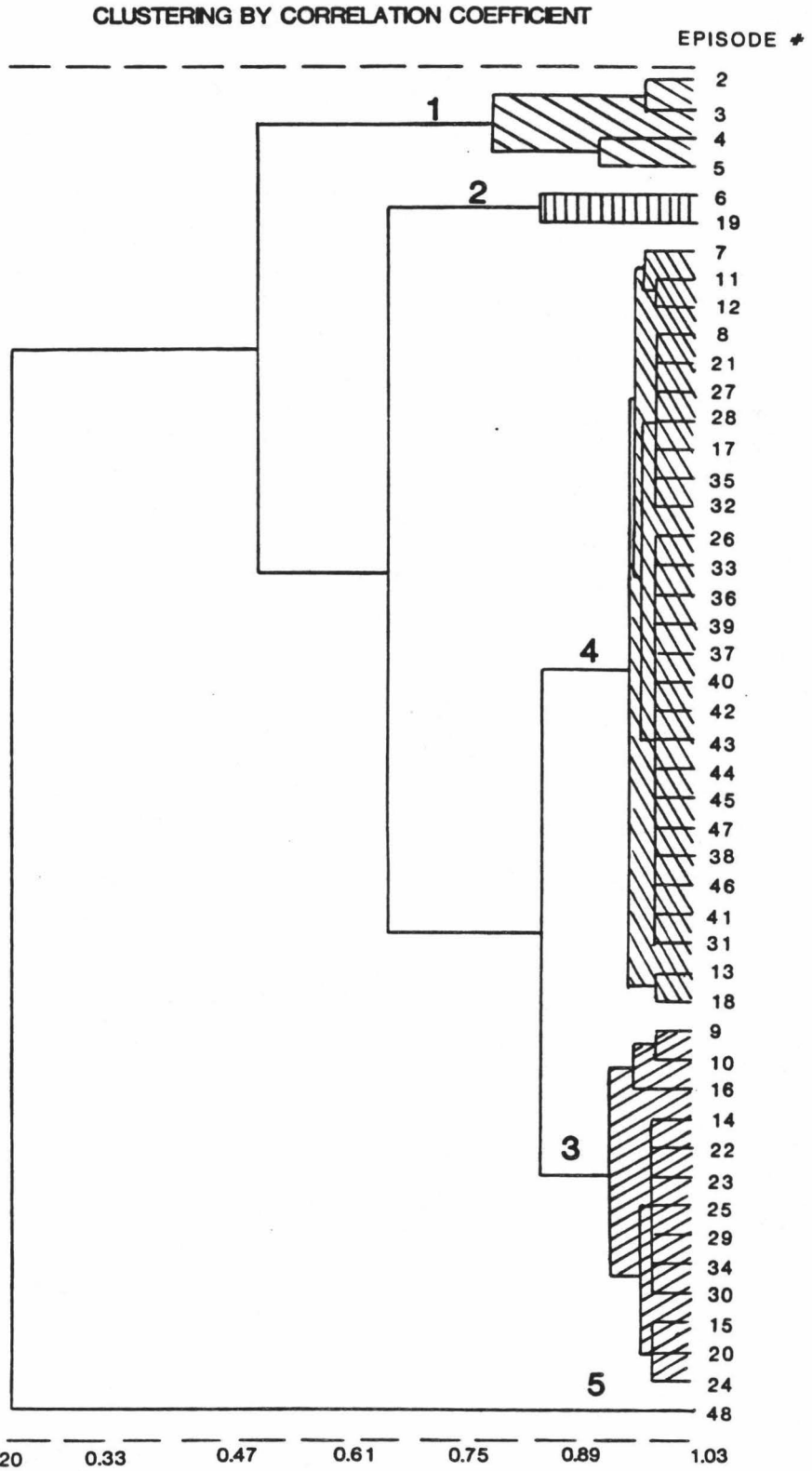

Figure 3. Dendogram produced from Q-mode analysis of data in Table 2.

deflation and eruption rates are greater for this group.

The final cluster contains only one episode. This, episode 48, was a 22-hour-long rift eruption at the base of the Puu Oo cone. After a 23-hour repose, a new fissure erupted about 3 kilometers downrift of Puu Oo where it is still erupting at the time of this writing. This eruption was not only dynamically different in its style (curtain of fire), but it had the highest deflation rate of all episodes. This high deflation rate is probably associated with intrusion of a dike during episode 48 (Ulrich, 1986, personal communication).

2. DISCRIMINANT ANALYSIS

To assess statistically the success of the assignment of the episodes to their respective cluster, the distinctiveness of the clusters, and the variables important to each cluster, the BMDP7M statistical routine (Jennrich and Sampson, 1985) was used to perform a stepwise discriminant analysis on the cluster-based data set. Each eruption is described by nine variables. As a first step in the analysis, centroids for each cluster are calculated (Table 3).

Table 3. Centroids for each group of eruptions constructed in a Q-mode cluster analysis (Fig. 3).

CLUSTER	DEFL	LENG	AVDR	MXDF	MXFT	RATE	INFT	DEFT	VOLU
1	186.5	161.0	8.8	22.3	130.0	116.3	13.7	15.5	19.2
2	63.0	58.5	16.5	45.5	130.0	84.0	12.6	11.0	5.5
3	29.6	24.0	54.1	98.1	349.0	508.7	10.6	13.9	10.0
4	27.0	18.8	60.1	138.8	285.9	843.0	12.9	13.3	11.6
5	16.5	21.6	114.0	260.0	30.0	330.0	15.2	18.8	7.2

Variables are selected as discriminators of sample clusters in a stepwise procedure based on an F-statistic. Entering and removing

variables is performed only if it improves the F-statistic by a previously determined amount. Weightings are the coefficients that maximize the distance between group centroids.

In the course of analysis, five variables were selected from the nine variables available and these are used in the discriminant function to discriminate clusters as listed in Table 4. The variables are listed in order of importance to the prediction of group assignment in Table 5. These weightings locate samples on a two dimensional display (Figure 4). The weightings are the coefficients which, in linear combination with the raw data value, determine the coordinates of a sample on Figure 4. Equations using weighted combinations and calculated intercepts for each axis are listed at the bottom of Table 5. Standardized coefficients provided by the discriminant analysis algorithm (BMDP 7M) indicate that the variables important in discriminating along the X-axis are DEFL and AVDR in a positive direction, and MXFT and DEFT in the negative direction. Variables important in discriminating along the Y-axis are MXFT in the positive direction and AVDR in the negative direction.

Table 4. Variables used as discriminators in the discriminant function.

CLUSTER PAIR	VARIABLES								
DISCRIMINATED	DEFL	LENG	AVDR	MXDF	MXFT	RATE	INFT	DEFT	VOLU
1-2	X								
1-3	X		X						
1-4	X		X						
1-5	X								
2-3	X				X			X	
2-4	X							X	
2-5								X	
3-4						X		X	
3-5					X			X	
4-5				X	X			X	

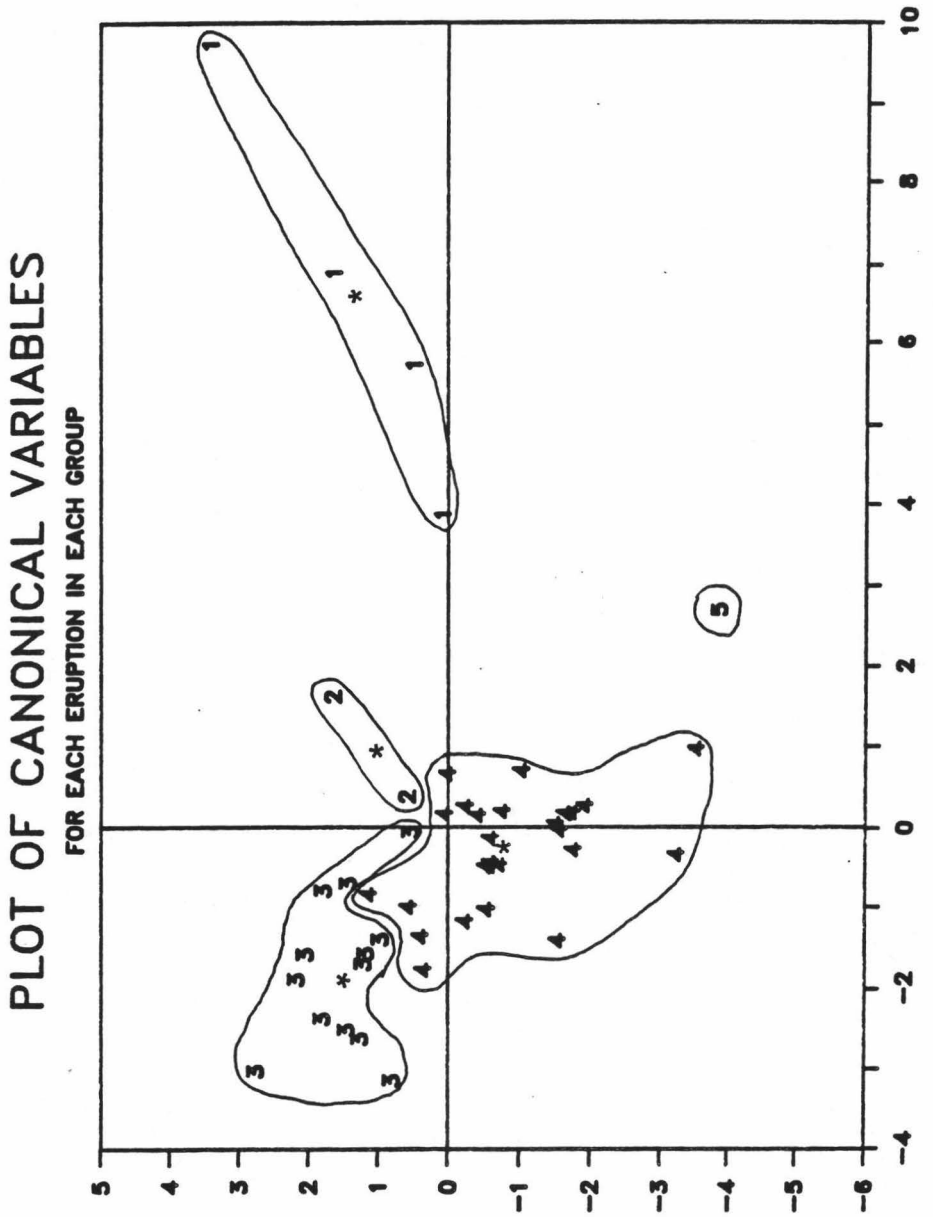

Figure 4. Plot derived from combining values of the discriminating variables with the weightings from Table 5 in linear combination.
* denotes centroid locations.

Table 5. Variables selected as discriminators of sample clusters. Variables are listed in order of their importance as discriminators. Weightings are the coefficients, which in linear combination with the raw data value, determine the position in Figure 4.

VARIABLE	X-AXIS	Y-AXIS
DEFL	0.060	0.004
AVDR	0.057	-0.029
MXFT	-0.012	0.014
RATE	0.001	-0.004
DEFT	-0.320	-0.060
CONSTANT	1.208	0.298

X=1.208+0.060(DEFL)+0.057(AVDR)-0.012(MXFT)+0.001(RATE)-0.320(DEFT)

Y=0.298+0.004(DEFL)-0.029(AVDR)+0.014(MXFT)-0.004(RATE)-0.060(DEFT)

The success of cluster choices is determined by comparing the location of each sample to the location of the centroid of each cluster. The distance from the centroid of the cluster to each sample is calculated and is tabulated by BMDP 7M. Each sample is then predicted to belong to the nearest centroid (cluster). About twenty percent of the samples were mis-classified according to this coefficient. Mis-classification probably resulted because the the correlation between clusters 2, 3 and 4 is very high (Figure 3). (Splitting clusters 3 and 4 may not be justified as suggested by preceding factor analysis). Another minor source of error probably resulted because the WPGA method of linking sample correlations is done by treating a cluster as one sample and when a new sample is entered into the cluster a simple arithmetic mean is computed to calculate the new correlation coefficient of the cluster.

In an attempt to better distinguish clusters 2, 3 and 4, the same stepwise discriminant analysis was performed on the samples from these clusters alone. The procedure results in a selection of a plane that better displays the separation of all three clusters (Figure 5). Variables important is discriminating these clusters

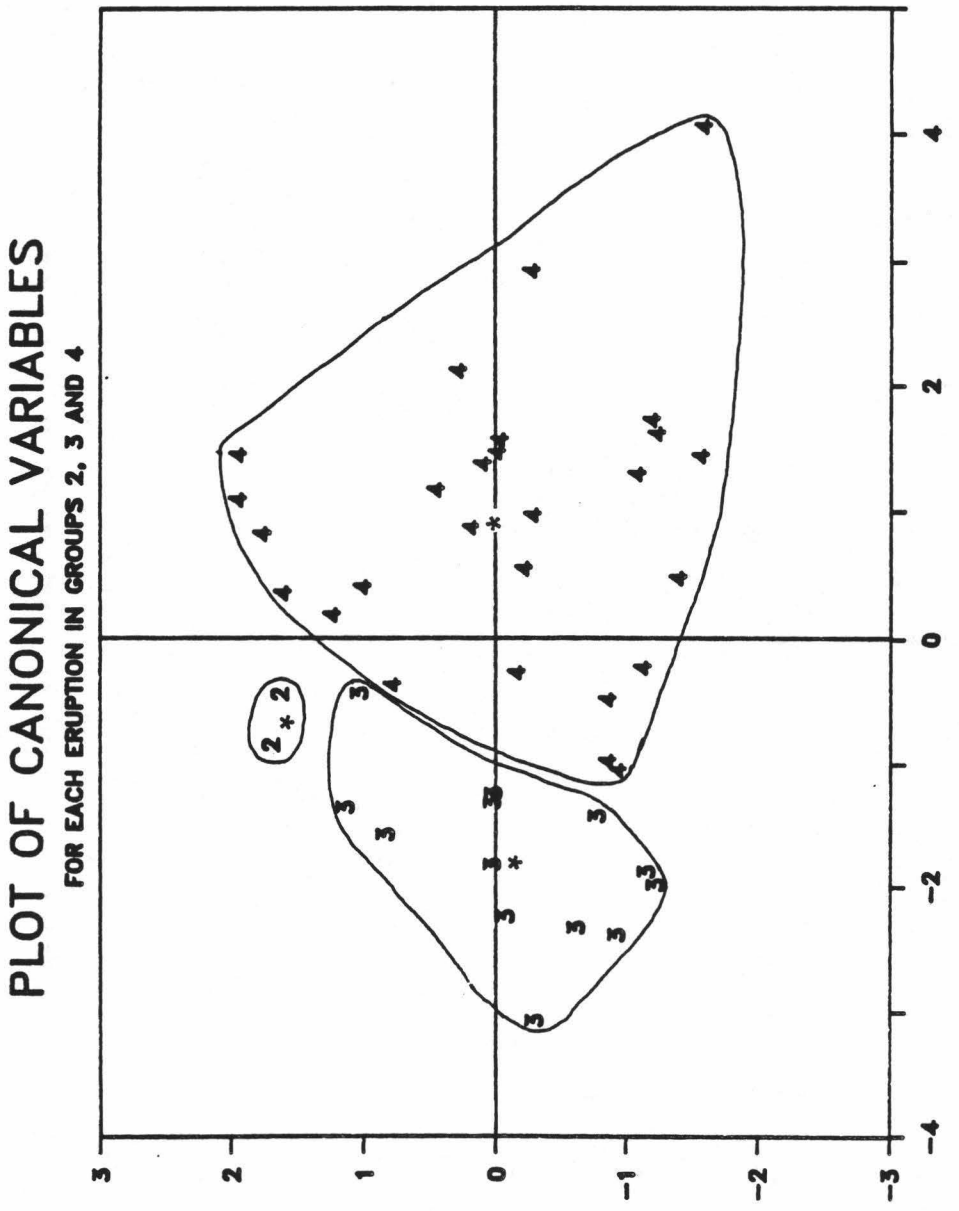

Figure 5. Plot derived from combining values of the discriminating variables with the weightings from Table 7 in linear combination. * denotes centroid locations.

are MXFT and RATE and are listed in Table 6. The weightings for each discriminating variable used are listed in Table 7.

Table 6. Variables in the discriminant function discriminating clusters 2, 3 and 4.

CLUSTER PAIR	VARIABLES							
DISCRIMINATED	DEFL	LENG	AVDR	MXFT	RATE	INFT	DEFT	VOLU
2-3				X				
2-4					X			
3-4				X	X			

Table 7. Variables selected as discriminators of sample cluster. Weightings are the coefficients, which in linear combination with the raw data value, determine the position on Figure 6.

VARIABLE	X-AXIS	Y-AXIS
MXFT	-0.015	-0.006
RATE	0.005	-0.001
CONSTANT	0.881	2.580

X=0.881-0.015(MXFT)+0.005(RATE)

Y=2.580-0.006(MXFT)-0.001(RATE)

Standardized coefficients provided in the BMDP output indicate that the variables important in discriminating along the X-axis in Figure 6 are RATE in the positive direction and MXFT in the negative direction. MXFT is important in discriminating along the Y-axis.

3. FACTOR ANALYSIS

The common objectives of factor analysis are to 1) identify and measure relationships of basic patterns in a data set, 2) minimize the covariance caused by the interrelationships between variables and 3) provide a means of rewriting the original data into another data set with more compact form.

The routine CABFAC.FORT (Klovan and Imbrie, 1971) performs a Q-mode factor analysis using a cosine theta coefficient and was applied to the same data set as CLUST.FORT (Table 2). CABFAC.FORT recasts the original data into a new data table; a table of factor loadings (Table 8). Each column of the new data table is a scaled and rotated eigenvector (or varimax factor), which is mutually independent of the other columns. Each factor has an associated eigenvalue, which measures the magnitude of the variance within the data explained by the factor.

The analysis reduces the size of the original data and the covariance between any pair of factors is near zero. The advantage of this result is that the table of factor loadings can be used in the same manner as the raw data were; the quantity of numbers is reduced and the covariances between variables is removed.

Samples marked by high values in a column of Table 8 are said to load highly on that factor. In general, most samples will load highly on factor 1 because that vector accounts for most of the variability in the data. Along with factor loadings, another new table of numbers is also generated in CABFAC; a table of factor scores (Table 9). The factor score table has a column for each

Table 8. Varimax factor loadings.

EPISODE	FACTOR 1	FACTOR 2	FACTOR 3
2	0.146	0.968	0.184
3	0.093	0.954	0.271
4	0.387	0.914	0.052
5	0.575	0.810	0.096
6	0.501	0.734	0.438
7	0.831	0.503	0.232
8	0.851	0.358	0.383
9	0.508	0.584	0.631
10	0.580	0.549	0.602
11	0.901	0.404	0.131
12	0.879	0.429	0.191
13	0.813	0.465	0.348
14	0.804	0.355	0.476
15	0.722	0.348	0.597
16	0.642	0.387	0.662
17	0.882	0.314	0.349
18	0.799	0.448	0.399
19	0.211	0.699	0.672
20	0.762	0.338	0.550
21	0.871	0.291	0.386
22	0.808	0.325	0.490
23	0.814	0.319	0.485
24	0.775	0.325	0.542
25	0.831	0.295	0.471
26	0.925	0.230	0.281
27	0.863	0.276	0.420
28	0.862	0.283	0.419
29	0.833	0.297	0.467
30	0.796	0.322	0.509
31	0.904	0.280	0.314
32	0.882	0.280	0.376
33	0.924	0.231	0.285
34	0.843	0.292	0.451
35	0.893	0.259	0.366
36	0.910	0.250	0.328
37	0.924	0.244	0.292
38	0.950	0.218	0.212
39	0.925	0.238	0.291
40	0.928	0.253	0.274
41	0.950	0.228	0.213
42	0.931	0.251	0.265
43	0.930	0.252	0.268
44	0.914	0.275	0.293
45	0.914	0.269	0.303
46	0.940	0.245	0.230
47	0.920	0.271	0.279
48	0.843	0.257	0.040
VARAINCE	65.272	18.777	15.113
CUM. VAR	65.272	84.049	99.161

factor and a row for each variable and quantitatively describes which variables are important to which factors. For instance, variables that have large values in a factor are said to score highly on that factor, and are important in describing that factor. Therefore, in statistical terminology, samples that load highly on factor 1 have characteristics that are strongly influenced by the variables that score highly on factor 1.

Table 9. Varimax factor scores. Most important variables are underlined. Eplanation of variable code names given earlier on page 6.

VARIABLE	FACTOR 1	FACTOR 2	FACTOR 3
DEFL	-0.108	0.705	-0.213
LENG	-0.104	0.618	-0.173
AVDR	0.076	0.036	0.013
MXDF	0.178	0.105	-0.038
MXFT	-0.051	0.273	0.960
RATE	0.968	0.137	0.015
INFL	0.004	0.075	-0.019
DEFT	0.004	0.068	-0.009
VOLU	0.003	0.069	-0.022

Postmultiplying the table (matrix) of factor loadings (Table 8) by the transpose of the table (matrix) of factor scores (Table 9) approximates the original data table (Table 2).

Factors that have eigenvalues (variance) of less than 1.0 account for a very small variation within the data and were deleted. This cut-off level resulted in retetion of three factors, collectively account for more than 99% of the variability within the data set (Table 8).

Varimax factor loadings indicate that factor 1 accounts for 65.3% of the variation (Table 8). The variable RATE scores most highly on factor 1 (Table 9), and is therefore assumed to be the

most important variable in factor 1. The plot of the varimax loading value for each eruption arranged sequentially with respect to time (episode), indicates a rapid increase in loading value until episode 11 (Figure 6a). By episode 31, the loadings are very consistant at a value of about 0.9.

Varimax factor 2 accounts for about 18.8% of the variability in the data set (Table 8). High scores for DEFL and LENG (Table 9) indicate the importance of these variables to factor 2. The plot of varimax loadings for each eruption indicates a rapid decrease in value until episode 8, followed by a slower decrease until episode 18 (Figure 6b). Episode 19 doesn't fit the temporal pattern, loading relatively highly on factor 2. From episode 20-48 the values decrease very gradually.

Varimax factor 3 accounts for about 15.1% of the variability in the data set (Table 8). MXFT scores most highly on factor 3 (Table 9), therefore, indicating that maximum fountain height is the most important variable in this factor. The plot of varimax loadings indicates an erratic increase in value until episode 19, followed by an erratic decrease in value until episode 48 (Figure 6c). Episodes 4,5,11,12, and 48 plot substantially lower than adjacent episodes.

Factor analysis has shown that only three eigenvectors are needed to explain the variability in the data set containing 47 samples and 9 variables. The most important variables describing these eigenvectors are RATE, LENG and MXFT. Since only three factors are necessary to explain 99% of the variation, the varimax loading can be normalized and plotted on a ternary diagram (Figure 7).

a.

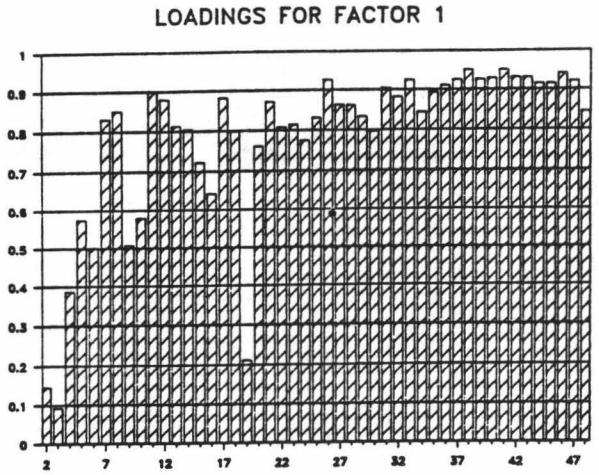

b.

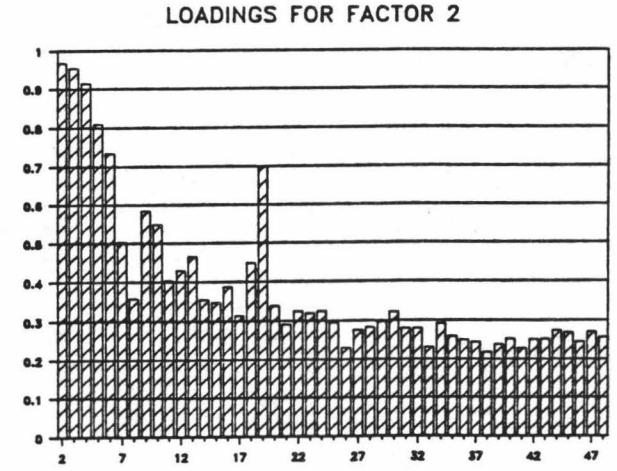

c.

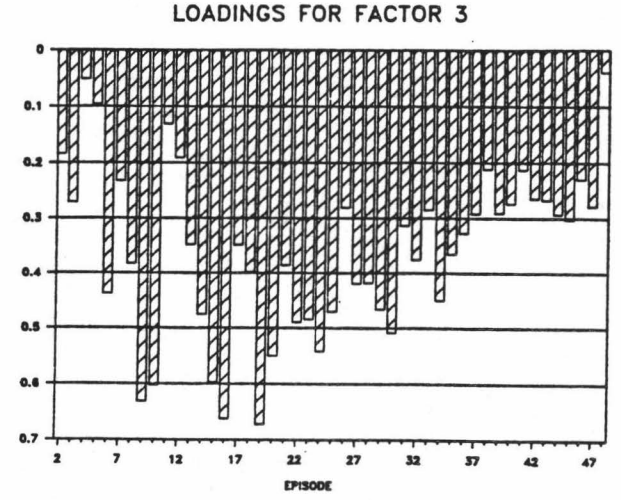

Figure 6a-c. Plot of the varimax factor loadings for each episode.

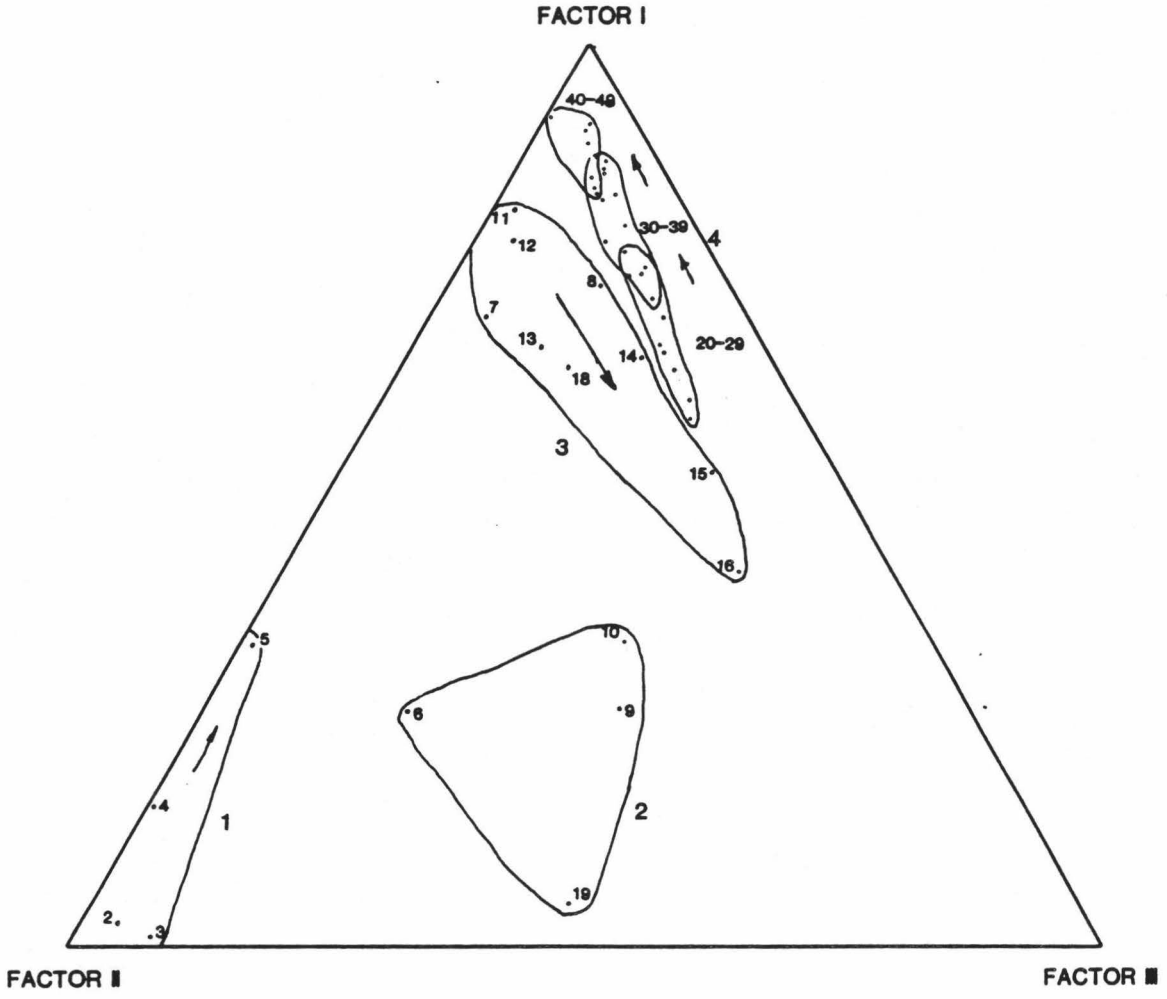

Figure 7. Ternary diagram of the three factors indicating an evolution of episodes with respect to time.

The ternary plot illustrates 4 groupings of episodes and indicates an evolution of episodes through time.

Group 1 on the ternary diagram consists of episodes 2,3,4 and 5. They plot near the Factor 2 corner, indicating eruption and deflation lengths were important variables in distinguishing the early eruptions from the later eruptions. Episodes represented in this group include those in cluster 1 (Figure 4). The four episodes in this group trend sequentially toward the factor 1 corner indicating an increasing influence from higher eruption rates with time and less influence from the length of eruption and deflation.

The second group is a group of losely clustered episodes near the center of the ternary diagram. These episodes are generally those in cluster 2.

The third group plots relatively high near factor 1 and trends down and to the right toward factor 3 with respect to episode number (time). Episodes in this group are generally the earlier episodes of cluster 3. This group can be distinguished from the first group by relatively high eruption rates (factor 1 component) and increasing amounts of factor 3 with time.

The fourth group consists of a continuum of episodes 20-48. When this group is divided into subgroups based on episode number a temporal trend is evident. Episodes 20-29 make up the lower part of the group, episodes 30-39 make up the middle section of the group and episodes 40-48 make up the top-most section of the group. This group, taken as a whole, is generally the same as the later episodes in cluster 3 combined with all of cluster 4, (this suggests that the

original splitting of clusters 3 and 4, to the degree of detail done, may not be justified). Samples within this group trend sequentially upwards toward the factor 1 apex, indicating they can be distinguished from other episodes by their eruption rates.

In summary, when factor analysis is applied to the data set in Table 2, episodes are classed into four distinct fields found to group together based on the ternary diagram. A temporal variation is evident for samples within the four groups described in the ternary diagram. In general, the four groups defined by factor analysis are the same as those defined by cluster analysis and the variables important in describing the factors are also similar to the variables found to be important in discriminating the five clusters. This comparison serves as a valuable test on the applicabilty of the two methods (cluster and discriminant analysis combined versus factor analysis) and the agreement between the two methods is interpreted as indicating that the results are well founded and that temporal patterns within this series of eruptions are quantifiable.

4. STEPWISE MULTIPLE REGRESSION

In an attempt to predict eruption episodes, sequence dates, volumes of extruded lava and repose lengths between episodes, multiple linear regression analysis was done on the data set found in Table 2. The relationships are assumed to be linear in the form:

$$E(y)=a_o+a_1x_1+a_2x_2+\ldots+a_mx_m \qquad (2.1)$$

where E(y) is the dependent variable, x_1, x_2, and x_m are the independent variables and a_o, a_1, and a_m are the coefficients.

The BMDP 2R Statistical routine (Dixon and Jennrich, 1985), was used in a stepwise multiple regression analysis. It is stepwise in that it enters and removes variables from a multiple linear regression equation in a stepwise manner, and reports a series of solutions at the different steps. Entering and removing variables is based on the F-statistic, where variables are either entered or removed if they improve the F-statistic by a previously determined amount, here set at 0.4. The hypothesis (assumption) the F-test tries to prove is that the 47 episodes have the same variance with respect to their system parameters (9 variables in Table 2). The goal of this stepwise multiple regression is to predict eruption episodes, sequence dates, repose lengths and eruption volumes given the measured system parameters found in Table 2. The dependent variables were selected for their utility at predicting the timing and magnitude of future activity.

The resulting equations for each dependent variable is listed in Table 10. The goodness-of-fit coefficient, standard error and calculated F statistics are also listed in Table 10. All calculated

F values indicate the relationships are statistically significant because they greatly excede the tabulated values of F for the appropriate number of degrees of freedom for a level of significance (alpha) of 0.05.

Table 10. List of regression equations obtained for various dependent variables. Listed in the table are the computed R, standard error, calculated F-statistic and F' value to compare against.

DEPENDENT VARIABLE	STEPWISE REGRESSION EQUATION	R	STD ERROR	CALC F	F'
EPISODE #	Y=12.42+0.19(MXDF)-0.71(DEFT)	0.89	6.3	85.4	3.2
SEQUENCE DAY	Y=345.0+5.07(MXDF)-17.36(DEFT)	0.88	175.8	70.3	3.4
REPOSE	Y=-0.81+1.90(DEFT)	0.65	8.8	33.0	5.4
VOLUME	Y=-4.76+0.06(DEFL)+(0.03)MXDF+0.79(DEFT)	0.91	2.3	70.7	2.8

EPISODE NUMBER and SEQUENCE DAY PREDICTED

Plots of predicted episode and sequence day versus observed episode and sequence day are found in Figures 8 and 9. For reference, a line with a slope of 1.0 has been added to the plots. Residuals are calculated by subtracting the predicted value from the actual value and bar graphs (Figs. 10 and 11). The pattern of values hints at a nonlinear relationship as the predicted episode and sequence day of earlier eruptions tend to be overestimated, whereas the later eruptions tend to be underestimated. However, given the sample size, the computed R values, and the statistical significance of the prediction, a linear relationship is assumed.

REPOSE PREDICTED

Repose and volume prediction plots are found in Figures 12 and 13, respectively. The variable RATE was not used as an independent variable when solving for VOLU as RATE is a function of lava volume and eruption length.

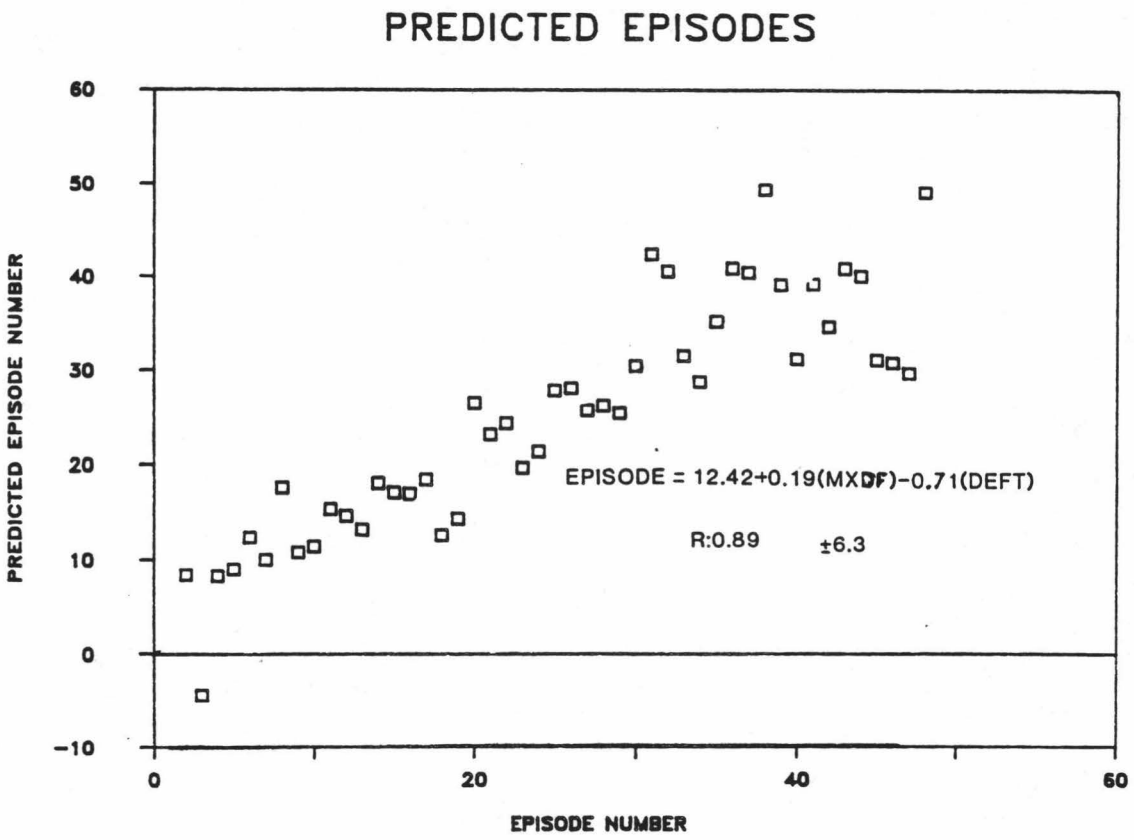

Figure 8. Predicted episode number obtained from multiple linear regression versus actual epiosde number.

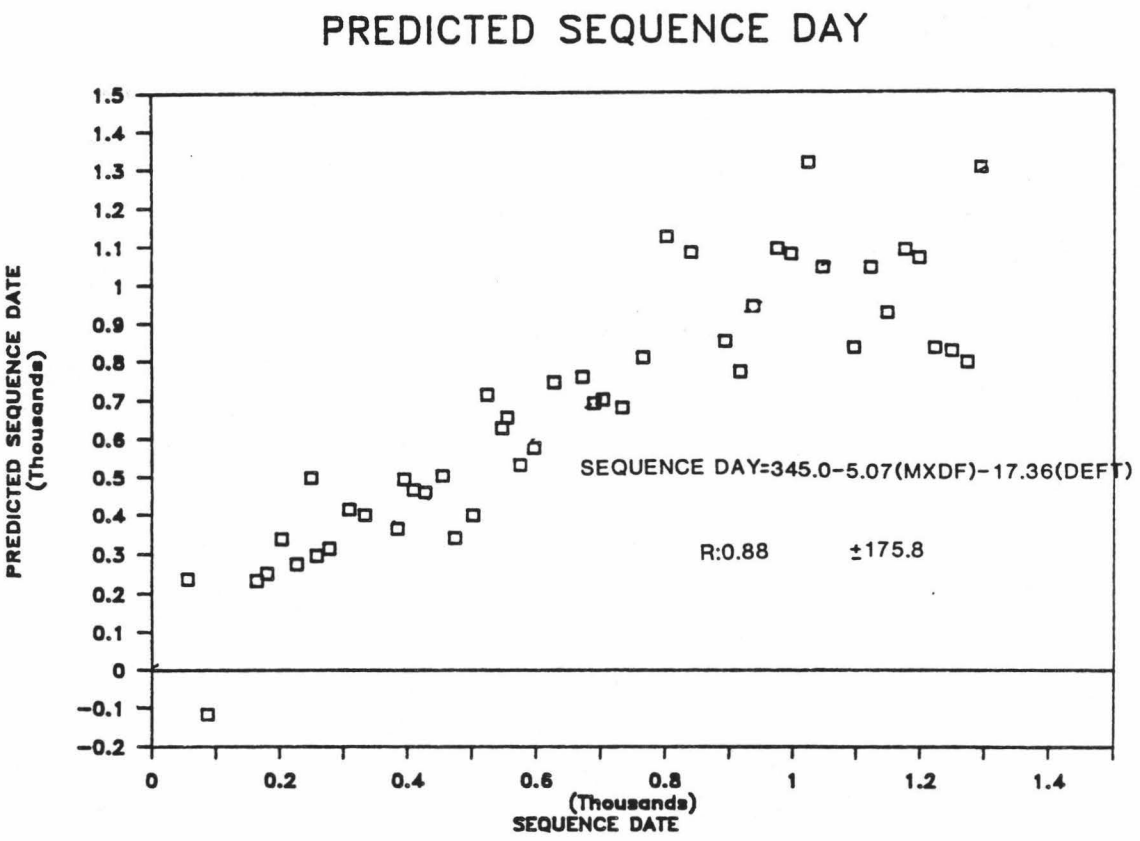

Figure 9. Predicted sequence day obtained from multiple linear regression versus actual sequence day.

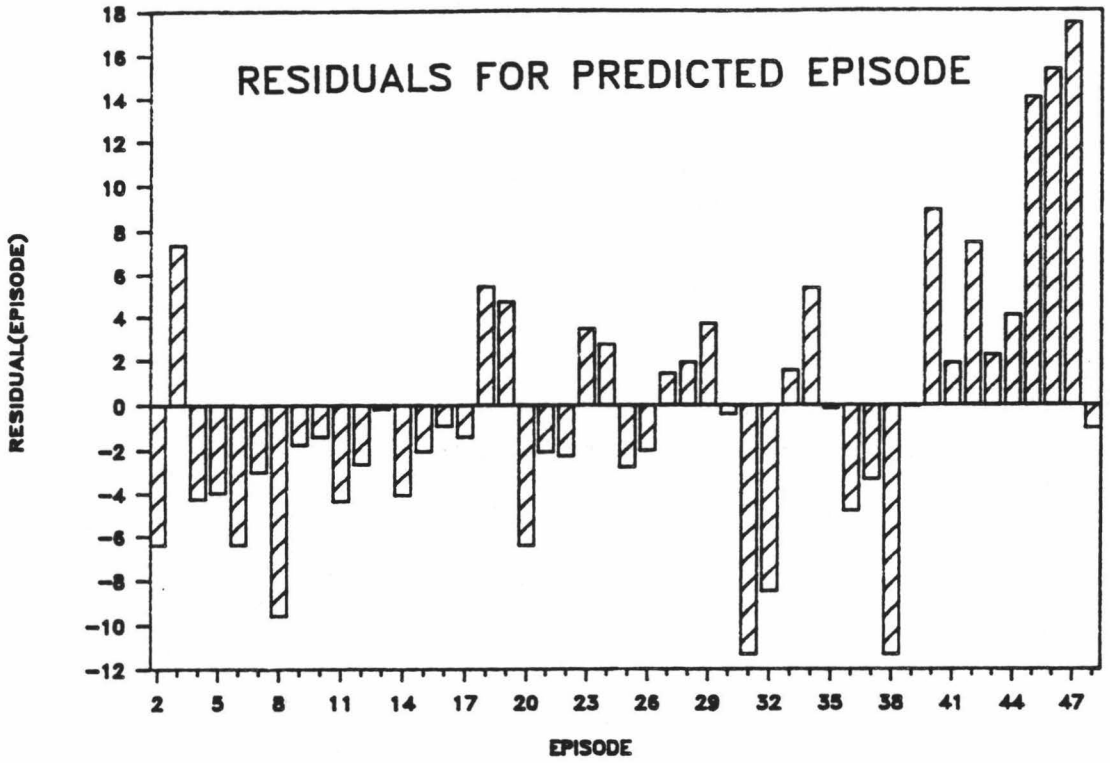

Figure 10. Bar graph of residuals for predicted episode number.

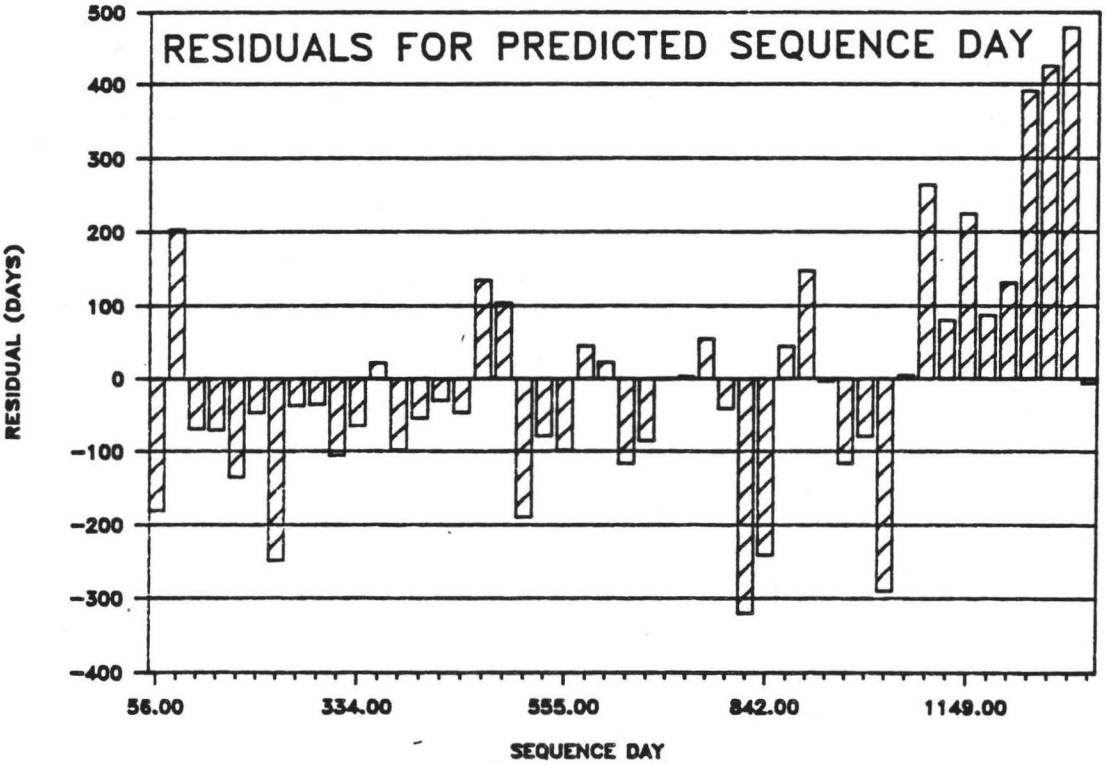

Figure 11. Bar graph of residuals for predicted sequence date.

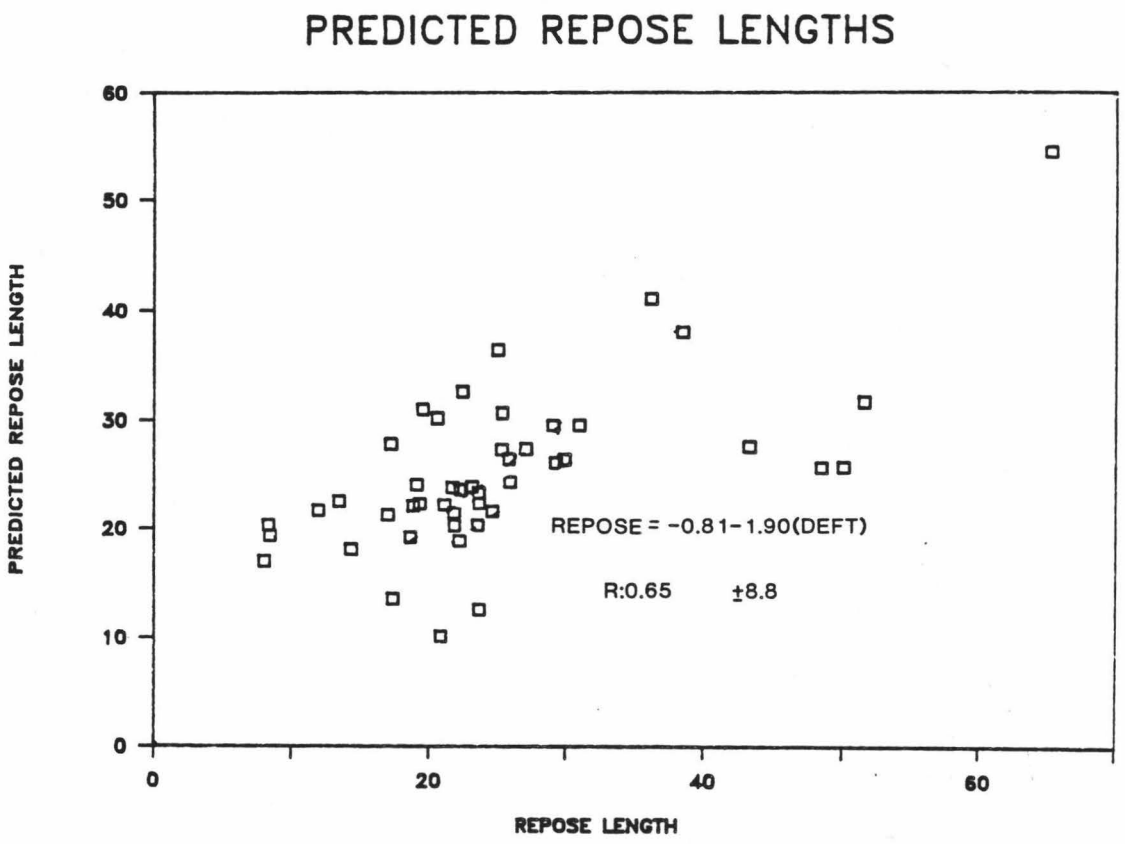

Figure 12. Predicted repose length obtained from multiple linear regression versus actual repose length.

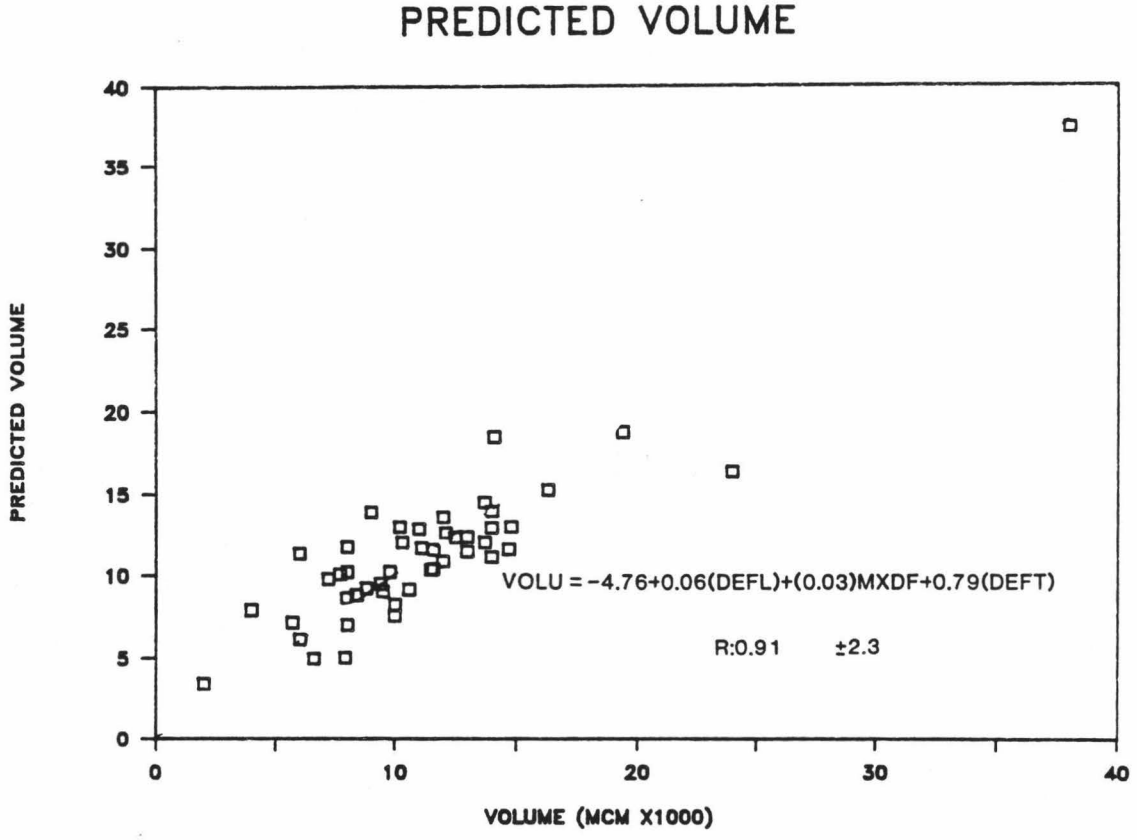

Figure 13. Predicted volume of extruded lava obtained from multiple linear regression versus measured volume of extruded lava.

The variable DEFT was found to be the only variable that helped predict the repose length (Table 10). The residual bar graph for predicted repose length (Figure 14) appears random and therefore a linear relationship can be assumed. The bar graph also indicates that the later episodes, with exceptions of 32, 33 and 39, are more acurately predicted.

VOLUME PREDICTED

Volumes are predicted by using the independent variables DEFL, MXDF, and DEFT (Table 10 and Figure 13). The residual volume bar graph (Figure 15) indicates a random pattern and therefore a linear model is appropriate. Predicted volumes for episodes 18 and 48 deviate the most from measured volumes.

Although the stepwise linear regression produced statistically significant results, with respect to their F-statistic, the results for sequence date, episode number and repose length were, in a practical sense, unusable. The standard error for predicted repose lengths ($\pm$8.8 days) is far too high considering the average length of a repose is only about 24 days. However, the VOLU values predicted using stepwise linear regression are perfectly acceptable with a standard error of 2.3 mcm. This method of predicting lava volumes could potentially be used in later episodes if the Puu Oo vent reactivates.

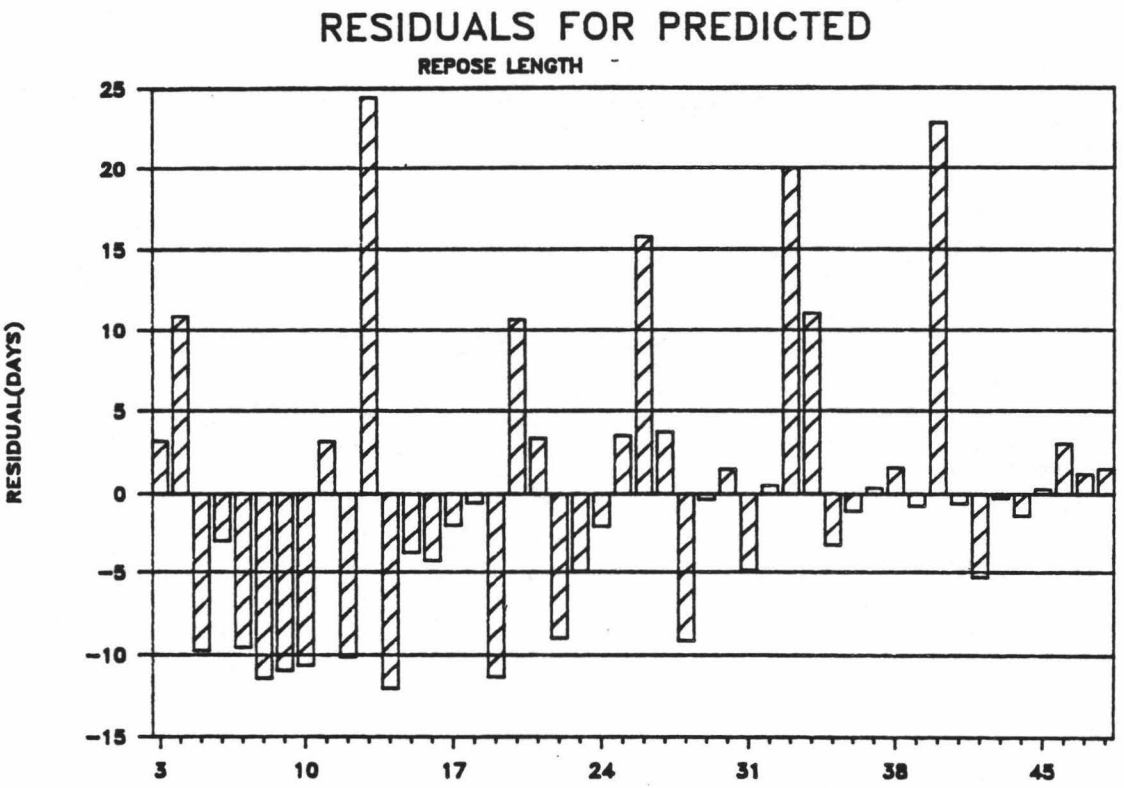

Figure 14. Bar graph of residual repose lengths.

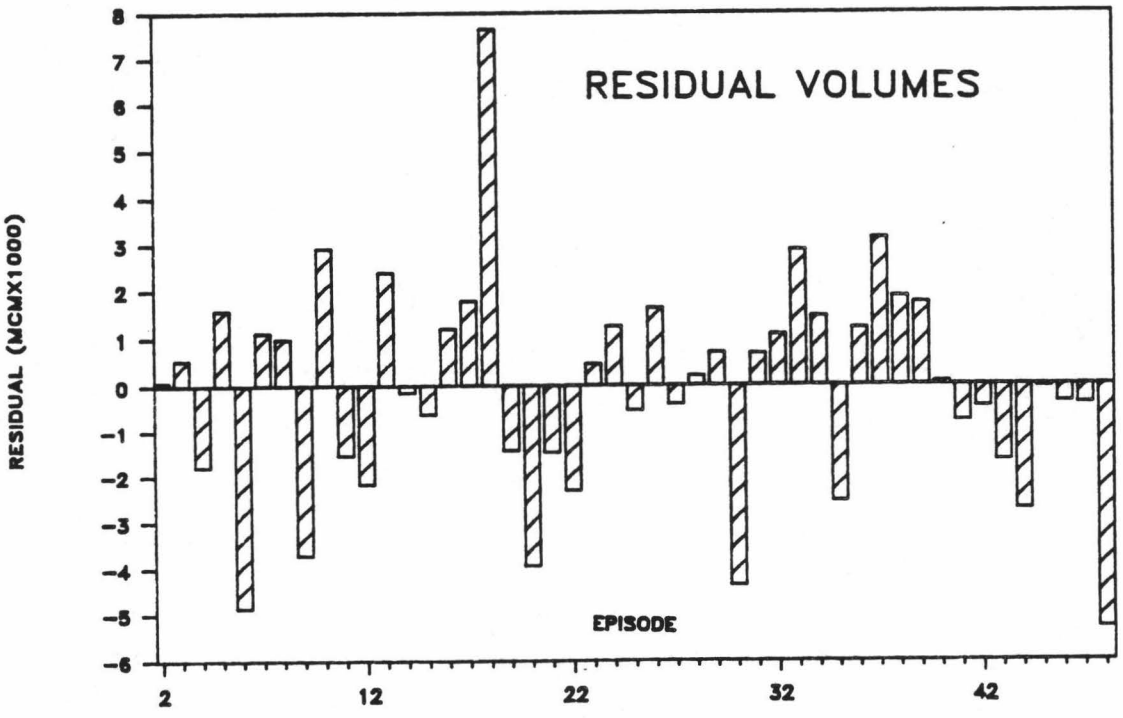

Figure 15. Bar graph of residual volumes.

The lack of "practical" predictability of the Puu Oo system is a function of our lack of understanding in both deterministic and stochastic variables. Most discussions of natural processes involve some mixture these methods, because even the most deterministic results involve uncertainities, and stochastic results often assume that some aspects of analysis can be expressed determistically. Of course, some distinction between deterministic and stochastic can be a matter of relative degrees of resolution in comparing patterns of repetitive process and their interaction.

Another approach at predictive modeling is found in numerical recursion. An example of the usefulness of recursive modeling follows.

5. NUMERICAL RECURSION

Data sets that form a sequence are common in geology. The data are usually not univariant, so the geologist needs some kind of quantitative method for summarizing, analyzing and forecasting the phenomena. One source of difficulty confronting the investigator is experimental error (noise). The fluctuation that occurs from one repitition to another is called noise and is often unavoidable. Large effects may obscure the noise; conversely, the noise may lead one to incorrectly beleive in effects that do not exist. In addition, the observed patterns result from the interaction of many factors, some deterministic and some stochastic.

The events and patterns exhibited by the Puu Oo eruption surely are the result of both deterministic and stochastic processes. Other processes may give rise to the same pattern, therefore symptoms are rarely unique. In this section, a recursive model of prediction is described.

Numerical recursion refers to some computational scheme (algorithm) wherein repetitive calculations are performed in which the current result, or state, is used to compute the next state. If the model is designed successfully, it transforms data into informative data and informationless noise; the model contains within itself all the information in the data.

The data to be analyzed in this recursive model is a bivariate

series of 250 pairs of values from the Puu Oo eruption. The input quantities are fountain heights measured at the Puu Oo eruption site during episode 19. A five point running average was applied to the data to smooth the trend. The output values are deflationary tilt measurements made at Kilauea's summit about 18 kilometers away. A three point running average was applied to this data set. Both data sets are equally space at 6-minute intervals. A plot of the raw input/output data is found in Figure 16; they are not plotted to the same scale.

The transfer function used by MICROCAPTAIN yields a full stochastic model of the Box-Jenkins type. The complete Box-Jenkins model can be written as a single equation:

$$y_k=(B(z^{-1})/A(z^{-1}))(u_{k-\delta})+(D(z^{-1})/C(z^{-1}))e_k \quad (2.2)$$

The following symbols are defined and used throughout this section.

y_k = output at the kth sampling instant

$\bar{y}$ = mean value of y

$u_{k-\delta}$ = input measured at sampling instants previously

z^{-1} = backward shift operator

δ = size of time delay (lag)

n = number of terms in A polynomial

m = number of terms in B polynomial

N = total number of samples

P_{ij} = covariance matrix

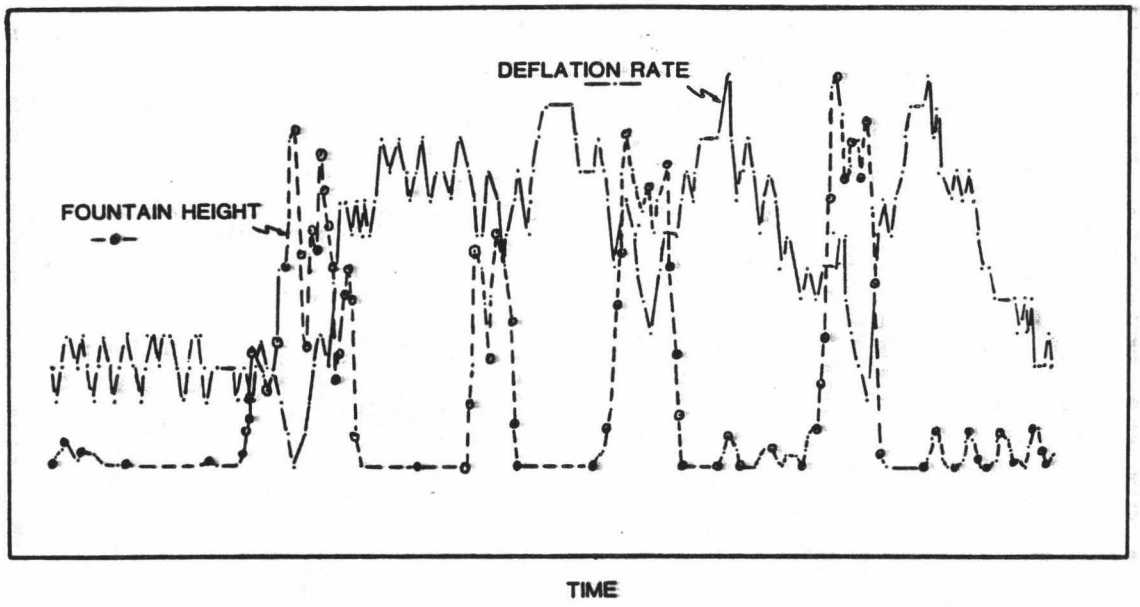

Figure 16. Raw input and output data plotted at different scales to allow comparison. Input data is fountain height; output data is deflation rate.

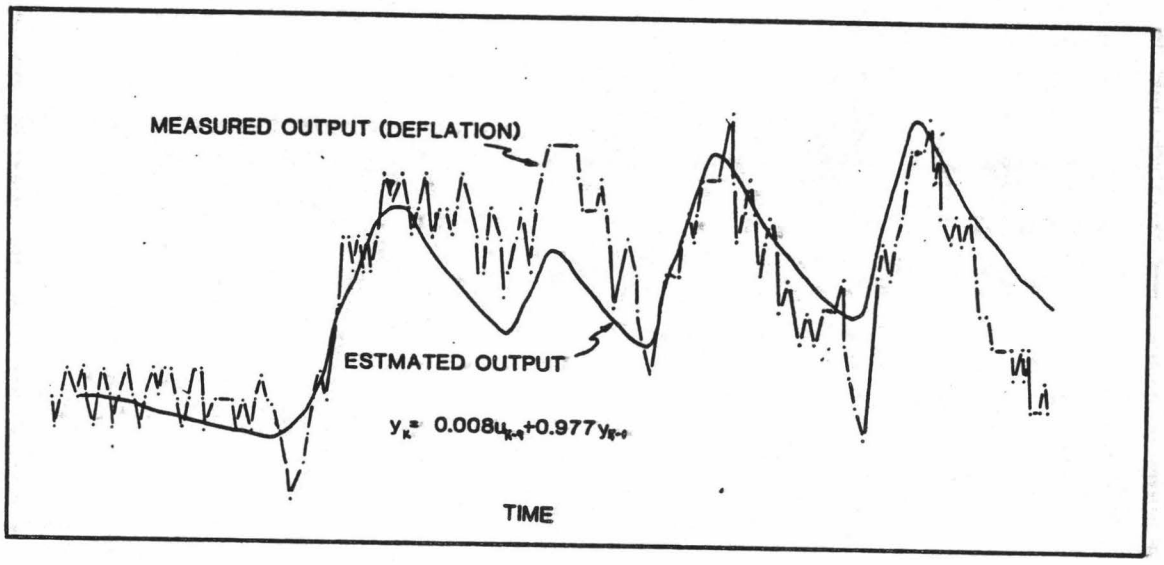

Figure 17. Calculated transfer function compared to observed output (deflation rate).

i = number of iterations

$\frac{B(z^{-1})}{A(z^{-1})}$ =discrete-time TF

$$\hat{x}_k = \frac{B(z^{-1})}{A(z^{-1})} u_{k-\delta} + E_k$$

$\hat{x}_k$ = deterministic output modelled as being causually related to u_k

$$E_k = \frac{D(z^{-1})}{C(z^{-1})} e_k$$ = noise term of stochastic disturbances

$\hat{E}_k = y_k - \hat{y}_k$ estimated value of noise

$A(z^{-1})$ polynomial $= 1 + a_1 z^{-1} + \ldots + a_n z^{-n}$

$B(z^{-1})$ polynomial $= b_o + b_1 z^{-1} + \ldots + b_m z^{-m}$

$C(z^{-1})$ polynomial $= 1 + c_1 z^{-1} + \ldots + c_p z^{-p}$

$D(z^{-1})$ polynomial $= 1 + d_1 z^{-1} + \ldots + d_q z^{-q}$

In MCAPT, the program allows the user to specify the model structure prior to parameter estimation. Table 11 lists the A (n) and B (m)

parameters, the size of the delay (δ), and the two relative merits of the models estimated for comparison; the coefficient of determination (R_T^2) and the error variance form (ln EVN). R_T^2 provides a normalized measure of how well the model explains the data and is defined as:

$$R_T^2 = 1 - \sum E_k^2 / \sum (y_k - y)^2 \qquad (2.3)$$

For a perfect fit of the data this value equals 1.0 with a small error term. Conversely, a poor fit will produce an R_T^2 near zero and have a high error term.

The EVN term indicates how well the parameters are defined in an overall measure of the variance associated with the parameter estimates. This helps prevent one from over parameterizing the model just to get a good R_T^2 value.

Table 11. Some models tested for the input-output data set.

n	m	lag δ	i	R_T^2	ln EVN
1	1	10	1	0.51	-8.1
1	1	9	1	0.53	-8.1
1	1	8	1	0.45	-8.0
1	1	11	1	0.51	-8.0
1	1	12	1	0.47	-7.9
1	1	9	1	0.53	-8.2
1	1	9	3	0.53	-8.2
1	1	9	5	0.60	-8.2
1	1	9	6	0.60	-8.3

For this system model, 1 A parameter, 1 B parameter, a time delay of 9 and 5 iterations produced the most favorable statistics and least noise variance. The model results in a goodness-of-fit coefficient of 0.60 and a lnEVN of -8.2. The simple first order equation implies a simple linear relatioship beteen the input (fountain height) and output (deflation rate) values and the time lag of 9 intervals illustrates the obvious lag in summit response.

The estimated A and B parameters are -0.977 and 0.008 respectively. Substituting these values in the TF results in

$$y_k=0.008u_{k-9}+0.977y_{k-1} \qquad (2.4)$$

This function is compared to the output data in Figure 17. The function more accurately predicts the peaks and troughs of the observed data and the intermediate values are sources of error.

This example of recursive modeling serves as an illustration of how two variables of unknown relationship can be coupled to stochastically predict one from the other. In the following chapter I will show that the relationship between fountain height and deflation rates is probably more deterministic than stochastic.

Recursive techniques can also be applied to other variables such as repose lengths and volumes (variables important for prediction and hazard assessments) and may lead to a better understanding of deterministic processes.

DISCUSSION: GEOLOGIC INTERPRETATION OF STATISTICAL RESULTS

The cluster analysis performed on the data set found in Table 2 deliniated 5 clusters of eruptions. Discriminant analysis was used to determine how well the clusters were discriminated and which variables were most important in their discrimination. Discriminant analysis indicated that 80% of the episodes were classified to be in the correct cluster according to a Mahalanobis distance coefficient. This success rate is very acceptable considering the similarity of many of the later episodes and the WPGA linkage method used (discussed earlier). Of the nine variables used to describe the series of eruptions, five were necessary in discriminating the 5 clusters; these are DEFL, AVDR, MXFT, RATE and DEFT. In support of the cluster and discriminant analysis, factor analysis applied to the same data set generally found similar groupings of episodes that followed nearly the same temporal variation. These groupings were also deliniated by similar variables.

Cluster 1 is composed of earlier episodes that had erupted from a complex of vents, suggesting a plexus of shallow conduits. They were long eruptions, with low deflation rates and low fountain heights. Discriminant analysis tells us that this cluster can be discriminated from all other clusters by DEFL and from clusters 3 and 4 also by AVDR (Table 4).

Cluster 2 is composed of later episodes. All episodes of cluster 2 were localized at what is now the Puu Oo vent. They were shorter in eruption length and had higher discharge rates. Erupting lava at a greater rate from a single centralized location suggests

that the Puu Oo conduit system had begun to establish itself and rapidly stabilize.

Cluster 3 includes still later episodes. These episodes include those with even higher deflation and discharge rates and shorter eruption durations. Fountains for this group were generally the loftiest. Theoretical studies (Wilson and Head, 1981) show that fountain height is controlled by gas content of the magma and effusion rate. The high fountains of this cluster may be explained by the increased rate of supply of magma to the eruption site. Increased magma supply will result in increased transport velocity. The higher velocity of magma leads to retention of more of the exsolved gas, as less time is needed for the magma to arrive at the eruption site. The higher deflation and discharge rates and shorter eruptions indicate that the conduit sytem between the summit and the eruption site was streamlining itself through time.

Cluster 4 generally includes the latest episodes in the series of eruptions. This group of eruptions is very similar (with respect to the nine system variables) to cluster 3 yet the summit deflation and eruption rates were slightly greater for this group. The similarity of cluster 3 with 4, with the exceptions just noted, indicates that the plumbing system of the Puu Oo system was well established in cluster 3 and only slight adjustments had been made during the later episodes of cluster 4. The slight adjustments made to account for the increased rates of deflation and lava production during cluster 4 both suggest that they were to further streamline the conduit system.

The pattern of eruptive behavior suggests that the plumbing system evolved quite rapidly. In fact most episodes included in cluster 3 or 4 follow episode 9. And all episodes including and beyond number 20 are included in clusters 3 or 4. Factor analysis applied to the data set also suggests a similar rate of system change. Therefore, it is assumed that by episode 10, the system had become well established and further changes made to the system are small and gradual.

Because the amount of inflation and deflation measured at the summit is related to the amount of lava leaving the summit reservoir (see following chapter and R-mode analysis performed earlier), one method of evaluating the state of equilibrium within the Kilauea system is to examine the amount of lava produced per microradian of deflation. Table 12 reveals that cluster 1 produced 1.3 million cubic meters per microradian of summit deflation. This value is almost twice as large as the value calculated for clusters 2 and 3 and substantially larger than cluster 4. The early episodes found in cluster 1 were influenced by the initial intrusion of the January 3, 1983 dike. The magma of this dike displaced much of the previously stored magma and resulted in the eruption of large volumes of differentiated and mixed magma. By cluster 2 and 3 the volume to microradian ratio stabilized at 0.77-0.78 probably reflecting some level of equilibrium between the summit tilt and lava extrusion. This ratio increased somewhat for those episodes in cluster 4 maybe reflecting an increased ease at which magma travels through the rift system as the system became more established.

Episode 48, the sole member of cluster 5, produced 0.38 million cubic meters of lava per microradian of summit deflation. This conspicuously low ratio is likely to be a result of a dike emplacement during this episode (Ulrich, 1986, personal communication).

Table 12. List of cluster number, episodes in reclassified cluster and amount of lava produced per microradian of deflation.

CLUSTER	EPISODES	VOLUME PER MICRORADIAN OF SUMMIT DEFLATION
1	2,3,4	1.30 mcm/urad
2	5,6,7,8,13,14,17,19	0.78 mcm/urad
3	9,10,15,16,18,20-25,27-30 34	0.77 mcm/urad
4	11,12,26,31-33,35-47	0.86 mcm/urad
5	48	0.38 mcm/urad

PETROLOGICAL AND GEOCHEMICAL EVIDENCE

The petrology and major oxide chemistry of the Puu Oo lavas has been studied by Garcia et al., (1984), Garcia and Wolfe, (in press) and Wolfe et al.,(1987). These studies show that the lavas from the early episodes (1-3) were erupted from various vents and are compositionally heterogeneous. The lavas contain less than 6.8% MgO, representing diferentiated basalt (Wright and Fiske, 1971). Wolfe interprets this lava as having resulted from fractionation of magma that had partly cooled and crystallized during a lengthy storage within the rift zone. The presence of resorbed xenocrysts and reversely zoned phenocrysts suggests that magma mixing had occurred.

By episode 4, the MgO content in the lava had increased to 6.8% or more. Episodes 5-10, 18 and 30-31 revealed a compositional variation within individual episodes as the MgO content in the lava

during these episodes gradually increased as the episode progressed.

Repose period crystal (olivine) fractionation of the magma within a local reservoir has been used to explain this intra-episode compositional variation. The resulting compositionally zoned local magma chamber near Puu Oo was completely erupted in episodes 5-10. Apparently, the local reservoir had grown considerably after episode 10 as the MgO depleted volume within this local reservoir was too large to be exhausted in following episodes except for episodes 18, 30 and 31, all of which produced a relatively large amount of lava. The volume of MgO-poor lava for episodes 6-10 is approximated to be about $3X10^6m^3$. Episode 11 produced $12X10^6m^3$ of lava that was all MgO-poor as was true also for lavas from most episodes following 10. Therefore, the reservoir in which the fractionation took place was enlarged prior to episode 11. Geodetic measurements are used in a later chapter to constrain the geometry and volume of the local Puu Oo reservoir.

This concludes the statistics portion of the thesis. The next chapter examines more closely the important distinguishing variables such as fountain heights, deflation rates and eruption rates. The apparent relationships between these variables is deterministically explained.

CHAPTER III

FOUNTAIN HEIGHTS AND SUMMIT SUBSIDENCE RATES

Characteristics of the recent Puu Oo eruption include fountain heights ranging from 10 to over 500 meters averaging 200-300 meters (for episodes after episode 20), and effusion rates of about 10 to 500 cubic meters per second averaging about 200 cubic meters per second. Wilson and Head (1981) have shown that fountain heights are controlled by effusion rates and gas content of the magmas. The relationship between fountain height and gas content has been shown to be the dominant and controlling relationship. This can be illustrated with a simple example of an eruption of a gasless magma. If a gasless magma erupts with an exit velocity of u, the resulting fountain height is calculated from:

$$H=u^2/2g \qquad (3.1)$$

where H is the fountain height above the surface and g is the acceleration due to gravity. Factors influencing u are pressure gradient, conduit geometry and friction factors (Wilson and Head, 1981), while effusion rates are affected by conduit geometry and eruption velocity.

Using the above equation to calculate the eruption velocity necessary for a fountain height of about 200 meters yields a velocity of about 63 meters per second. Vent observations (Wolfe et al., 1987) suggest the vent is nearly circular with a diameter close to 20 meters. Multiplying the velocity of the gasless magma

by the cross-sectional area of the vent yields an effusion rate of 200,000 cubic meters per second. This value is two orders of magnitude greater than any observed effusion rate for the Puu Oo eruptions. Conversely, when an eruption velocity is calculated by using typical effusion rates and a radius of 10 meters a value of 0.65 cubic meters per second is obtained. Using this velocity value to calculate a fountain height yields heights of only a few centimeters. This value is obviously much smaller than any observed fountain height at Puu Oo. This discrepancy can be attributed largely to the fact that the magma is not gasless, but in fact has a large gas volume component. As the magma rises through the near vent vertical conduit the exsolution of gases (presumed to be mostly water, Greenland, et al., 1985) disrupts and buoyantly propels the magma in a vertical direction resulting in high fire fountains of low-density tephra.

Wilson and Head (1981) have used numerical methods to show relationships between effusion rates and fountain heights for a variety of gas contents. Their figures illustrate a weak dependence of the fountain height on effusion rate. The Puu Oo eruption has had maximum fountain heights of about 500 meters indicating a gas content of 0.6 to 0.8 wt% H_2O for typical effusion rates (Figure 7b in Wilson and Head 1981). The average fountain height of about 200 meters suggests a gas content of about 0.4 wt%. Greenland et al.,(in press a) has COSPEC measurements indicating that the east rift zone magma degasses about 0.4 wt% gas during eruption. Therefore, both field and numerical methods have been shown to be

very similar and a gas content of 0.4 to 0.8 wt.% is assumed throughout the text.

The above argument suggests that fountain heights are indicators of exit velocities of magma which are strongly influenced by gas content and only weakly influenced by magma effusion rate. Large variation in fountain height during a single eruption probably reflects changing volatile content. Small variations in fountain height may reflect changing volatile content and/or changing effusion rates.

I will present data that correlates fountain heights to eruption rates. At first sight, this appears to be in direct conflict with the argument that correlates fountain heights with gas content and only very little with eruption rate. I will show later that correlating fountain heights with eruption rates does not conflict with the above argument.

FOUNTAIN HEIGHT DATA

All fountain height data and corresponding times were obtained from the collection of 8mm-time-lapse film stored at the Hawaiian Volcano Observatory. The times corresponding to each fountain height were derived by marking the time at the beginning and end of each roll of film. The time it took from the beginning time-mark to the ending time-mark is divided by the number of frames and an average frame rate is obtained. This average frame rate was assumed constant and used to interpolate the times of intermediate frames. Our on-site observations and comparisons with the time-lapse record

suggest that a time discrepency does exist, however, it is virtually never more than ±10 minutes.

Fountain heights were obtained by digitizing the fountain directly from the film and multiplying the digitized result by a scale constant. The scale constant is dependent on the focal length of the camera and the distance from the camera to the fountain. Inherent errors exist in the digitizing process due to poor visibility at the vent or uncertainty in the pinpointing of the actual fountain height on the images. However, our on-site observations and comparisons suggest the fountain heights are accurate to ±20 meters.

SUMMIT DEFLATION AS A MEASURE OF ERUPTION RATE

Many investigators have documented the positive correlation between the magnitude of summit subsidence and the volume of erupted lava. Linear, least-squares fit of erupted lava volumes against microradians of summit deflation yields an estimate of 0.33 million cubic meters per microradian for Kilauean eruptions spanning a time period from 1956 to 1983, (Dzurisin et al., 1984) and an estimate of 0.45 million cubic meters per microradian for a time period spanning 1966 to 1983 (Dvorak, et al., 1985).

The average ratio of volume of erupted lava to summit deflation (determined from Puu Oo field measurements and measurements at the summit tilt meter) yields a relation of 0.83 million cubic meter (±0.24) per microradian (0.62 ±0.18 after correction for void space). Figure 18 illustrates the positive relationship between summit deflation and volume of erupted lava.

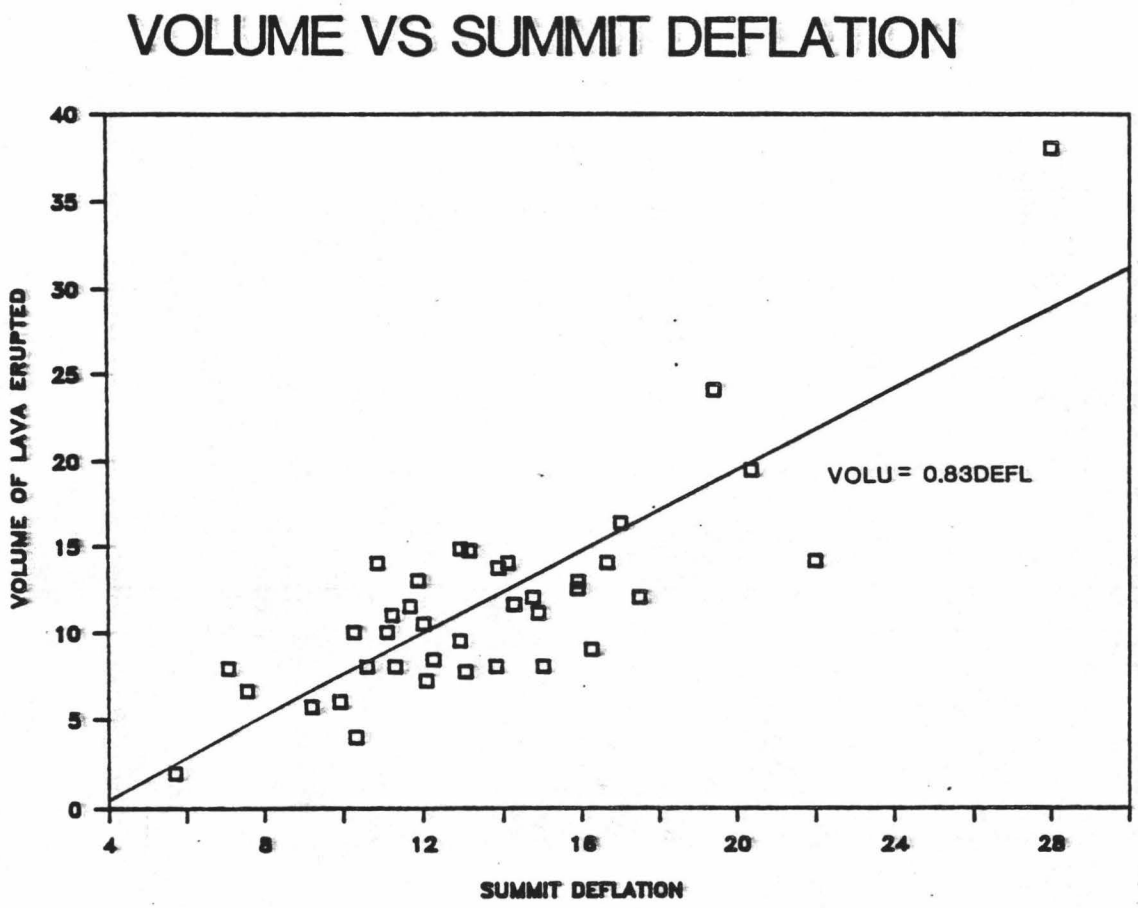

Figure 18. Measured volume of lava extruded versus summit deflation.

FOUNTAIN HEIGHTS AS A MEASURE OF ERUPTION RATE

Like the relationship between summit deflation and volume of erupted lava, a relationship exists between fountain height and erupted volume. Fountain heights of 16 eruptive episodes were plotted to the same scale and digitized for relative areas beneath the curves. Episodes were chosen on the basis of their superior fountain height record and volume estimates: each of these 16 eruptions produced a single distinct fountain and HVO had a near-complete photographic record with good visibilty and stable cameras. The volume estimates were made with the aid of aerial photographs and ground measurements. Typical examples of a well recorded fountain height and deflation rate are illustrated in Figure 19.

A remarkable correlation results when the digitized fountain areas are plotted against lava production and summit deflation (Figures 20 and 21, Table 13). This suggests that for eruptions of a given length, those with relatively high fountains will produce more lava than those eruptions with relatively low fountains. It also suggests that the summit will experience more net deflation for those eruptions with higher fountains. This, therefore, suggests that fountain heights are related to effusion and deflation rates. When the area of the fountain height is determined on the digitizing tablet its units are converted to cm x hrs. This calculated area is divided by the duration of the eruption resulting in an average fountain height (the average height is in cm measured on the digitizing tablet). The 16 Puu Oo average fountain heights measured

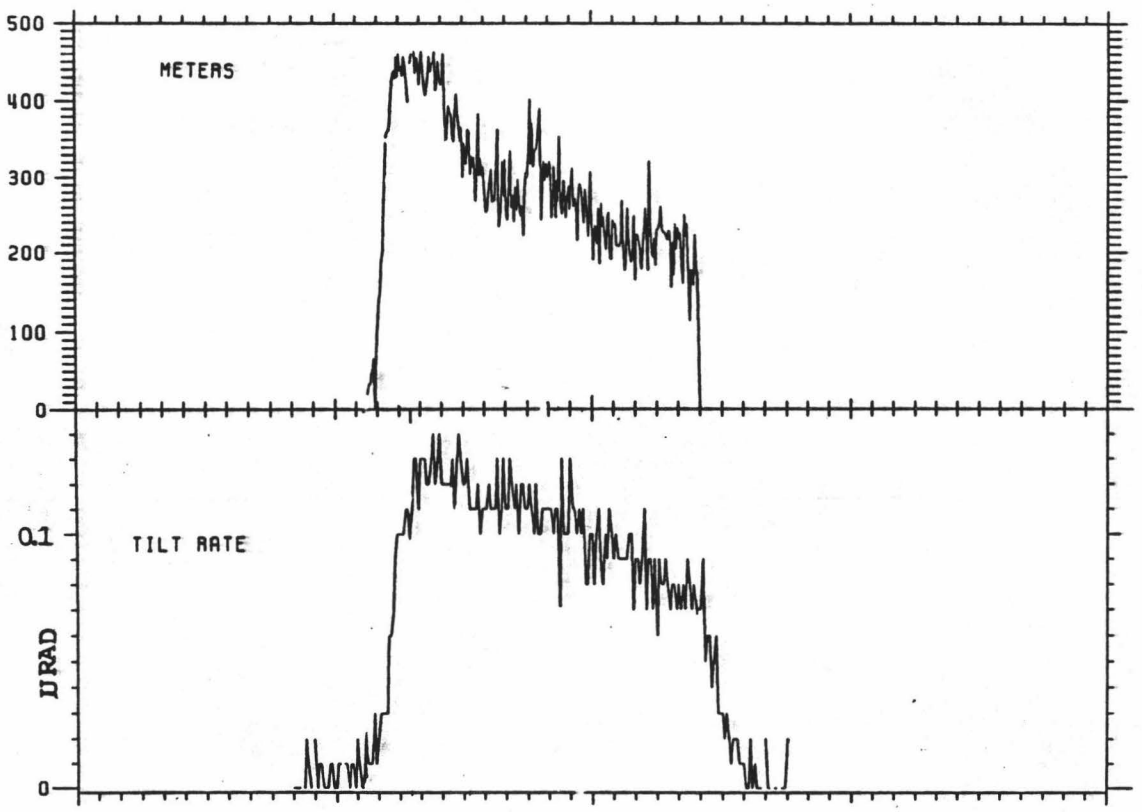

Figure 19. Typical examples of fountain heights (top) and deflation rates (bottom). Vertical scale for plots differ for easier comparison; horizontal scale the same.

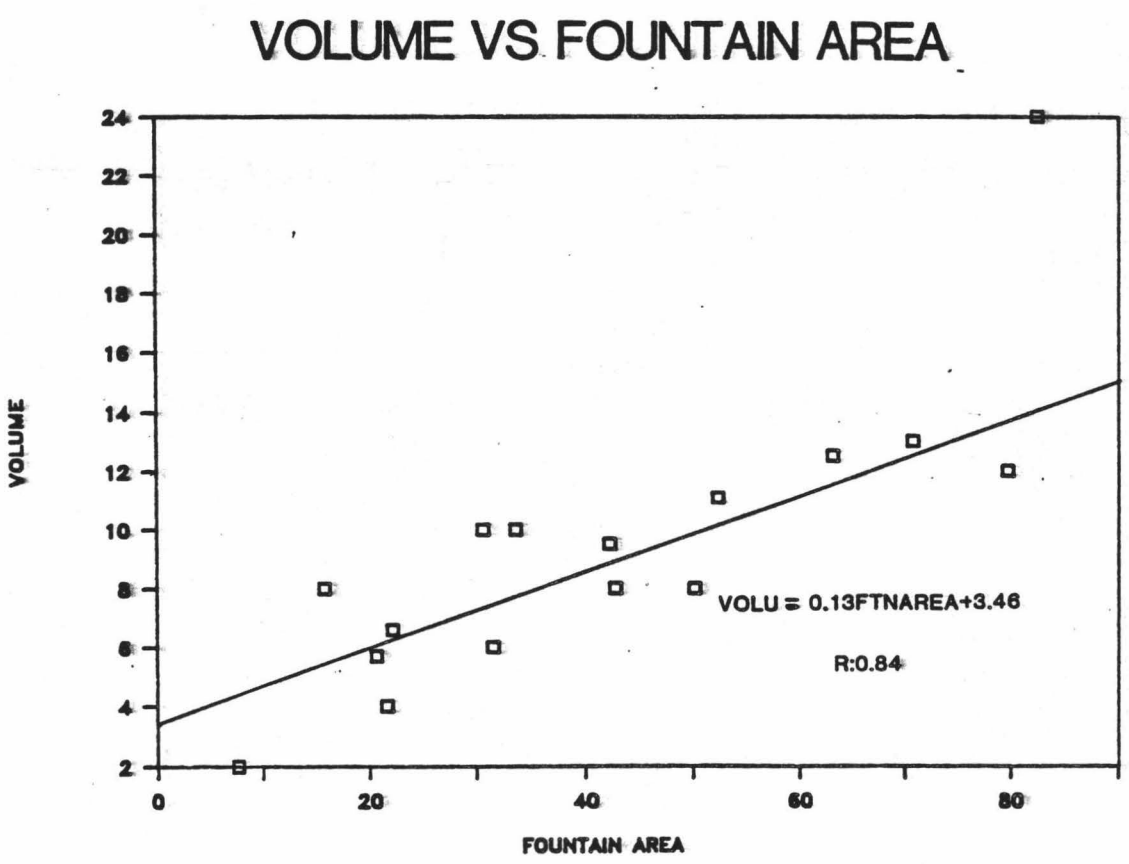

Figure 20. Volume of erupted lava versus digitized fountain area.

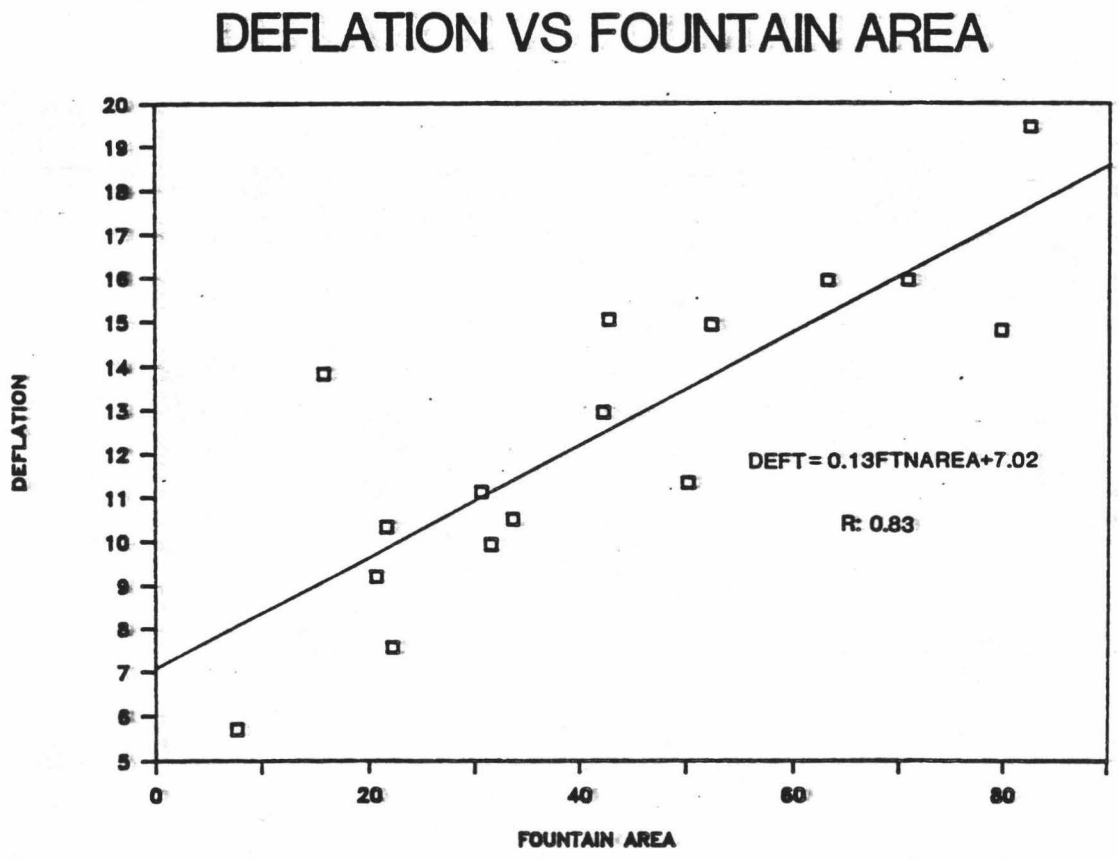

Figure 21. Summit deflation versus digitized fountain area.

Table 13. Tabulated digitized fountain heights with other system parameters.

EPISODE	FNT AREA	VOLUME	DEF	MAX FIN	MAX DEF	AVE FIN	AVE DEF	RATE
9	42.78	8.0	15.02	200	0.47	0.823	0.25	154
12	15.76	8.0	13.82	65	0.63	0.450	0.34	229
13	30.65	10.0	11.10	116	0.47	0.730	0.26	238
14	31.52	6.0	9.91	195	0.66	1.659	0.41	316
15	50.18	8.0	11.31	350	0.67	2.641	0.45	421
16	79.76	12.0	14.77	390	0.78	2.493	0.45	375
17	33.56	10.0	10.49	180	0.70	1.459	0.43	435
18	82.50	24.0	19.44	220	0.73	1.375	0.29	400
19	7.20	2.0	5.70	130	0.31	0.164	0.11	45
20	21.65	4.0	10.32	330	1.11	2.406	0.36	444
21	20.63	5.7	9.20	320	0.90	2.579	0.24	713
23	42.25	9.5	12.93	320	0.85	2.347	0.57	528
25	52.40	11.1	14.90	470	1.35	3.881	0.75	822
26	22.14	6.6	7.55	394	1.09	4.428	0.47	1320
28	63.24	12.5	15.91	420	1.30	4.361	0.84	855
29	70.86	13.0	15.92	460	1.26	4.429	0.76	813

here display a good correlation to average eruption rate (Figure 22). A similar correlation between average fountain heights and eruption rates was recognized earlier for the Mauna Ulu series of eruptions (Swanson et al.,1979). Furthermore, when Puu Oo maximum fountain height is plotted against maximum deflation rate a positive relationship is found (Figure 23) also suggesting that fountain heights are a partial measure of the deflation rate and hence eruption rate.

To examine further the dependence of fountain heights on deflation rate (and hence eruption rate) fountain height data for five eruptions were plotted in concert with summit deflation rates (Figures 24-28). Theses plots have the same horizontal scale but differ in vertical scale to allow an easier comparison between the two variables. The five episodes were chosen because they experienced a relatively large variation in fountain height and had a complete photographic and summit deflation record. In all five cases the summit tilt correlated in magnitude to the fountain height record as high deflation rates were associated with high fountains and low deflation rates were associated with low fountains. This correlation was amplified when the summit tilt record was shifted backwards (to the left) by 1.5 to 2.3 hours.

A leftward shift of the summit tilt record illustrates that the summit response followed the eruption site response (fountain production). In other words, the eruption could start with the summit only realizing it hours later. An increase in fountain height would signal an increase in deflation rate up to two hours

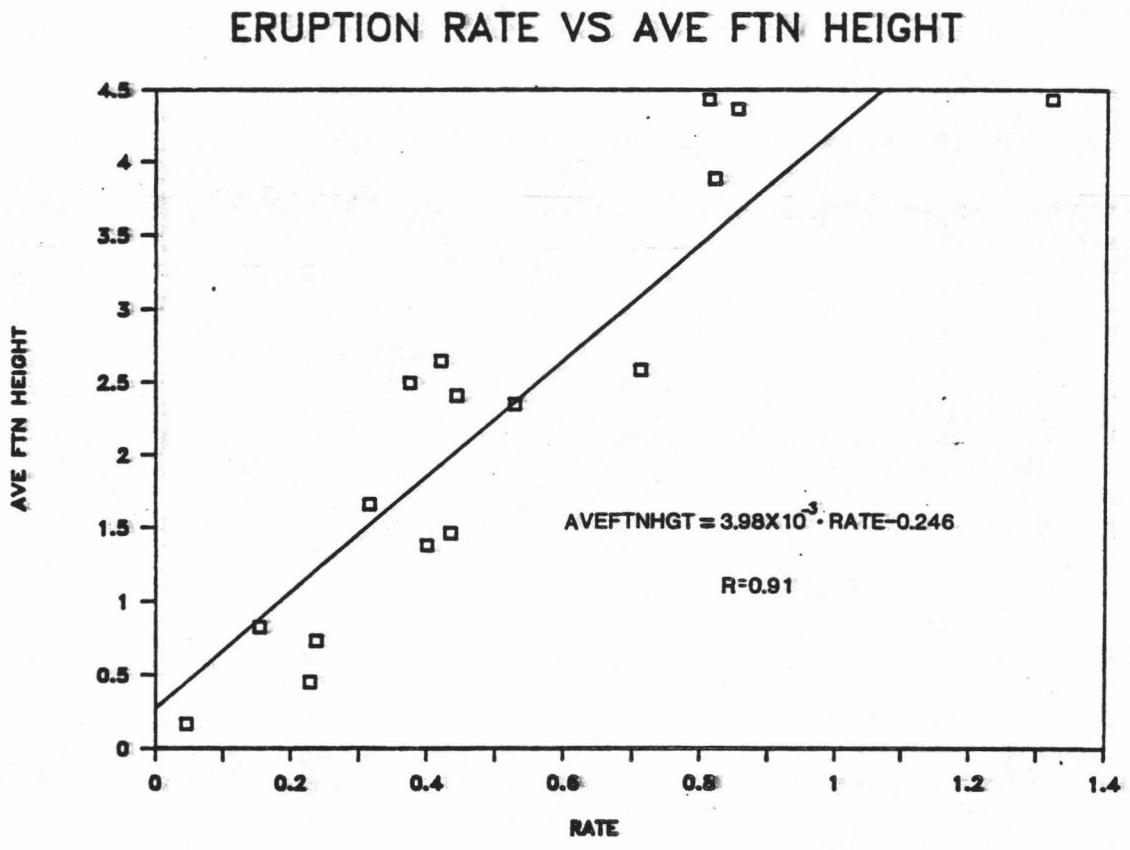

Figure 22. Average fountain height versus average eruption rate.

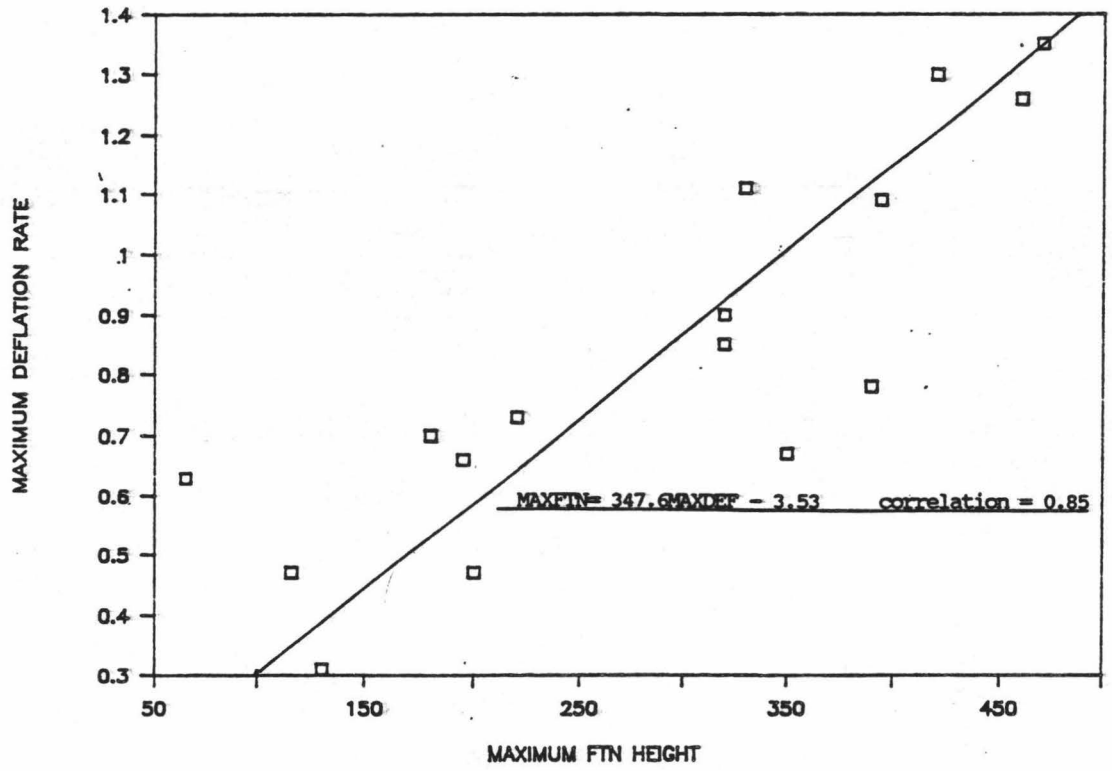

Figure 23. Maximum fountain height versus maximum deflation rate.

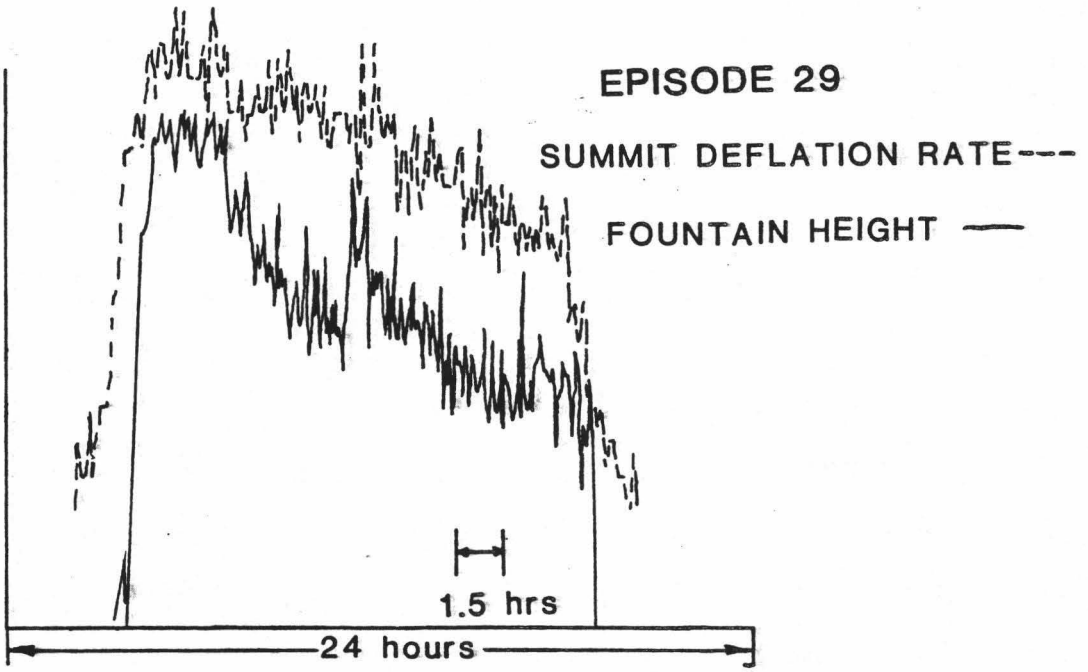

Figure 24. Summit deflation rate and Puu Oo fountain height for episode 29 plotted together. Summit deflation shifted to left by 1.5 hours.

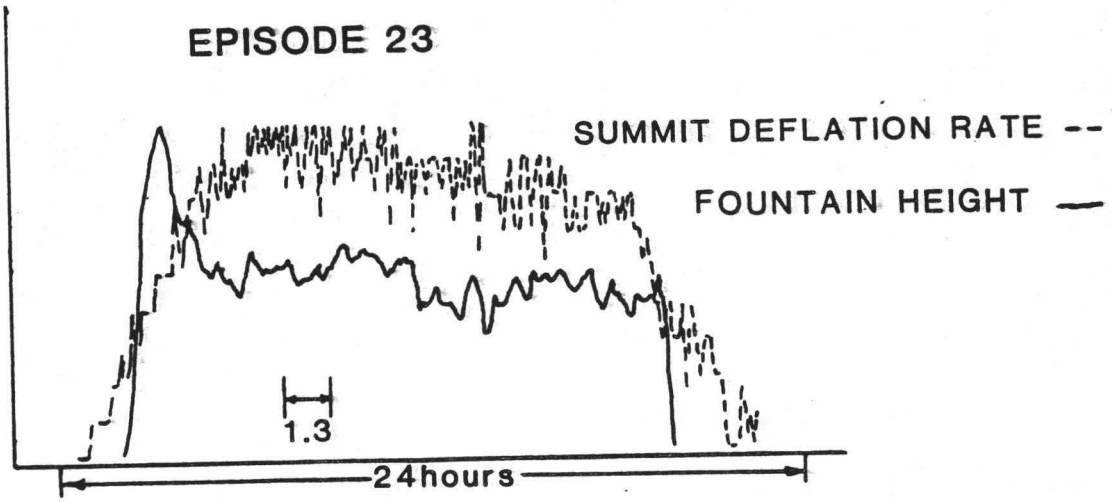

Figure 25. Summit deflation rate and Puu Oo fountain height for episode 23 plotted together. Summit deflation shifted to the left by 1.3 hours.

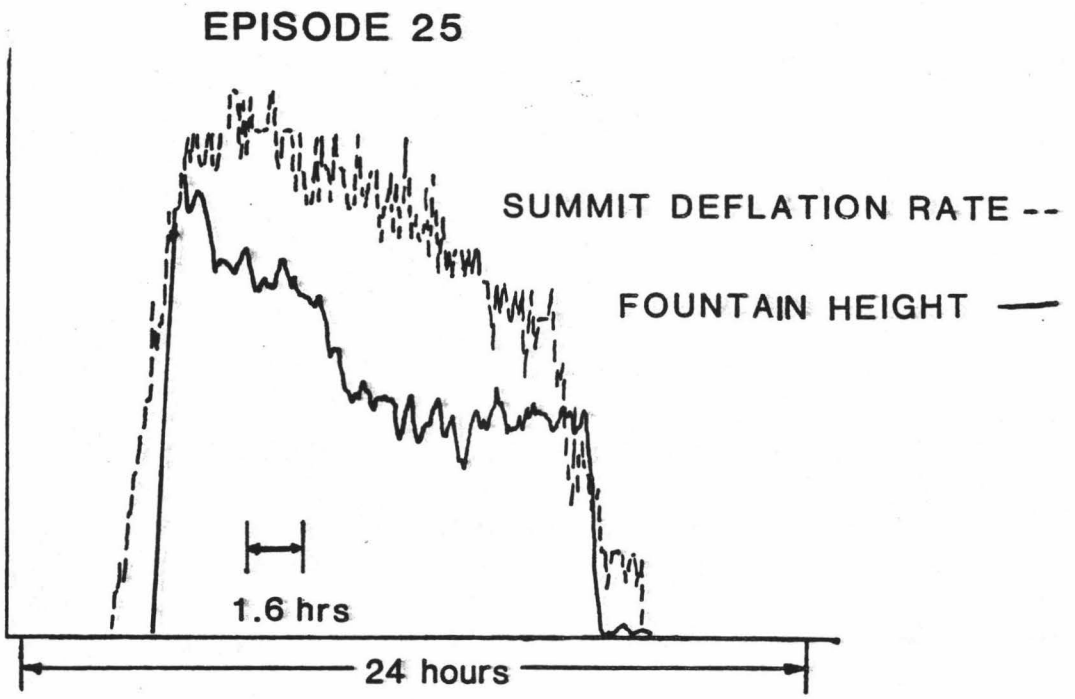

Figure 26. Summit deflation rate and Puu Oo fountain height for episode 25 plotted together. Summit deflation shifted to the left by 1.6 hours.

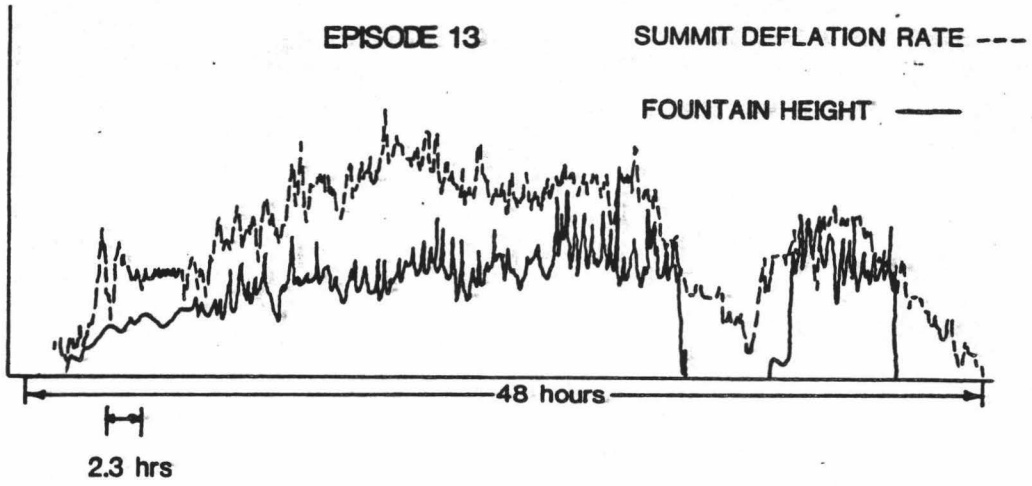

Figure 27. Summit deflation rate and Puu Oo fountain height for episode 13 plotted together. Summit deflation shifted to the left by 2.3 hours.

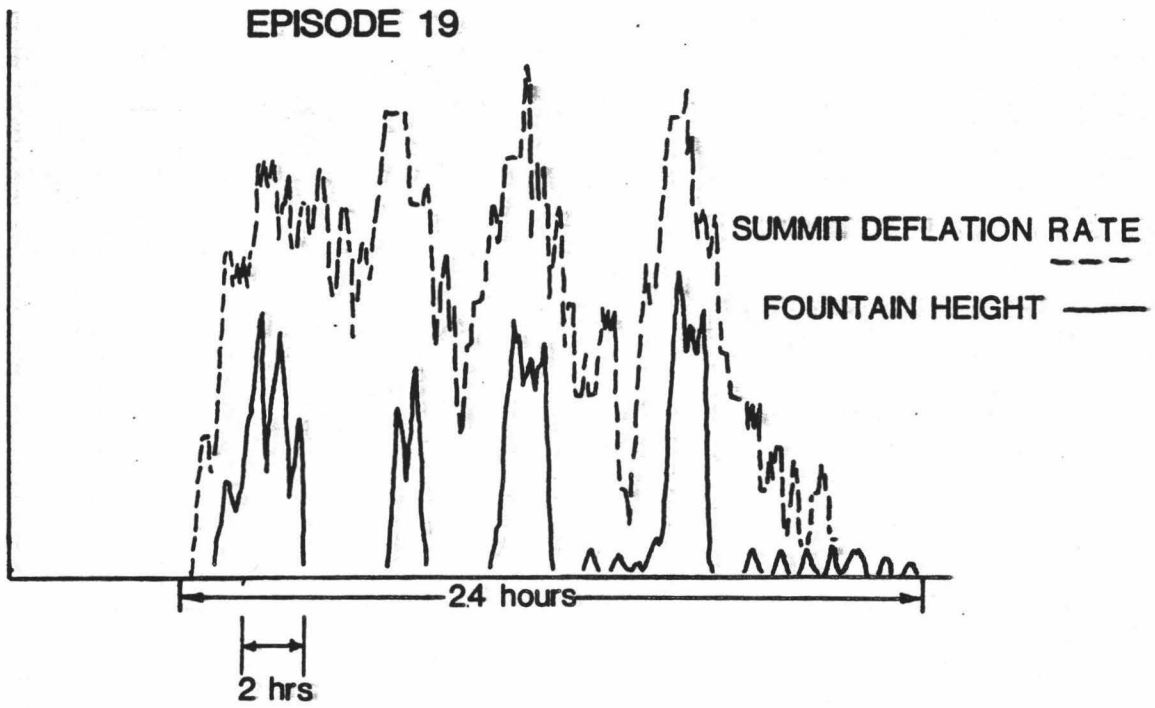

Figure 28. Summit deflation rate and Puu Oo fountain height for episode 19 plotted together. Summit deflation shifted to left by 2 hours.

later. This communication pulse between the eruption site and the summit travels at a rate of about 2.5 m/s. This may suggest something about edifice inertia and the strength of the volcano or may imply that it is a near vent phenomena that controls the timing of the eruptions and that the summit plays a lesser role. It is interesting to note that the first few episodes experienced the onset of summit deflation prior to the onset of eruptive activity.

DISCUSSION

The above discussion apparently conflicts with the notion that fountain heights are strongly influenced by gas content and only very slightly influenced by eruption rate. However, I contend that a magma erupting at a higher eruption rate travels at a higher velocity and can therefore carry with it more gas. In contrast, an eruption with a lower discharge rate travels slower and therefore "leaks" some of its gas before eruption leading to lower fountain heights.

Wilson and Head (in press a) have used fluid dynamic arguments on data from the series of Puu Oo eruptions to calculate the geometry and describe the dynamics of the dike system between the summit and the eruption site. They find that the dike system can be described as a blade with a thickness of about 1.8 meters and a dike height close to 3.0 km. The typical speed of magma transport was determined to be about 0.1 m/s during eruption. They used the relationship from Knudsen and Katz (1958), relating magma velocity to the pressure gradient dP/dx, where the driving pressure is

balanced by wall friction losses. From Knudsen and Katz:

$$D(dP/dx)=frhoU^2 \qquad (3.2)$$

where f is the fanning friction factor calculated from:

$$f=24/Re \qquad (3.3)$$

for laminar flow in a dike and Re, the Reynolds number, is calculated from:

$$Re=(2DUrho)/mu \qquad (3.4)$$

where mu is the magma viscosity and is assumed to be 200 Pa s. rho is the magma density and is assumed to be 2700 kg/m3. D is the average dike thickness in meters. Calculated Reynolds numbers indicate that the magma motion was laminar.

Decker et al., (1983) showed that the summit pressure could be estimated by the summit tilt, using a value of $8.5x10^4$ Pa per microradian of summit tilt. Therefore, on the average, the excess summit pressure prior to eruptions was close to 1.25 MPa. Assuming a dike length of about 18 km this indicates a pressure gradient of about 70 Pa/m. Wilson and Head assume the pressure at the eruption site to be negligble, however, this probably is an incorrect assumption. Ground deformation measurements discussed in following chapter show that pressures at the eruption site are about one-third to one-half of the summit pressures. Therefore the pressure gradient should be halved and the resulting magma velocity is reduced to about 0.07 m/s (compared to 0.1 m/s). Also, they used an average mass flux rate of $4.3x10^5$ kg/s. This rate is an accurate estimate of the average eruption rate over the entire series, but the rate varied by a factor of ten during the series of eruptions.

Mass flux is directly porportional to velocity, assuming the dike geometry remains the same, the velocity should vary accordingly. Therefore I use values of about 0.05 to 0.15 m/s as the high and low extremes of magma velocities.

Wilson and Head also show that most of the magma resides at depths greater than 1 km during its lateral movement toward the eruption site, therefore exsolving only small amounts (less than 1 wt %) of water and sulfur dioxide. Most of the degassing occurs near the eruption site. Figure 29 shows the simplest case in which the dike connecting the summit reservoir to the eruption site forms a straight line and is inclined at an angle of about 5 degrees. The slope of the volcano is about 1.4 degrees, therefore the dike, in this case, meets with the eruption site at about 6.4 degrees (note that the figure is not to scale). The geometry of this conduit system, with respect to its slope approaching the eruption site, is probably unlikely. In the next chapter, previous seismic studies are used to examine the geometry of the rift zone conduit system and recent ground deformation studies are used to better define the near-vent geometry of the conduit system. However, this simplified geometry presented in Figure 29 can be assumed for the time being to illustrate the effects of degassing magma at shallow levels.

Of the three abundant gas phases present in magma (CO_2, SO_2 and H_2O) H_2O is the most abundant and therefore most important gaseous phase. H_2O doesn't begin to exsolve until the shallow depth of about 300 meters (Wilson and Head, 1981), therefore the exsolution of water begins about 2.7 km uprift of the eruption site according

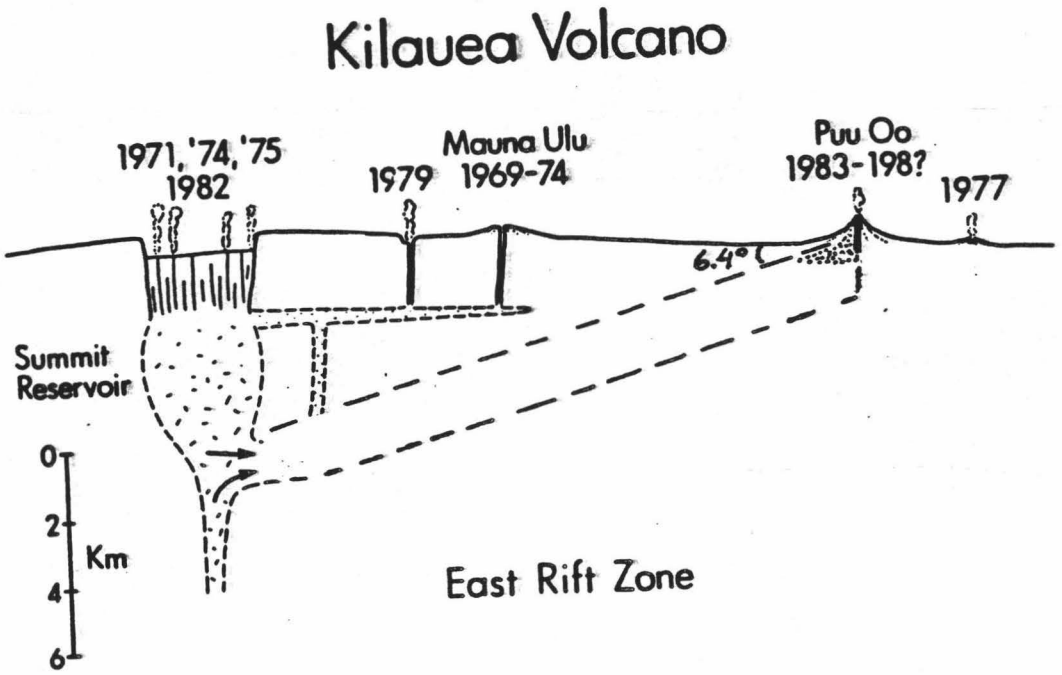

Figure 29. Relatively unrealistic model of the most simple possible conduit system conecting the summit reservoir and eruption site. Magma begins to exsolve gas near Puu Oo. Not to scale.

to Figure 29. The time that the magma takes to pass through this section of the dike will determine the eventual gas content of the erupting magma, therefore affecting the fountain dynamics. It is easy to see that the longer the magma resides in this shallow section the more degassed the magma will become. Magma travelling at a velocity of about 0.05 m/s will take about 15 hours to cover the 2.67 km, while magma travelling at a velocity of 0.15 m/s will take about 5 hours.

Sparks (1978) has shown that the rise of gas bubbles in basaltic magma is largely controlled by bubble size, magma viscosity and magma density. Bubble growth is assumed to be by pressure release only. Simple calculations from Sparks (1978) using Boyle's Law, a magma viscosity of 200 pa and magma density of 2700 kg/m^3 were used. Bubble growth is also possible by diffusion, however, this effect is considered to be negligible as the transit time between nucleation and escape (via eruption or leakage) is small. Surface tension is also considered to be negligible. Average rise rates of bubbles were predicted to be about 0.10 m/s for the top 300 meters of the conduit system. This rise rate is in good agreement with recent studies done by Vergniolle and Jaupart (1986) who examined separated two-phase flow in basaltic magma. This velocity is also similar to the estimated rise velocity of magma through the conduit of 0.1 m/s (Greenland, et al., in press b; and Wilson and Head, in press a).

The rise of gas bubbles is a complex process and difficult to evaluate. If our simplifications and assumptions are reasonable

then we can begin to explain some of the differences between some of the Puu Oo episodes. A bubble rise-rate of 0.1 m/s will result in bubbles rising faster than the magma for those episodes with lower discharge rates (lower magma transport rates of about 0.05 m/s-see previous reasoning). This will result in leakage of gas and hence a more sluggish eruptive style. Conversely, those episodes with the higher discharge rates and therefore higher magma transport velocities of about 0.15 m/s (see previous reasoning) will prevent rising of bubbles through the melt. The retention of a larger portion of the gas phase will cause the erupting melt to be more energetic producing higher fountains.

The previous paragraphs suggests that one very important variable in determining the eruptive style is eruption rate and therefore transport velocity of the magma. An increase in magma velocity has been assumed to increase with the progression of the series of episodes. This probably was a result of streamlining the rift zone conduit system with repetitive "intrusions". The exsolution of the gas phase in the magma is also important. Exsolution of H2O mostly occurs in a shallow portion of the conduit. Figure 29 illustrates a model of the shallow portion of the rift zone. Seismic evidence (Klein et al., 1987) show that the conduit leaving the summit reservoir is nearly paralellel to the surface travelling at a depth of about 3 kilometers. Therefore, a shallow near vent reservoir may be used to explain the degassing process.

A near vent reservoir may also be used to explain the time-lag

between the eruption site behavior and summit response. The time-lag discussed earlier suggests that the onset of the eruption is in fact controlled, in part, by a near-vent phenomenon. The following chapter uses ground deformation data to revise Figure 29 and constrain the geometry of the postulated near vent reservoir.

CHAPTER IV

EAST RIFT ZONE DEFORMATION

GEOLOGIC SETTING

Kilauea volcano, located on the southeast side of the island of Hawaii, is buttressed on the northwest by the larger Mauna Loa volcano and open to the Pacific ocean on the southeast. Two rift zones, the southwest rift zone (SWRZ) and the east rift zone (ERZ), extend outward from the summit caldera (Figure 1). Seismic and surface-deformation data have suggested that magma of mantle origin accumulates at a shallow (2-6 km) depth beneath the summit region and may be discharged into the rift zones as long, bladed dikes (Fiske and Kinoshita, 1969; Koyanagi et al., 1976; Ryan and others, 1983; and Klein and others 1987).

PREVIOUS GROUND DEFORMATION STUDIES

Many earlier investigators have analyzed surface deformation patterns associated with intrusions and eruptions of Kilauea volcano to develop an understanding of the magma storage and conduit system of the volcano (Mogi, 1958; Eaton, 1962; Fiske and Kinoshita, 1969; Jackson et al., 1975; Dietrich and Decker, 1975; Swanson et al., 1976; Duffield et al., 1982; Dvorak et al., 1983; Dzurisn et al., 1984; Ryan et al., 1983; Pollard et al., 1983; and Okamura et al., in press). These studies showed that gradual inflation of the summit region overlying the magma reservoir occurs during repose

periods reflecting a near-continuous supply of magma from the upper mantle. A summit eruption may occur or a magma intrusion into one of Kilauea's two rift zones may occur, when sufficient pressure has accumulated. Rift-intruded magma may or may not reach the surface (Klein et al., 1987). If intruded magma does reach the surface, a linear curtain-of-fire is characteristic of the initial eruption style. The eruption will eventually become localized to a single eruptive locus.

DESCRIPTION OF HAWAIIAN RIFT ZONES

Hawaiian rift zones are considered to be shallow-level features whose locations are dictated by gravitational stresses within an edifice, and by the shape and positions of preexisting shields (Fiske and Jackson, 1972). The magma in the ERZ has a depth of 2-6 kilometers and extends 120 kilometers from the summit to a point about 70 kilometers off Cape Kumukahi (Moore, 1971).

Intrusion of magma is generally an intermittent, pressure-driven process resulting in magma moving at large volume rates and accompanied by shallow seismic swarms due to sudden rock fracturing. However, Dzurisin et al., (1984) have shown that near-continuous leakage of magma into the rift also occurs. These slower intrusions of rates less than 10 m^3/s are weakly seismic to aseismic in nature, implying that the rift is open or nearly open and fracturing is not required. However, earthquakes may be produced at the terminus of the intrusion where the magma accumulates. Summit tilt may rise, fall or remain relatively flat during these slow leakages into the rift zone, but the tilt rate is

never more than a few microradians per day. Epp et al., (1983) have shown that the slower intrusion rates of less than 10 m^3/s are more common in the upper 20-30 km of the ERZ while the larger intrusion rates of 100 to 1,000 m^3/s accompanied by shallow seismic swarms, are more common in the lower ERZ.

THE JANUARY 1, 1983 ERZ DIKE INTRUSION AND THE EVENTS LEADING UP TO THE INTRUSION

The ERZ seismic swarm of January 1, 1983, associated with an intrusion of a dike, lead to a long-standing eruption that is still in progress at the time of this writing (July, 1988). Rift zone earthquakes accompanied only the early phases of the January, 1983 eruption. By March, the successive eruptions were localized at the Puu Oo vent area. No additional seismicity or new dikes were created (Koyanagi et al., in press).

The January seismicity extended 17 km from Makaopuhi to just east of Kalalua and earthquakes were centered along the ERZ at a depth of about 2.5 to 3.5 km (Koyanagi et al., 1987, and Klein et al., 1987). Eruptive vents were confined to an 8 km section from Napau Crater to Puu Kahaualea (Wolfe et al., 1987, and Wolfe et al., in press). Seismic and eruptive activity generally moved downrift, but in a complex pattern, eventually stabilizing at the Puu Oo vent area . The complex pattern of activity suggests a complicated interaction of multiple intrusions in the conduit system from Makaopuhi to the Puu Kamoamoa area.

Okamura et al., (in press) have examined the ground deformation leading up to and associated with the emplacement of the January,

1983 intrusion which initiated the long-standing Puu Oo erption. They find evidence that the ERZ experienced a series of cyclic slow intrusions from Nov 1978-July 1979 and May-October 1980. They have shown the presence of a large east rift zone magma storage body extending from Napau Crater to beyond Kalalua. As magma was discharged downrift, the summit tilt oscillated, coinciding with tilt peaks and shallow seismic swarms near Puu Kamoamoa. Following the emplacement of the January 1983 dike, Okamura et al., used tilt data with a simple three-dimensional elastic model of a thin, rectangular dike to model the emplacement of the dike at the start of the 1983 Puu Oo eruption. Their model dike is estimated to be 15 km long, 2.5 km high, and 3.5 m wide.

Following the emplacement of the dike and the subsequent eruption in early January 1983, the ERZ continued to be active. Eruptions became centralized at the Puu Oo eruption site by episode 4 and continued through episode 48 (see previous chapters). Kilauea's summit indicated a systematic inflation prior to each episode that was followed by a rapid deflation during each episode suggesting a close-to-direct link between the two 'ends of the pipe' nearly 20 kilometers apart.

I will concentrate on the low-volume-rate aseismic intrusion (sometimes refered to as leakage) that occurs in the upper part of the ERZ during repose periods of the recent series of episodic Puu Oo eruptions and examine the resulting horizontal ground deformation at two locations on the rift zone: one at the eruption site and the other 9 kilometers uprift from the eruption site. I will use the

ground deformation measurements in an attempt to model the geometry and pressures of the near-vent storage system.

One of the most comprehensive studies of dike propagation is by Pollard et al., 1983. They used cross-sectional displacement and strain curves, derived from geometric models of large planar sheets, generated by pressurizing a fluid filled crack. This chapter presents horizontal surface deformation data from Kilauea's ERZ and is compared to predicted cross-sectional deformation curves.

To evaluate the character of deformation associated with the gradual intrusion of magma into the rift zone during the repose periods of the recent series of eruptions, two networks of segmented, horizontal deformation lines, crossing and approximately normal to Kilauea's ERZ, were installed and regularly reoccupied between June, 1984 and February, 1986 (Figure 30). The first network installed was located 700 meters uprift from the active Puu Oo vent while the second was located uprift near Mauna Ulu. Frequent (daily to monthly) measurements were made with an electronic distance meter (EDM) at both the near vent and the upper-east-rift deformation network near Mauna Ulu.

NETWORK DESCRIPTIONS

KMM INSTRUMENT SITES

The near-vent instrument station (KMM) was positioned on a topographic high point (at Puu Kamoamoa, a pre-historic volcanic vent) near the center of a 3.3 kilometer-long segmented deformation

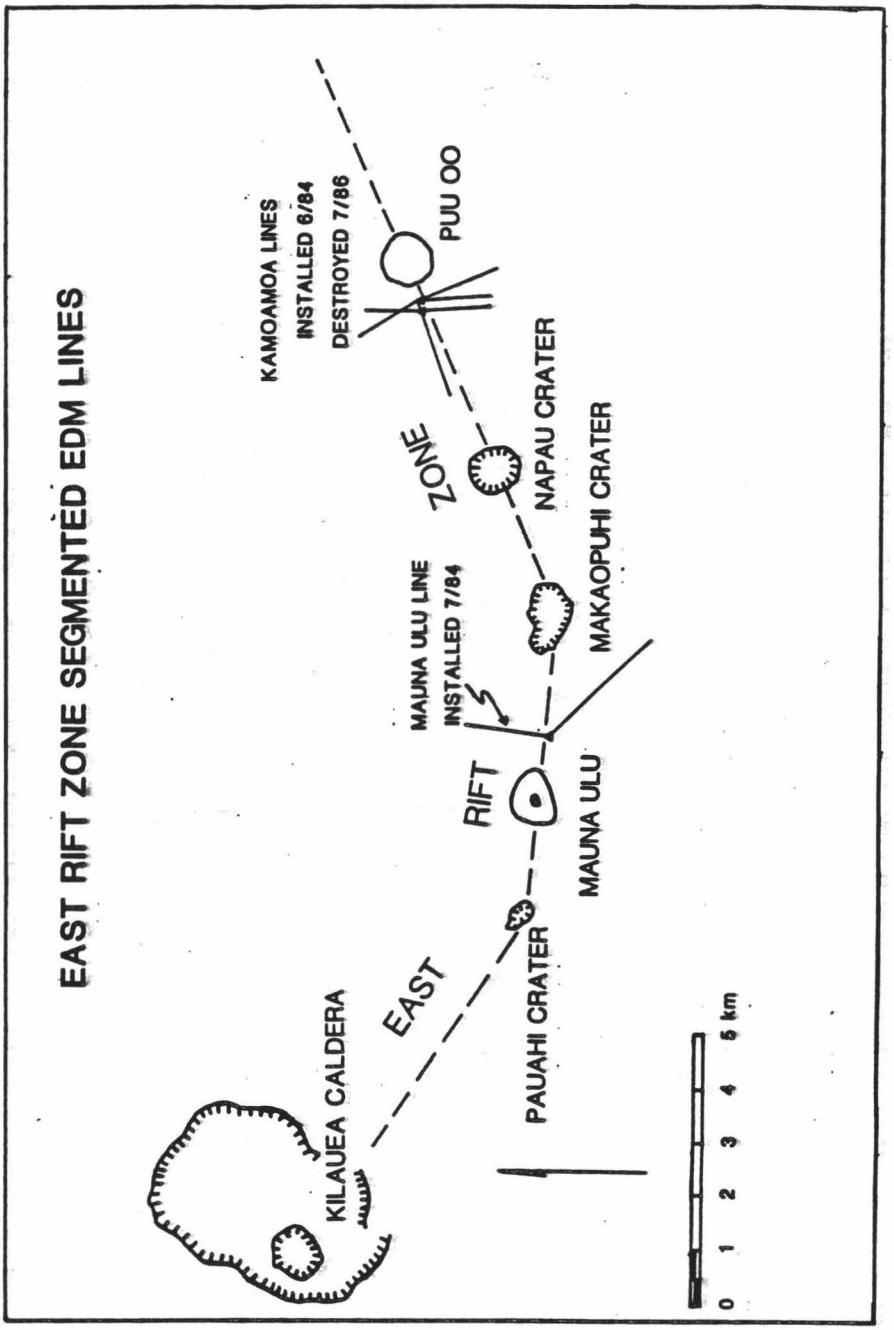

Figure 30. Location of segmented, horizontal deformation lines on Kilauea's east rift zone.

line (Figure 31). Extending 1.5 kilometers to the northwest from KMM the line was segmented with as many as 7 targets. Extending southeast from KMM, the line was 1.8 kilometers long and segmented with up to 6 targets. The KMM line had a continuous record for episodes 22 through 29, however, poor weather and the destruction of some southeast targets caused poor documentation of the ground deformation patterns for the repose period prior to episode 28. The best documented deformation patterns during repose periods prior to eruptions are those that had at least 4 measurements made on a full network of targets. Based on these criteria, the best documented patterns of deformation prior to eruptions include those prior to episodes 23, 24, 25, 26, and 29. By the end of episode 29, the growth of the Puu Oo cone necessitated a move of the southeast line to a shorter and more southerly directed line segmented with 4 targets (Figure 31). This newly adjusted line lasted until episode 32 and was most successful in documenting the deformation patterns during the repose periods prior to episodes 30 and 31.

A further increase in the size of the Puu Oo cone required a move of the instrument site following episode 32, to KMMS, offering a better view of the recently altered south line (Figure 31). A fissure eruption during episode 35 destroyed the southern line and blanketed most of Kamoamoa with shelly pahoehoe lava, requiring yet another new instrument site (KMMW) and deformation line to be occupied. The best documented deformation measured from the KMMS instrument site was for the fissure opening of episode 35.

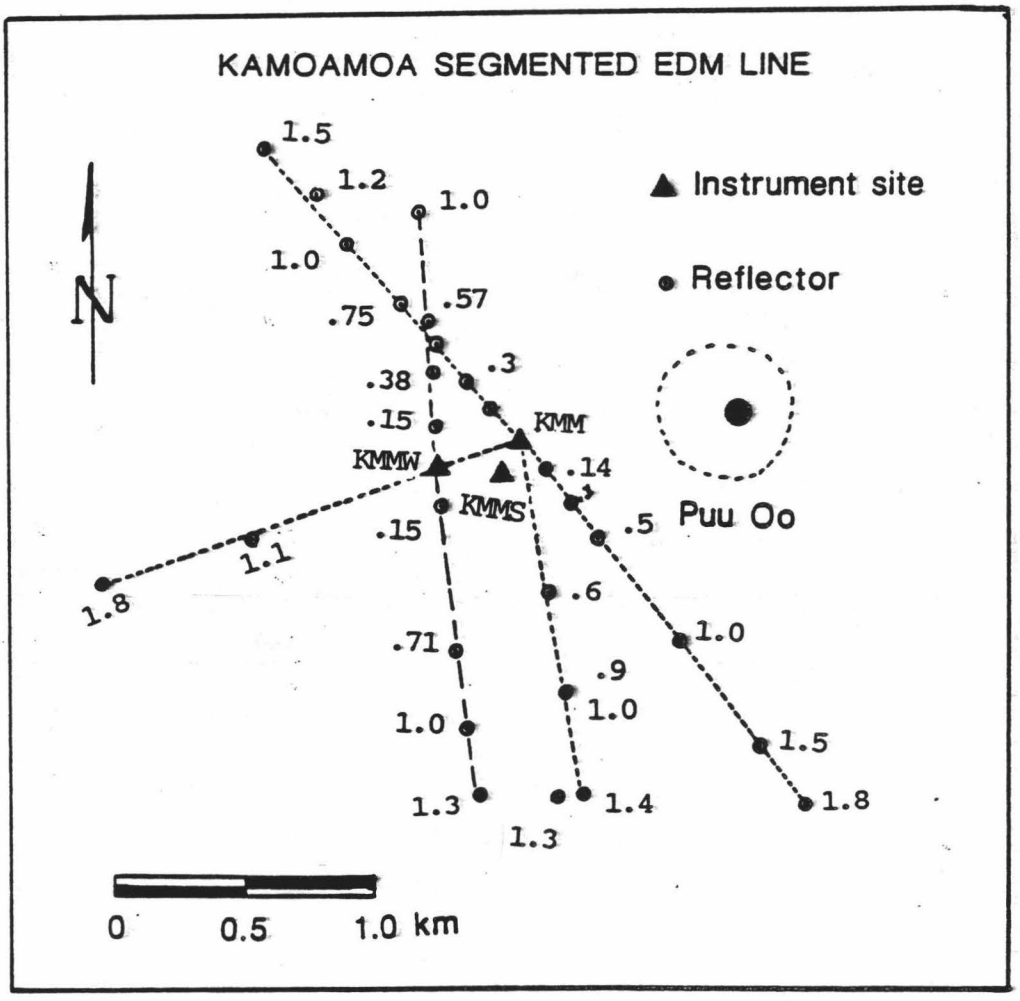

Figure 31. Near-vent segmented deformation lines.

The new KMMW instrument site, about 300 meters west of the original instrument site, was near the center of a 2.3 kilometer-long segmented line and was used for episodes 37-47 (Figure 31). The northern limb was 1.0 kilometer long and segmented with 4 targets, while the southern limb was 1.3 kilometers long also segmented with 4 targets. The best documented patterns of deformation were for repose periods prior to episodes 39, 40 and 42.

From this point on, the three cross-rift lines will be collectively referred to as the KMM lines. More than 30 targets have been used on the KMM lines. A list of the targets used, their location and the dates used can be found in Table 14. Rapid replacements of destroyed or obscured targets and the movement of instrument sites offered a near continuous record of ground deformation near the eruption site from episodes 22 through 42. Infrequent measurements made after episode 42 made it impossible to identify a deformation trend corresponding to individual eruptions (see following results section).

Table 14. A list of the instrument stations, their targets, their locations and the episodes they were used.

STATION/TARGET	LATITUDE	LONGITUDE	DATES USED	EPISODES
KAMOAMOA	19.3909	155.1149	06/26/84-05/20/85	21-32
1.5NW	19.4009	155.1242	06/26/84-05/20/85	21-32
1.0NW	19.3975	155.1213	06/26/84-05/20/85	21-32
.75NW	19.3958	155.1195	07/19/84-05/20/85	23-32
.5NW	19.3942	155.1180	06/26/84-05/20/85	21-32
.3NW	19.3929	155.1166	07/19/84-04/17/85	23-32
.15NW	19.3918	155.1158	07/19/84-01/31/85	23-30
.14SE	19.3899	155.1141	08/16/84-11/01/84	25-26
.3SE	19.3891	155.1137	07/19/84-11/01/84	23-26
.5SE	19.3872	155.1122	06/26/84-07/26/84	21-23
.6SE	19.3855	155.1139	01/10/85-04/17/85	30-32
1.0SE	19.3837	155.1091	06/26/84-01/03/84	21-29
1.0SE	19.3819	155.1133	01/10/85-04/17/85	30-32
1.4SE	19.3784	155.1125	01/10/85-03/12/85	30-31
1.5SE	19.3800	155.1062	06/26/84-01/03/85	21-29
1.8SE	19.3780	155.1044	06/26/84-01/03/85	21-29
KMMS	19.3896	155.1200	05/20/85-08/19/85	33-35
1.5NW	19.4009	155.1242	05/20/85-08/19/85	33-35
1.2NW	19.3986	155.1220	05/20/85-08/19/85	33-35
1.0NW	19.3975	155.1213	05/20/85-08/19/85	33-35
.75NW	19.3957	155.1195	05/20/85-08/19/85	33-35
.6SE	19.3855	155.1139	01/10/85-04/17/85	30-32
.9SE	19.3814	155.1129	05/20/85-07/24/85	33-35
1.3SE	19.3794	155.1140	05/20/85-08/01/85	33-35
1.5SE	19.3780	155.1062	05/20/85-07/24/85	33-35
KMMW	19.3897	155.1180	08/19/85-06/02/86	36-46
.15S	19.3883	155.1178	09/02/85-06/02/86	37-46
.71S	19.3833	155.1174	08/19/85-06/02/86	36-46
1.0S	19.3812	155.1170	08/19/85-06/02/86	36-46
1.3S	19.3783	155.1163	08/19/85-05/08/86	37-45
.15N	19.3912	155.1181	08/28/85-06/02/86	37-46
.38N	NA	NA	08/28/85-06/26/86	37-47
.57N	19.3975	155.1184	08/28/85-06/02/86	37-46
1.0N	19.3988	155.1188	08/28/85-06/02/86	37-46

MAUNA ULU INSTRUMENT SITE

The Mauna Ulu deformation network was installed 9 kilometers uprift from Puu Oo, in July, 1984 (Figure 30). This line is 4.2 kilometers long with 4 targets to the southeast and 3 to the north. This line has an uninterrupted record since July 16, 1984, however, the frequency of measurements was somewhat less than the KMM lines and was curtailed after episode 40.

INSTRUMENTATION

The measuring device used was a Hewlett Packard 3808-A medium-range infrared distance meter. This electronic distance meter (EDM) is aimed at a reflector station and sends out a beam with a fixed wave-length. The difference in phase between the beam going out and returning is converted to a distance between the instrument and reflector. Each digitally observed reading, having the precision of one part per million ($\pm$ 1 mm per kilometer), is the average of 70 internal measurements. Five to ten readings were taken for each target to increase the precision.

Barometric pressures and temperatures were measured at both target and instrument to correct for refraction errors. The targets used were six sided prismed glass reflectors. They were bolted onto a one-and-one-half meter iron bar that was hammered approximately one meter into the surface.

The data were reduced at the Hawaiian Volcano Observatory using a program adapted (by Arnold Okamura) for EDM purposes and are presented as changes of Clark Arc Spheroid distances in this thesis.

RESULTS OF EDM MEASUREMENTS

Results indicate that horizontal changes have been small (less than 50 millimeters) but systematic trends exist on the KMM, KMMS and KMMW lines and correlate with eruptive activity. Line-length changes suggest extensional movement of many of the targets during the repose periods, and following each eruptive episode, a nearly equal contraction was measured (Figures 32 and 33). Presumably, the deformation patterns result from an elastic response to the addition and removal of magma.

ERROR CONSIDERATIONS

Since the line-length changes are small, possible sources of error such as instrument set-up, local site instability, incorrect atmospheric assumptions due to a change in air temperature and the precision of the instrument, are considered. As for set-up errors, an automatic error of $\pm$ 2 mm is assumed, but since the instrument site is located near the center of the deformation line and adding changes on either side of the instrument would cancel any set-up error. Changes between targets on the same side of the instrument site will also be free of any instrument set-up error and therefore a 2 mm error is probably an overestimate. Reflectors were regularly checked for stabilty and corrosion. It is highly unlikely that even unstable reflectors would have wandered in the patterns (shown in Figs. 32 and 33).

Another possible source of error could be due to incorrect atmospheric assumptions. Temperatures were measured at both the

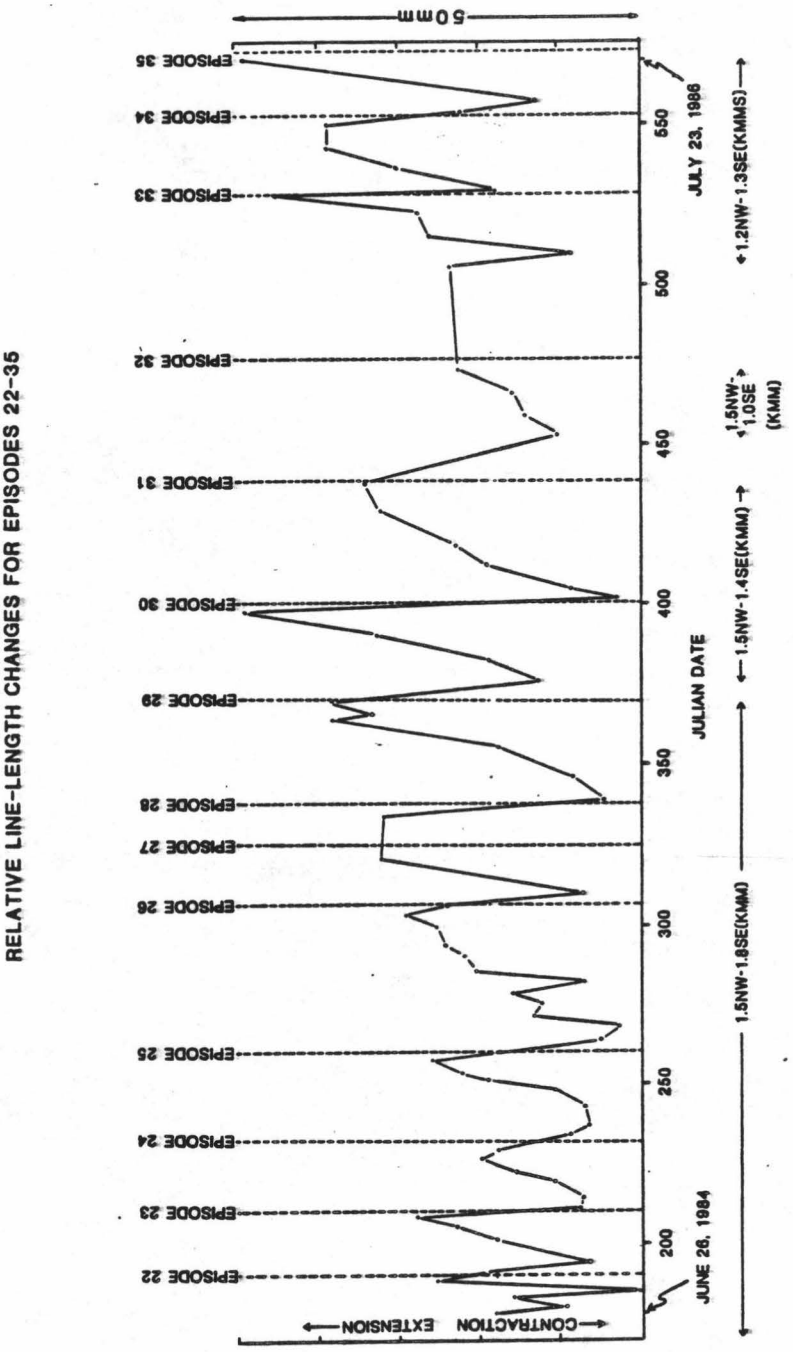

Figure 32. Overall line-length changes between targets at extreme ends of the line for episodes 22-35.

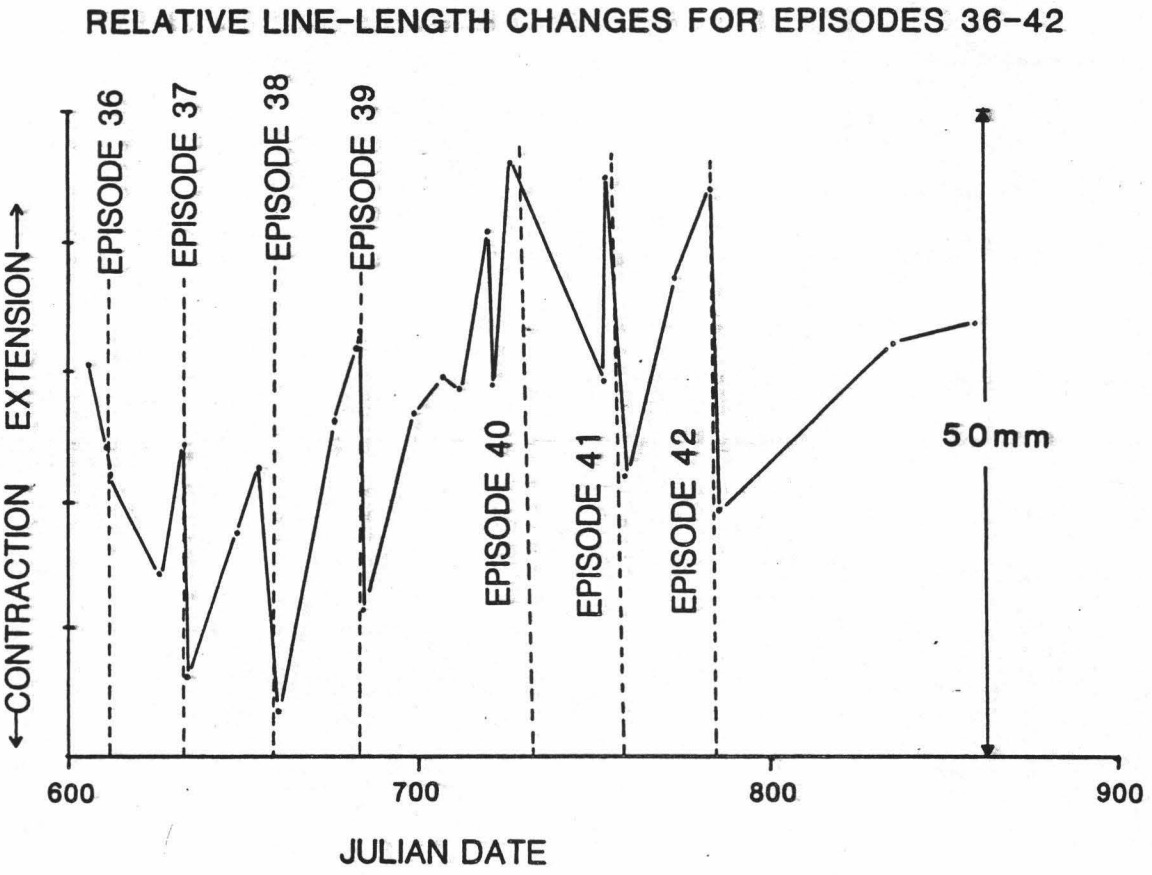

Figure 33. Overall line-length changes between targets at extreme ends of the line for episodes 36-42.

instrument and reflector at the beginning of the installation of the line and the differences were assumed to remain the same for all subsequent measurements. However, this assumption is probably not valid when the line of sight of the EDM is directed over a hot, young lava flow. There are three reasons why I believe that this error is small and can be nearly neglected. First, there were only a couple of times when the EDM had to view directly over a hot flow and this was on the SE line only: the view to the NW was never over a new lava flow. Second, although it was necessary to occasionally shoot the EDM over a hot flow, the instrument site was located on a local topographic high and therefore the shot was directed through only a small portion of the heat shimmer. Third, the line length is changed only 1 mm per km for every change in 1^{o} C. The distances to most of the targets were less than 1 km and even the longest were only a few hundred meters longer than 1 km. I am therefore using an estimated error bar of 4 mm which includes the built-in $\pm$ 1 mm per kilometer, 2 mm for a set-up error and 1 mm for atmospheric error.

Pollard et al., (1983) have convincingly shown that the intrusion of a rectangular dike results in both vertical and horizontal deformation. Elastic displacements elevate (extend) the flanks relative to a central depression forming a ridge-trough-ridge displacement profile, where the trough is centered near the dike. Symmetry of the ridge-trough-ridge profile is strongly dependent on the dip of the dike: as the dip of the dike decreases the displacements on the foot side decrease and those on the hanging side increase. They have shown that a change in dip from 90^{o} to

80^{o} changes the ratio of ridge heights from 1 to 0.4. They have also illustrated that the location of the trough is dependent on the dip of the dike.

A ridge-trough-ridge structure of the horizontal strain profiles along the three KMM lines (Figure 34) suggests application to the buried, steeply dipping rectangular dike model. I have obtained a computer program (DIS3D) from Paul Delaney of the Hawaiian Volcano Observatory and have used it exclusively to model the deformation at the eruption site as due to the growth of a previously emplaced steeply dipping, rectangular dike.

THE DIS3D PROGRAM

The original DIS3D is an unpublished geodetic program written by Scott Dunbar in 1984 for the USGS. The program calculates displacements, tilts, strains and stresses due to strike-slip and/or dip slip motion and due to an opening motion across a dislocation surface. The rectangular dislocation planes are located in a linear elastic half space. The half-space is idealized as an isotropic, homogeneous material with a specified Poisson's ratio and shear modulus. DIS3D is a 3 dimensional dislocation program that calculates displacements and other elastic fields at specified observation points. DIS3D can also calculate changes in line length between any two observation points and changes in angles between any three observation points. I have employed the program to calculate line-length changes between observation points due to a dilational

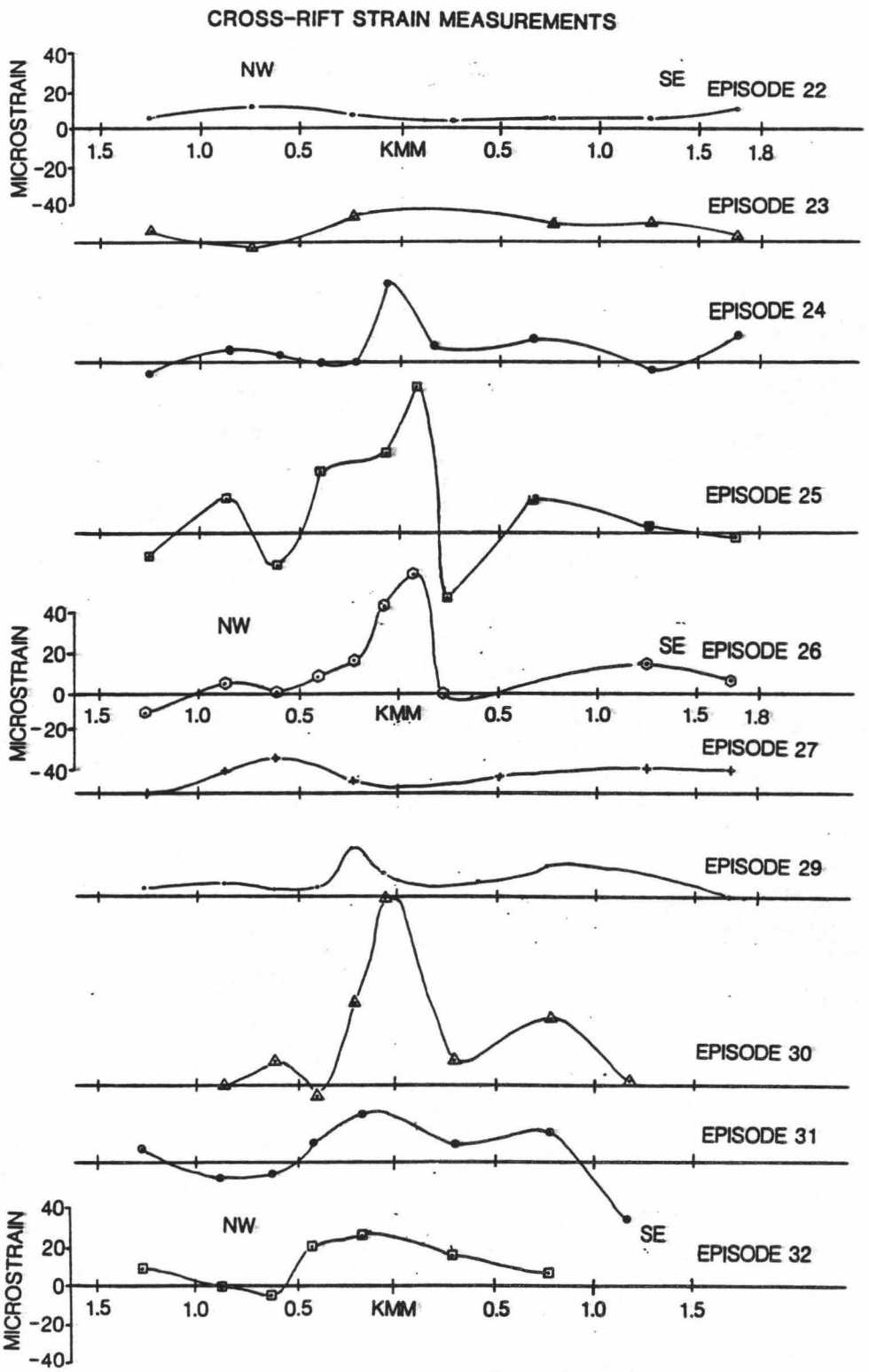

Figure 34. Horizontal strain profiles for near-vent deformation line.

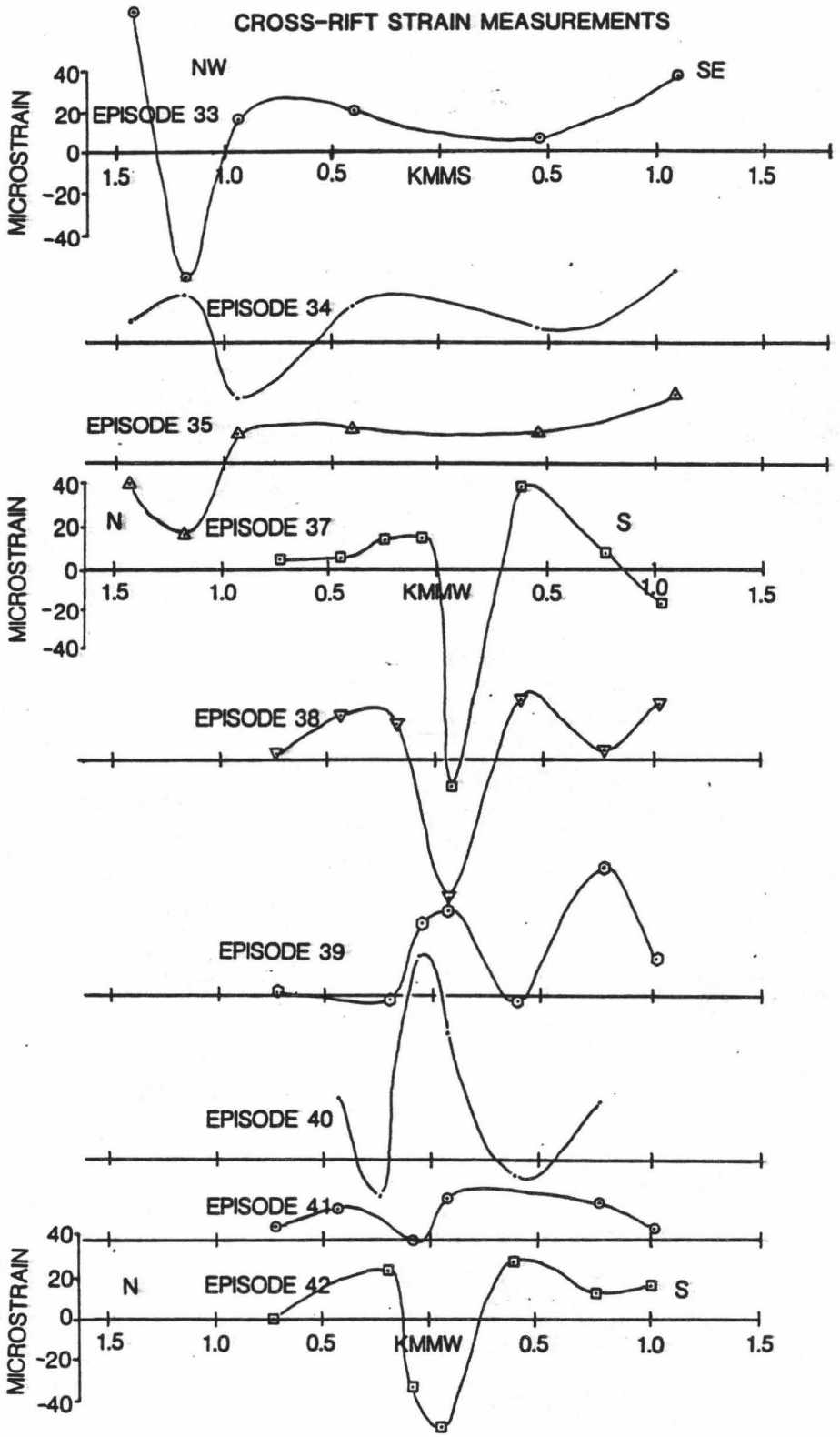

Figure 34 continued. Horizontal strain profiles for near-vent deformation line.

opening across a dislocation surface to model the expansion of a dike. The equations for the elastic fields are from Yang and Davis (1986) who integrated Volterra's formula using Mindlin's (1936) point force solution for an elastic half space (commonly referenced as Maruyama, 1964).

The DIS3D program was modified by Erickson in 1986 to handle singularity problems. She also added subroutines for non-horizontal observation planes and wrote the user's manual reflecting the changes and additions for her Master's Thesis (Erickson, 1986). I used this user's manual to guide me through the necessary steps to run the program and obtain the output.

To run the program DIS3D, an input file is passed to the program and the resulting output is directed to an output file. The input file specifies the coordinates of the points, relative to the center of the dislocation plane, at which the elastic fields are to be calculated. In this case these coordinates correspond to the location of the reflector targets.

The input file also specifies the parameters needed to describe each dislocation plane in the model. Those used to describe the dislocation plane (a dike in this case) are; H, the dike half-length; ϕ, the strike relative to a local coordinate system; θ, the dip relative to the horizontal free surface; DU and DL, the distance measured down-dip from the free surface to the upper and lower edges of the rectangular dike plane respectively; and op, the amount of opening across the dislocation surface.

The user must specify which elastic fields are to be calculated in the input file. The output file lists the elastic fields values used and predicts line-length changes for each observation point using the defined parameters just mentioned. After a comparison of observed and predicted line-length changes is made, the parameters are adjusted so as to improve the match. Figure 35 is a schematic diagram illustrating the idealized half-space.

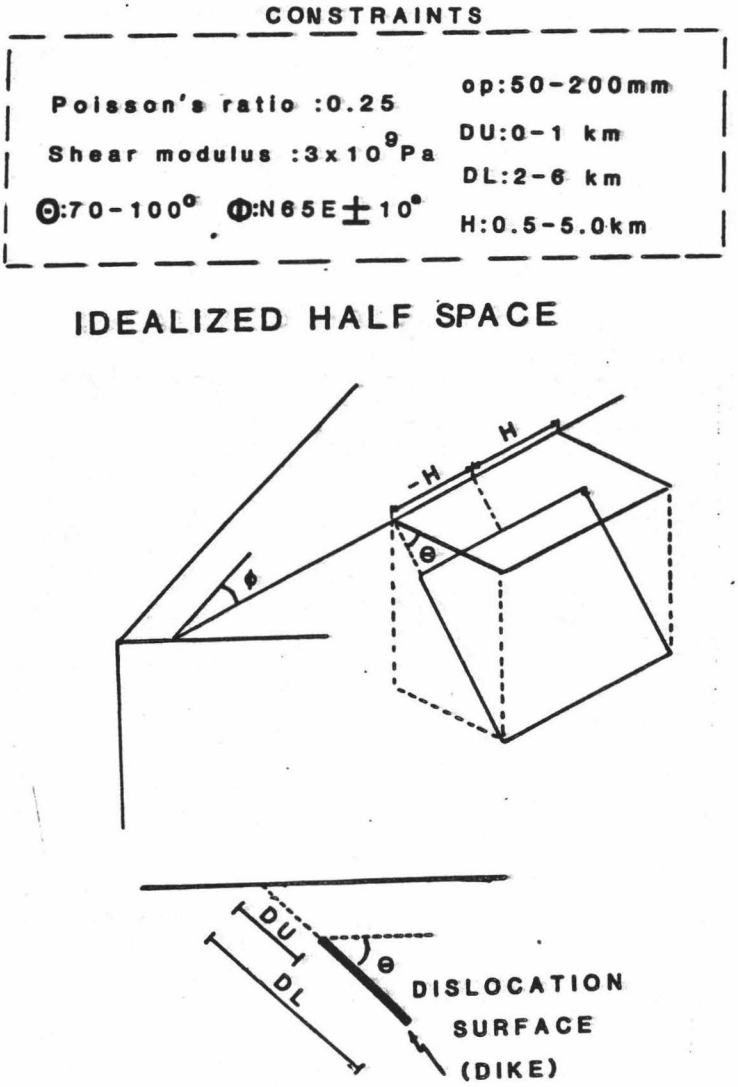

Figure 35. Schematic diagram illustrating the idealized half-space assumed in DIS3-D.

MODEL CONSTRAINTS, SENSITIVITY AND DISCUSSION OF RESULTS

To derive a dike expansion model that would match the line-length changes recorded on the KMM EDM lines, the seven parameters (H, ϕ, θ, DU, DL, op and the coordinates of the observation points relative to the center of the dike) were allowed to vary one at a time, until the best graphical comparison was found. Some parameters were allowed to vary more than others as tighter constraints could be made for them. For example, the strike of the dike, ϕ, is assumed to be about N65E $\pm$ 10^{o} which corresponds to the strike of the ERZ and many of the newly formed surface cracks near the eruption site (Wolfe et al., 1987 and Ulrich, 1985, personal communication). The dip of the dike θ, is assumed to be near vertical but was allowed to fluctuate from 70^{o} to 110^{o}. This constraint can be made as field observations of eroded rift zones for virtually all Hawaiian volcanoes indicate that dikes are emplaced as near vertical sheets, (Macdonald and Abbott, 1970) but commonly vary by as much as 20^{o} from vertical (Walker, 1987). Also, geophysical surveys (Kinoshita, 1965 and Hill, 1969), deformation studies (Duffield et al., 1976) theoretical and comparative studies of ancient dikes (Delaney and Pollard, 1981) demonstrate that magma travels in steeply dipping dikes. Seismic data (Klein et al., 1987 and Koyanagi et al., in press) is used to constrain the maximum depth (DL) of the dike to about 5-6 km. The depth to the dike top has been arbitrarily constrained to a depth of just a few meters below the free surface.

The location of the center of the dike is constrained by the

ground deformation patterns indicate which a primary zone of deformation just south of the instrument site near the 0.3SE reflector target (Figure 34). However, the half length (H) of the dike is poorly constrained and was allowed to range from 0.7 km to 5 km. The shorter end-member of 0.7 km is the approximate distance from the EDM line to Puu Oo. A short duration, lower resolution theodolite deformation study (carried out by Christina Heliker and George Ulrich of HVO, and myself, prior to episode 25) suggested no pre-eruption extension on the down-rift side of Puu Oo. The upper end of the half length parameter (5 km) can be constrained as another EDM line, located 9 km uprift of Puu Oo, near Mauna Ulu, shows a smaller pre-eruption extension and post eruption contraction (Figure 36). The deformation on this line is presumably also due to the expansion of the east rift zone due to an addition of magma. However, the expanding dike in this case is the conduit system that magma passes through enroute to the eruption-site storage system. It is presumably deeper due to its closer proximity to the summit and therefore does not affect the line-length changes nearly as much as the shallow dike below the near-vent KMM-lines. As the H parameter is increased to beyond 5 km no substantial differences in the model occur. Therefore, the H values have been constrained to 0.7 and 5 km. The final parameter to be adjusted is the widening (op) of the dike. In an attempt to constrain this value, the pattern of deformation over the series of eruptions was considered. The systematic pattern of extension and contraction of the line-lengths had all been aseismic and elastic in nature. The

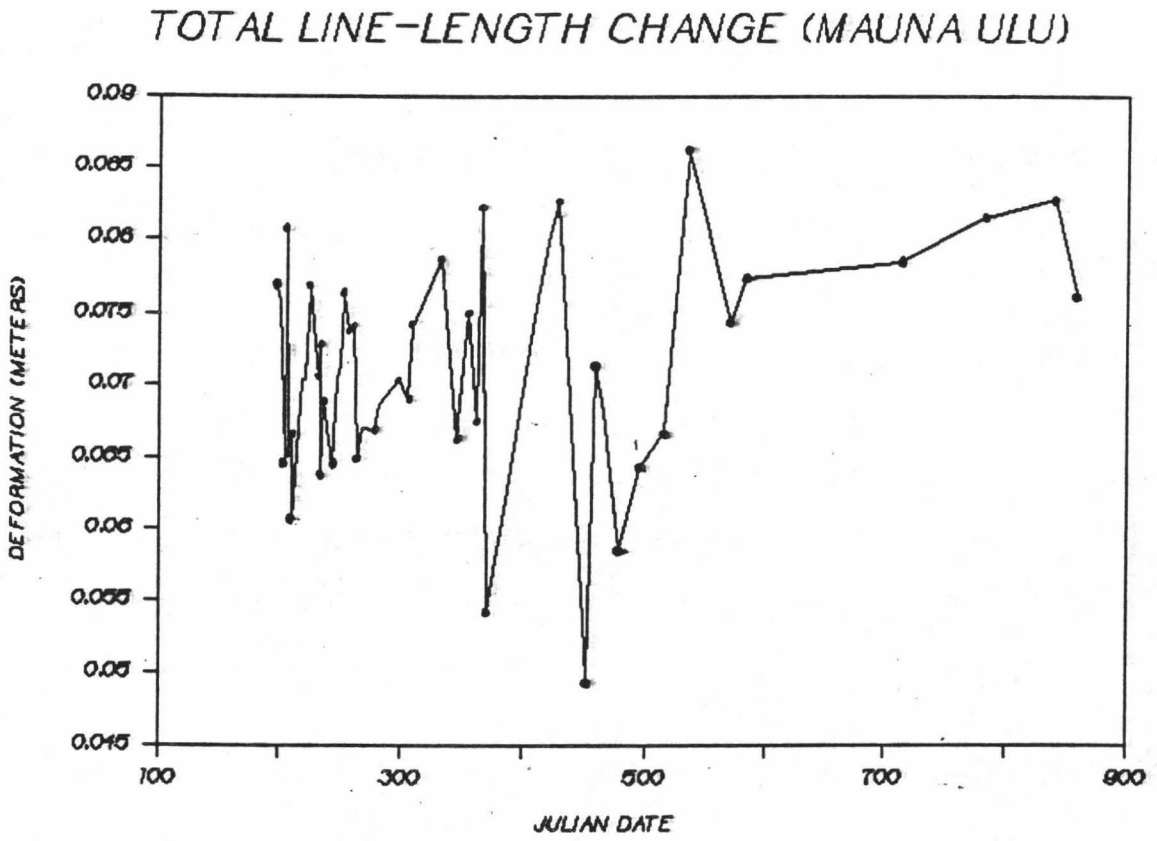

Figure 36. Overall line-length changes for Mauna Ulu deformation line.

widening of the dike was not large enough to cause brittle deformation of the host rock but must have been at least as large as the extension of the EDM line. The op parameter was therefore varied from 50 to 200 mm.

To summarize, the parameters best constrained are strike and dip of the dike. The depth to the top and bottom of the dike as well as dike opening are constrained fairly well. The least contrained parameter is the dike half length.

The elastic parameters used in DIS3D program are Poisson's ratio and shear modulus. Values for these parameters were assumed to be the commonly used values of 0.25 and $3x10^9$ Pa, respectively.

In order to record the bulk of the displacement, it is important that a measurement is made at both the beginning and end of the repose period. Two additional measurements made at intermediate times are used to further substantiate any deformation. The frequent (daily to weekly) EDM measurements on the near-vent KMM lines has been successful in documenting the deformation patterns for 20 of the 21 repose periods spanning episodes 22 through 42. The repose prior to episode 28 was missed due to poor weather conditions.

Of the 20 repose periods, 3 are classified as "very well" documented (those with many measurements on a full set of reflectors) and 6 of them are classified as "well documented" (those with at least 4 measurements made on a full network of targets). If only two or three measurements are made but they are made at the beginning and end of the repose periods, then the deformation may be

classified as moderate-to-well documented, while three others are classified as moderately documented. Other repose periods are classified as poorly documented. See Table 15 for a listing of the repose periods and their respective classification.

Table 15

EPISODE	DOCUMENTATION CLASSIFICATION	H /(km)	DU /(km)	DL /(km)	θ (degrees)	φ	OP /(mm)
22	Moderate-to-Well	1.00	0.70	2.2	89	15	103
23	Well	1.10	0.57	2.7	86	10	91
24	Well	0.90	0.61	3.0	80	15	100
25	Well	0.60	0.25	3.0	102	24	100
26	Very Well	0.76	0.26	2.5	91	15	90
27	Moderate-to-Well	0.80	0.72	3.0	79	11	103
28*	Poor	no data available					
29	Very Well	0.80	0.32	4.0	82	16	100
30	Very Well	0.80	0.42	4.0	97	12	160
31	Well	0.76	0.42	3.0	93	12	97
32*	Moderate	0.80	0.40	4.0	100	12	93
33*	Moderate	0.78	0.33	4.0	95	12	105
34	Well	0.79	0.35	3.0	82	12	125
35	Moderate-to-Well	0.70	0.31	2.0	88	16	105
36*	Poor	no data available					
37*	Poor	0.62	0.30	2.5	93	12	52
38*	Moderate	could not model successfully					
39	Moderate-to-Well	0.72	0.39	3.0	70	18	158
40	Well	0.71	0.42	3.5	95	13	156
41*	Poor	0.72	0.46	2.5	77	20	82
42	Moderate-to-Well	0.75	0.35	1.5	77	21	87

* Data is too suspect to be used in Figure 38 and calculations in Figure 39.

Nearly 700 plausible combinations of the 7 parameters were used in an attempt to model the deformation patterns near the eruption site on the three KMM EDM lines for episodes 22 through 42. Generally satisfactory results were obtained for the eruptions with better than moderate documented line-length changes and will be presented in a graphical analysis.

Results of the model calculations indicate that the displacement of the targets relative to the instrument station is most sensitive

to the depth to the top of the dike and to the lateral location of the center of the dike. Small variations in these parameters resulted in large calculated changes in line-length. Other sensitive parameters include the amount of displacement of the dike (assumed to be perpendicular to the dislocation plane), length of the dike and often the dip of the dike. The less sensitive parameters include the depth to dike bottom, and strike of the dike. Generally speaking, the most sensitive parameters were the least constrained ones.

To summarize the results of the modeling for each episode the final parameters (boundary conditions) are tabulated (Table 15) and calculated displacement profiles are plotted together with observed displacement profiles (Figures 37a-37q). Figures 37a through 37q clearly illustrate the generally good fit between calculated and observed deformation profiles. The ridge-trough-ridge profile is closely followed in nearly all cases; however, in some cases the outer flanks of the ridges are not well constrained. Longer line-lengths on both the south and north side are necessary to observe the complete structure of the ridge flanks. Unfortunately, longer lines were imposible due to the obstruction of view by the nearby forest. The DL parameter will affect the outer flanks of the curve the most: larger DL values result in larger displacements of the distant stations. It could be argued that since the outer flanks of the curve are not observed, the DL parameter could be even larger. However, there are a number of fairly well documented episodes that suggest the that both the north and south sides of the

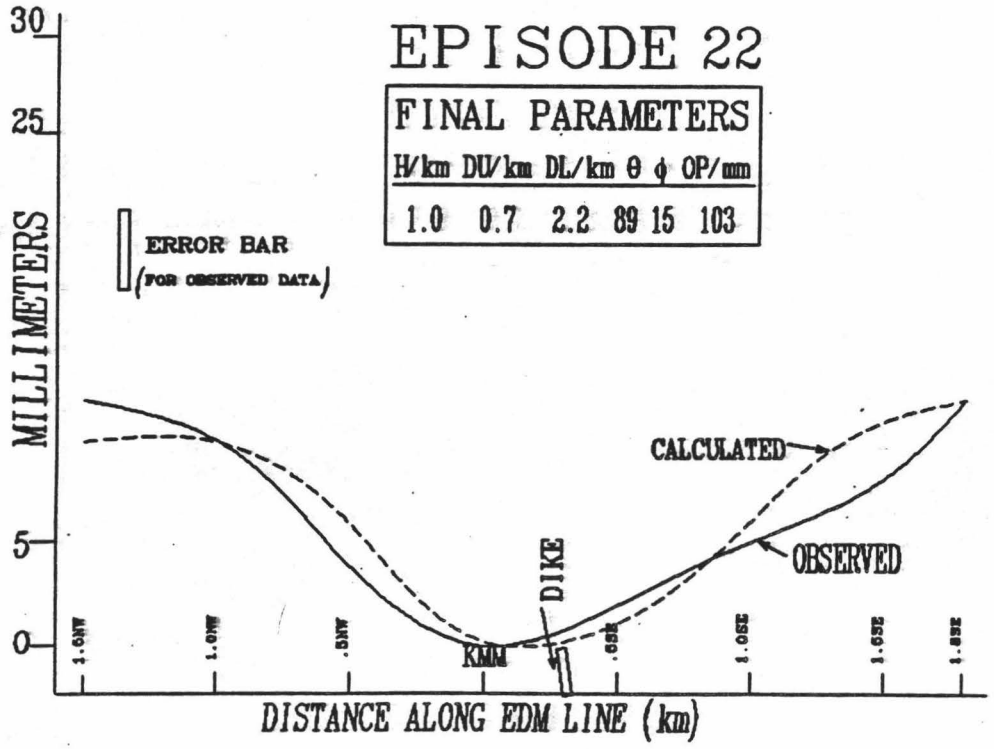

Figures 37a-q. Calculated displacement profiles plotted with observed displacement profiles. 37a displayed here.

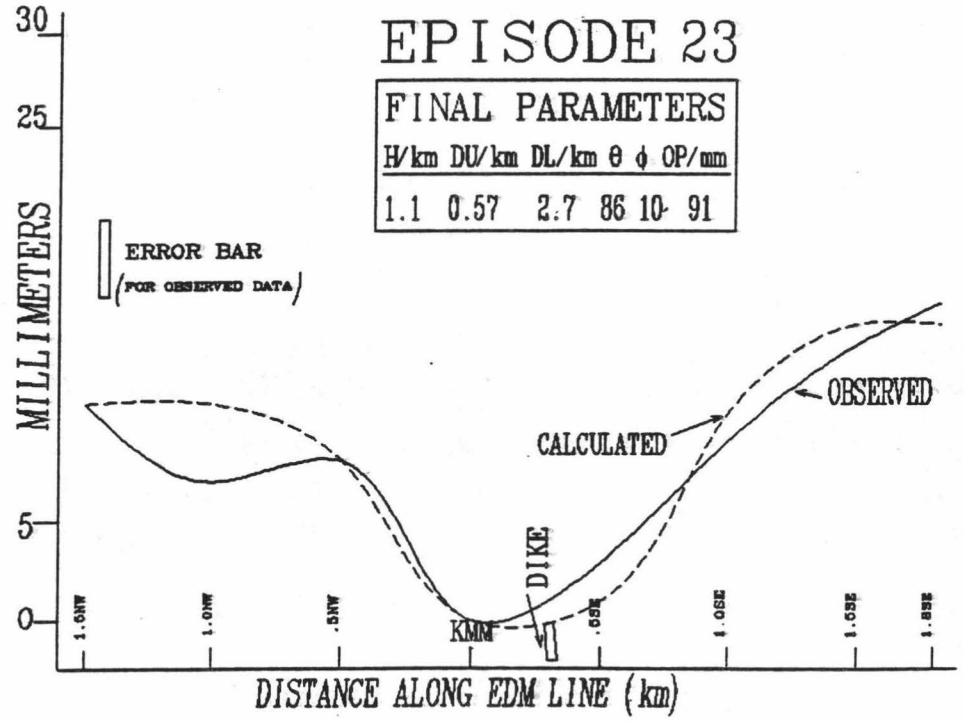

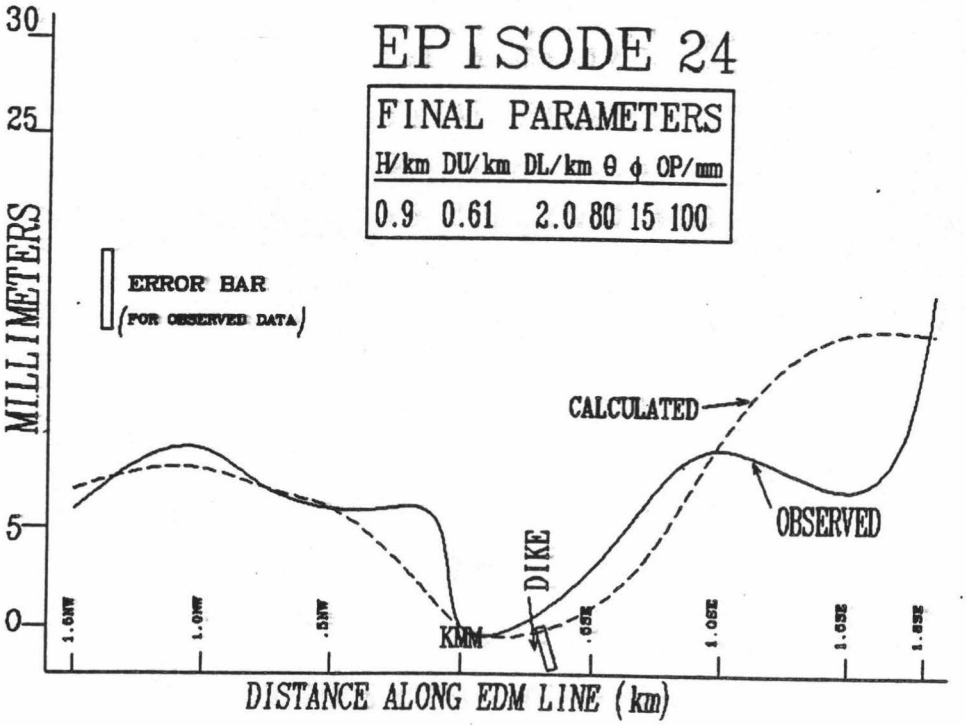

Figure 37b-c. Calculated displacement profiles for episodes 23 and 24.

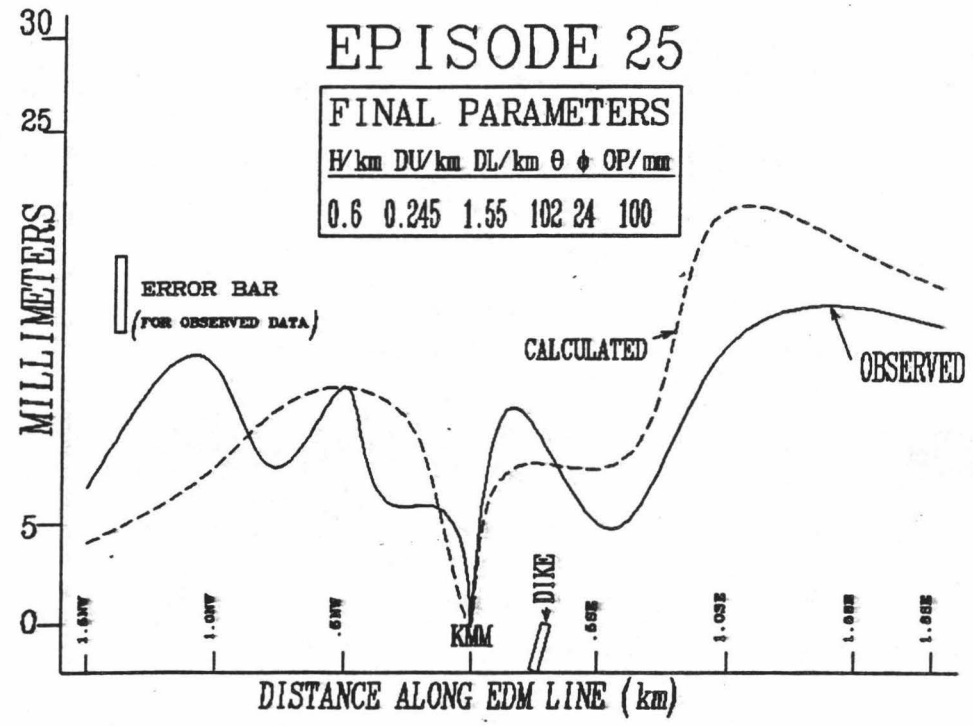

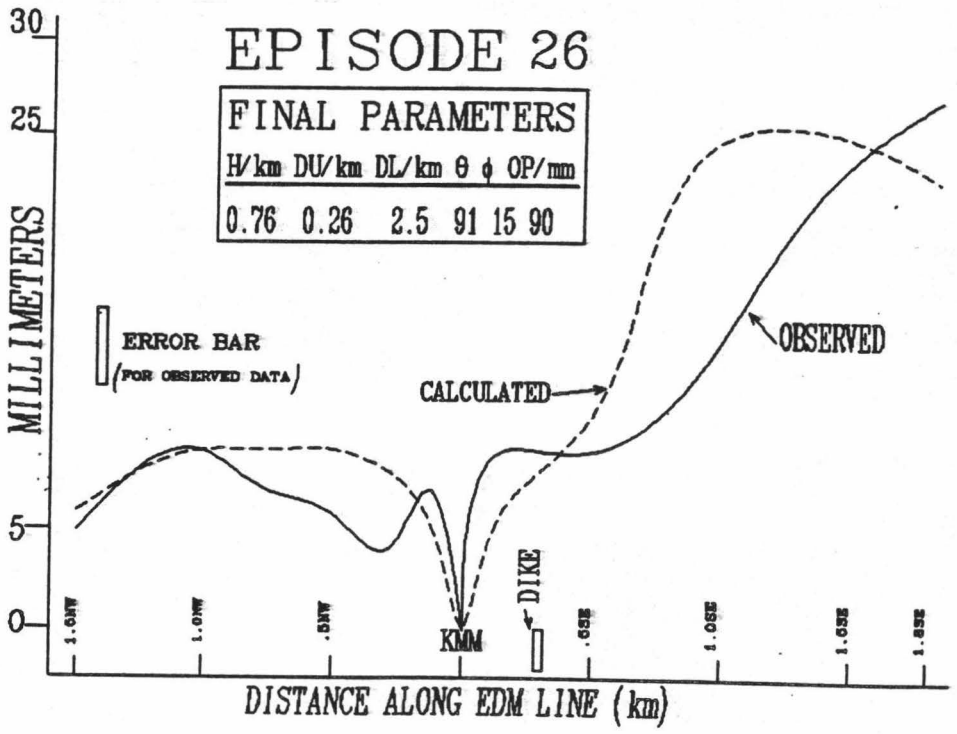

Figure 37d-e. Calculated displacement profile for episodes 25 and 26.

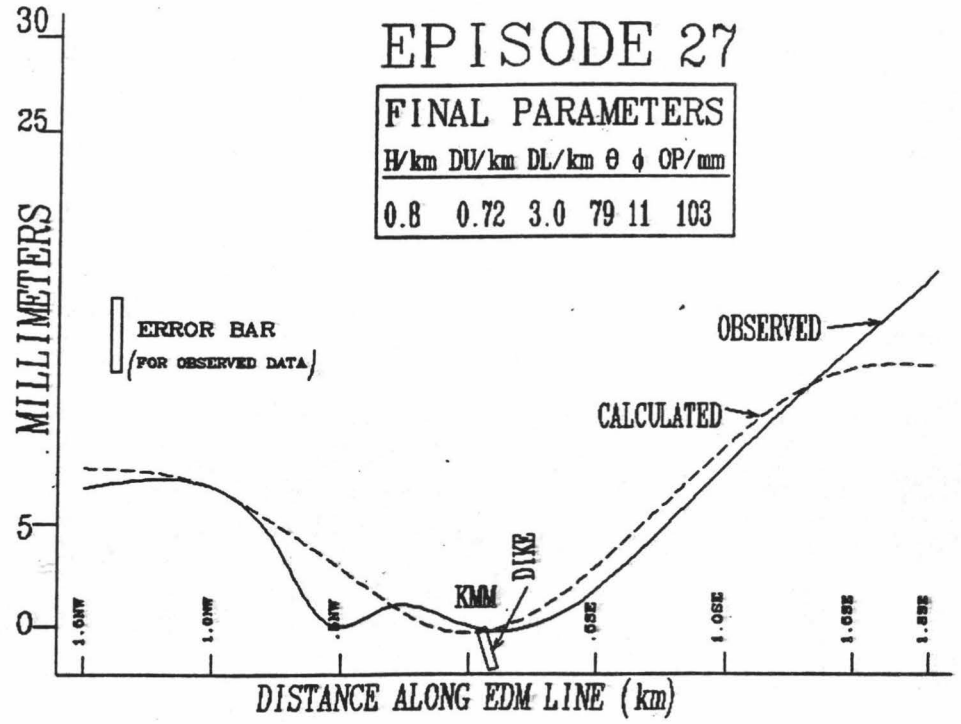

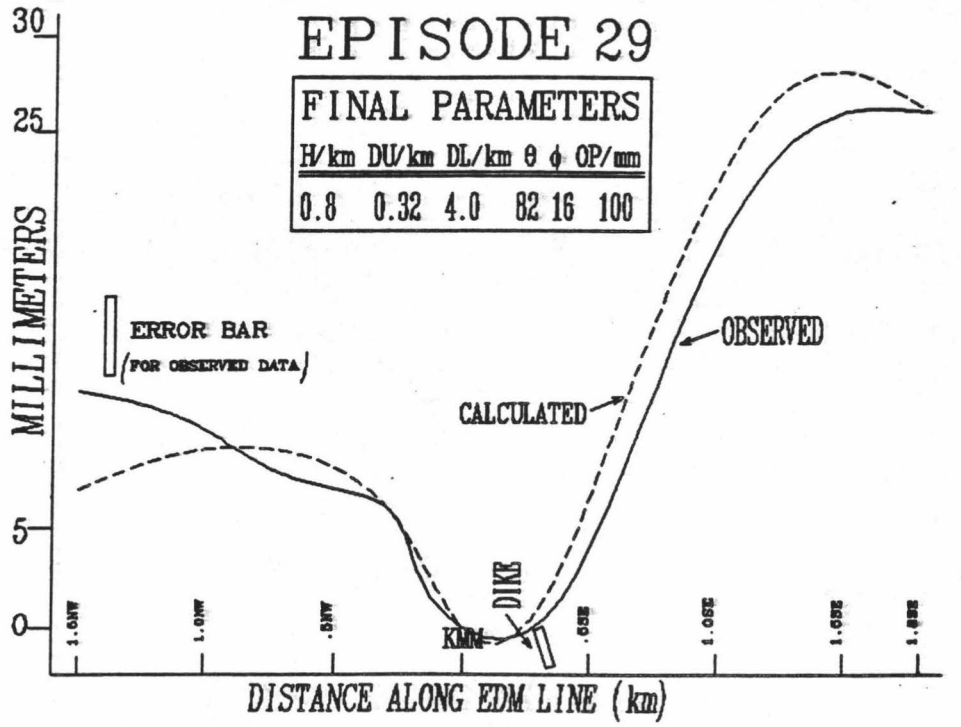

Figure 37f-g. Calculated displacement profiles for episodes 27 and 29.

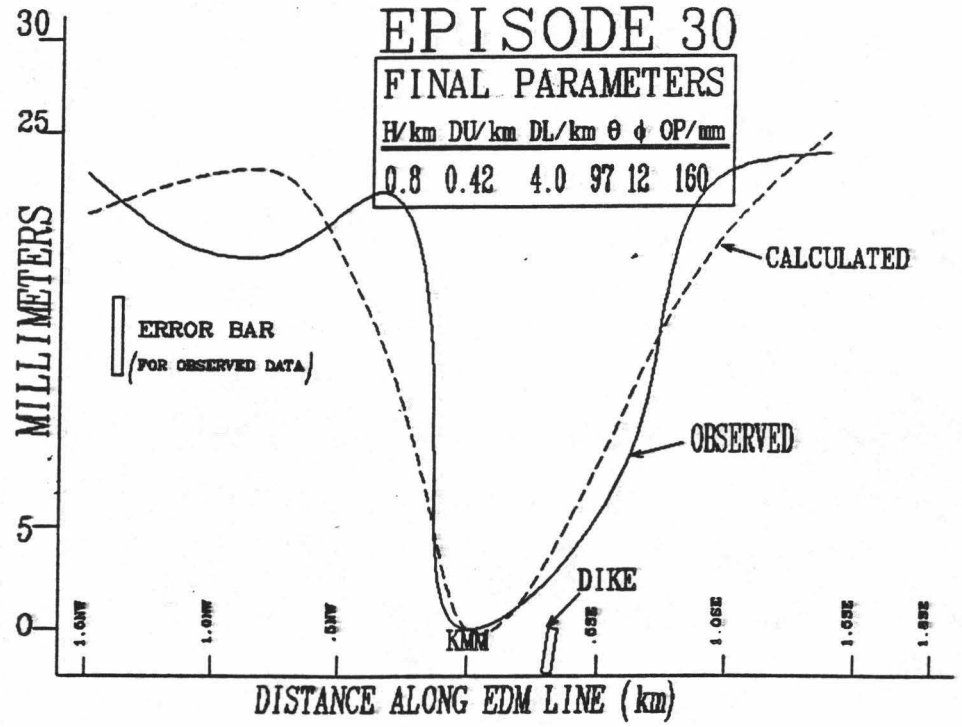

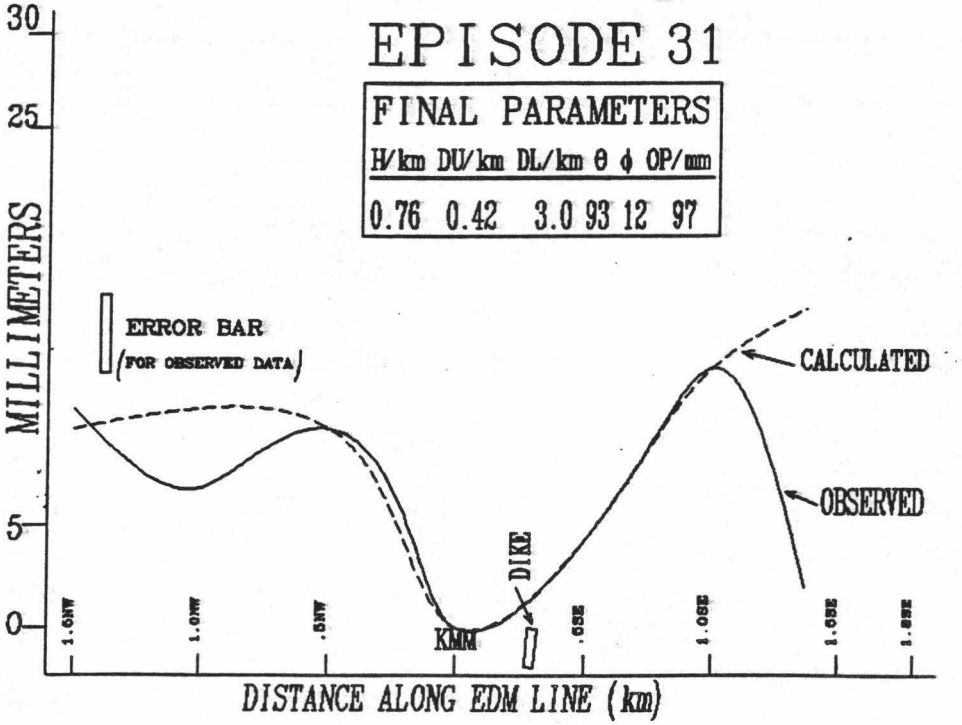

Figure 37h-i. Calculated displacement profiles for episodes 30 and 31.

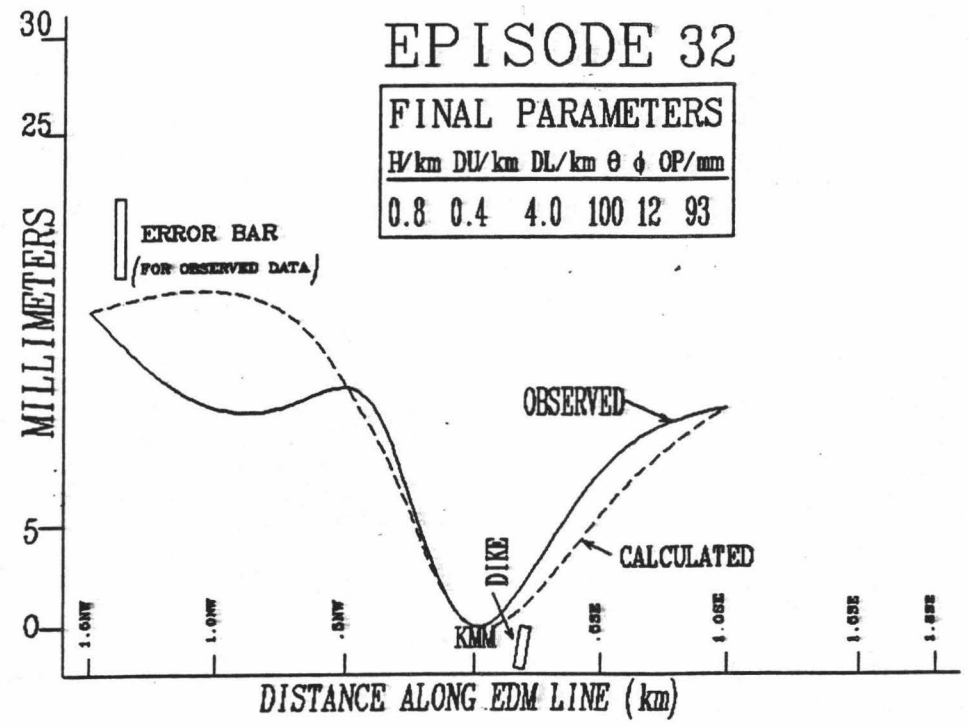

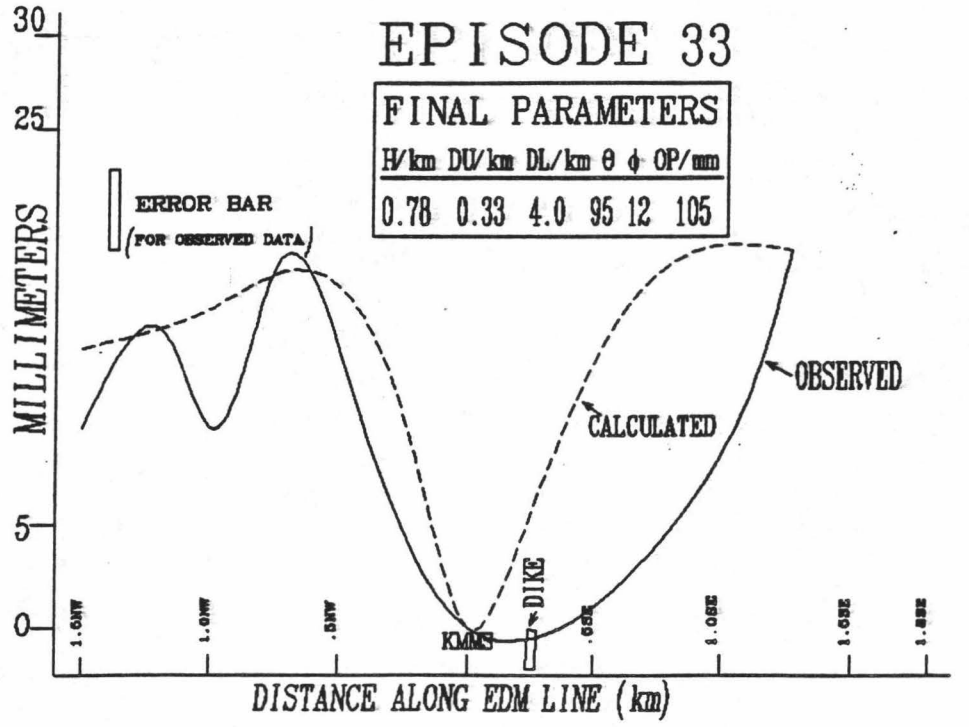

Figure 37j-k. Calculated displacement profiles for episodes 32 and 33.

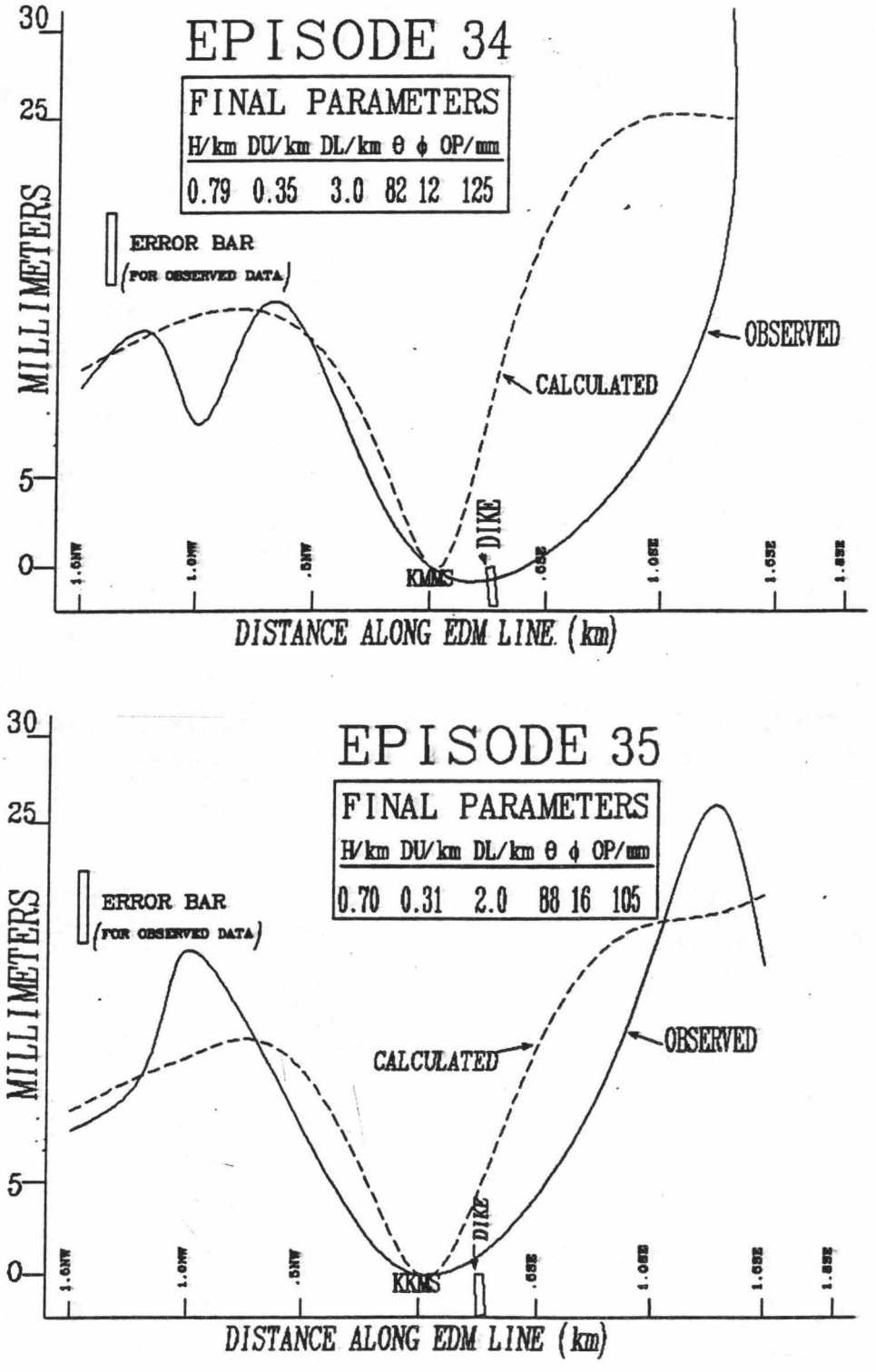

Figure 371-m. Calculated displacement profiles for episodes 34 and 35.

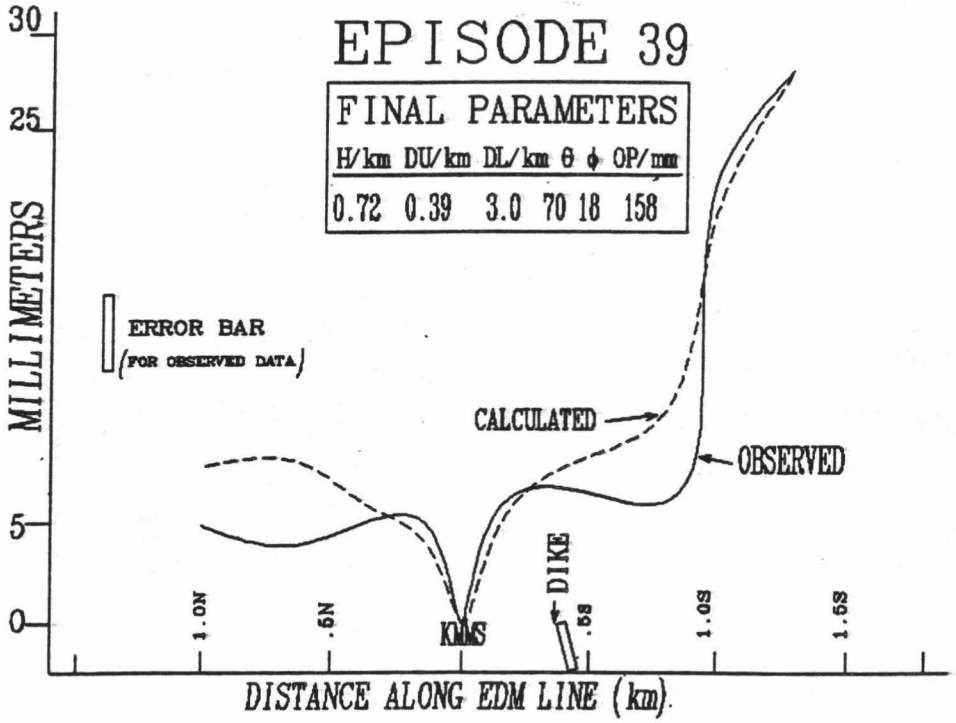

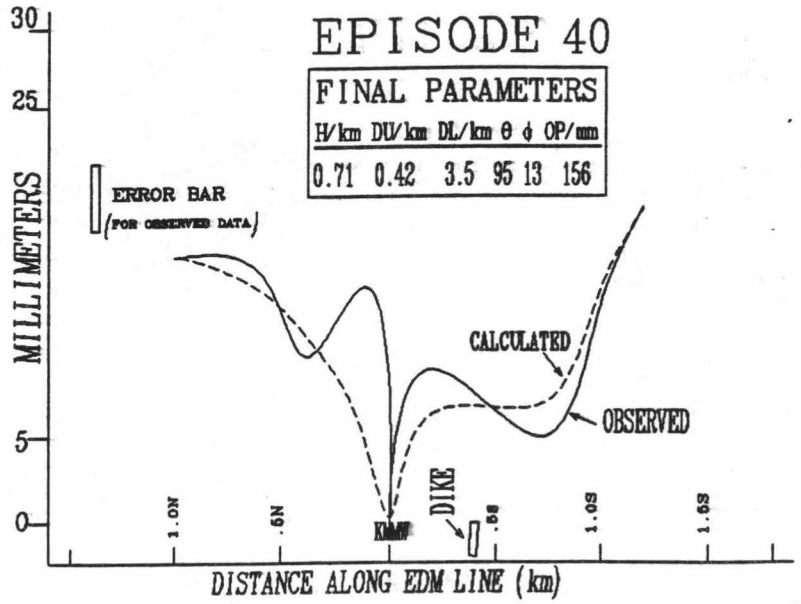

Figure 37n-o. Calculated displacement profiles for episodes 39 and 40.

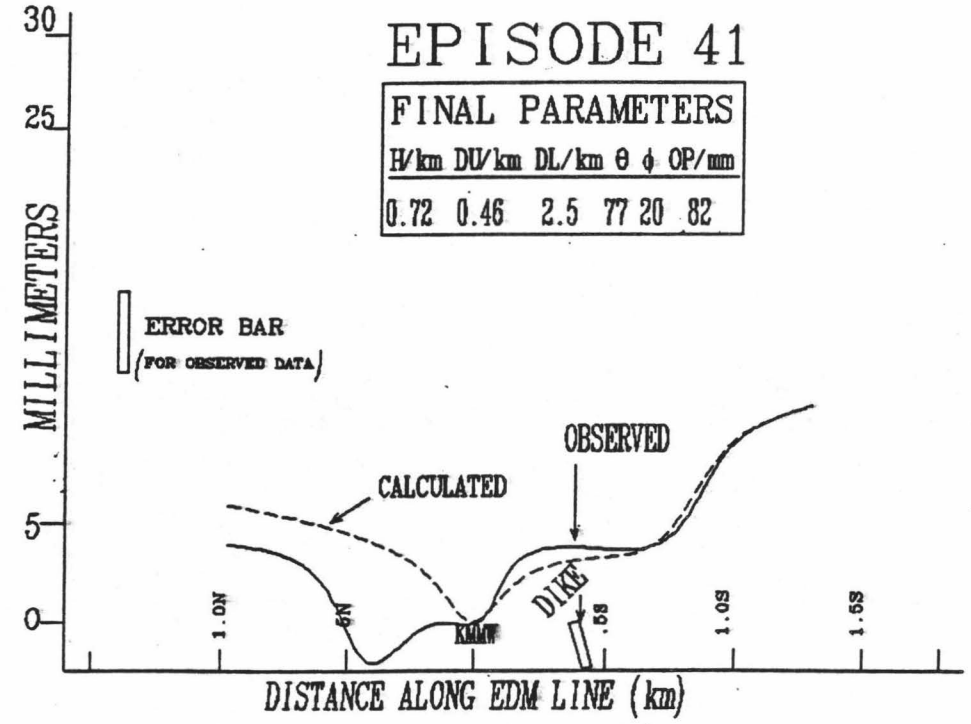

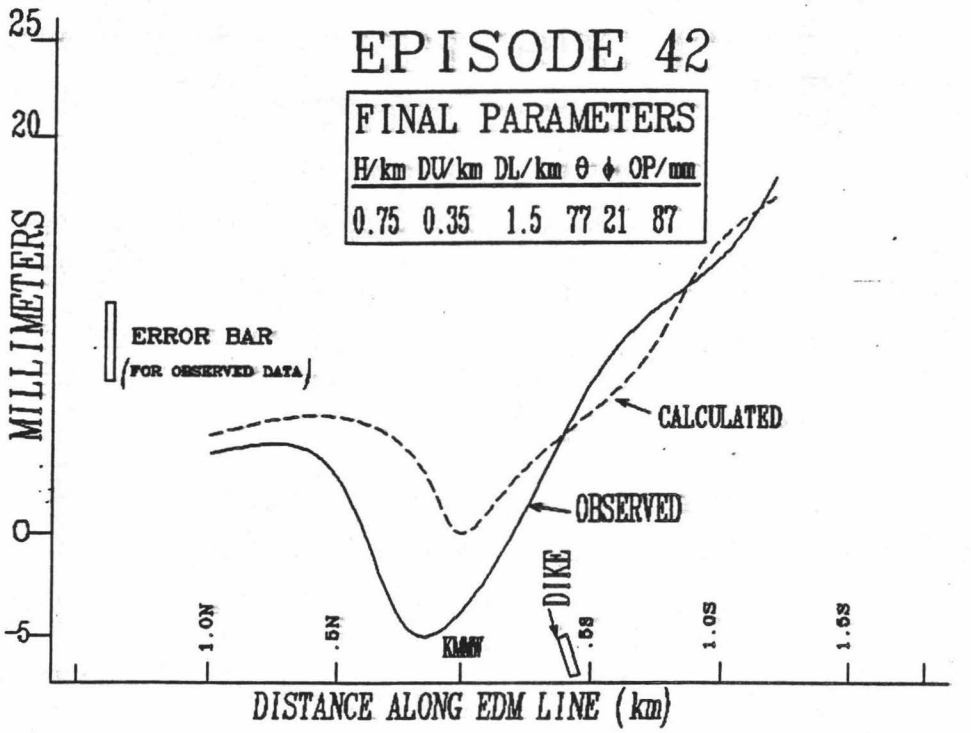

Figure 37p-q. Calculated displacement profiles for episodes 41 and 42.

displacement curve is in fact beginning to turn over. The south side was generally displaced more than the north side which may be due to a southerly dip of the dike. The larger displacement to the south may also be associated with the mobility of the south flank. However, the repetitive elastic-like recovery of the south line suggests a southerly dip of the dike be the cause of the relatively large southern displacement.

Figures 37a through 37q demonstrate that only 'moderately well documented' (Table 15) repose periods are necessary to have generally good comparisons between calculated and observed profiles. Documentation beyond 'moderately well' proves also to be as informative, however,does not improve the fit between calculated and observed curves significantly. These measurements also demonstrate that the ground displacement profiles across the rift zone include components of inelastic deformation in an inhomogeneous medium. This type of deformation appears as discontinuities in an otherwise smooth curve with systematic deviations from the calculated curve. The discontinuities and systematic deviations from the calculated profile correlate spatially with cracks on the north side of the KMM line (Figures 37b,e,h,i,j,k and l). Presumably, these cracks accomodated some of the horizontal deformation. This is another reason the deformation on the south side was greater than the north side. Another possible explanation is the expansion of a more northerly distant dike.

There is a systematic extension-contraction trend that correlates positively with the timing of eruptions (see Figs. 32 and

33). Extension of the line-length occurs during the repose period and is followed by nearly the same amount of contraction soon (usually within a couple of days) after the eruption. Elastic recovery, toward a state of extension, usually begins less than a week after the eruption and continues right up to the next eruption. It is for this reason measurments should be made near both ends of the repose period.

Superimposed on the extension-contraction pattern of episodes 22-25 (Figure 32) is an approximate increase in extension and contraction with time for episodes 24 through 30. The extension of the line prior to episode 24 was about 12 mm, and the extension prior to episode 30 was about 40 mm (note that the line returns to nearly the same length after each contraction). The EDM measurements were made less frequently after episode 31, so the extreme ends of the repose periods were not always measured; however, the line-length changes remained relatively consistent and high for the better documented repose periods. This implies that the storage system near the eruption site was evolving between episodes 24 through 30 in a sense that its geometry and/or position affected the line-length changes more and more. This change in geometry could be explained by a combination of factors including an increase in the width of the dike, a decrease in the depth to the top of the dike, or the position of the dike (half-length) relative to the targets and the dip of the dike. Beyond episode 30 and until episode 35, the dike presumably stabilized itself with respect to its geometry and position.

An examination of the estimated parameters for each episode (Figure 38), however, does not indicate an obvious systematic trend in calculated parameters with time. The dike's dimensions may have changed slightly from episodes 22 to 25 as the values of H and DU decreased from values of about 1.0 km to 0.7 km and about 0.6 km to 0.3 km respectively. The large DU value for episode 27 could be somewhat erroneous reflecting the "moderate" level of documentation for that repose period. Beyond episode 25, the calculated H and DU remained relatively stable at a level of 0.7-0.8 km and about 0.3 km respectively. The calculated op parameter suggests that the amount of opening became more variable with time as episode 22-29 had calculated values of about 100 mm; after episode 29, the op parameter varied from 60 to 160 mm. This variation is probably greater than the variation caused by the noise and differing degrees of documentation from episode to episode. Other parameters for instance show no systematic trends and the variations within each are considered to reflect a combination of the noise and differing degrees of documentation from episode to episode. I therefore assume that the strike and dip (ϕ and Θ, respectively) of the dike remained nearly constant throughout the series of episodes. The average of the calculated strike and dip are about 14^{o} (corresponds to about N65^{o}E: the targets were referenced in DIS3D relative to a coordinate system having N51^{o}E as the starting strike) and 87^{o}, respectively. However, I am assuming that the depth to dike top and bottom (DU and DL, respectively), opening (op) and half length (H) varied somewhat from episode to episode.

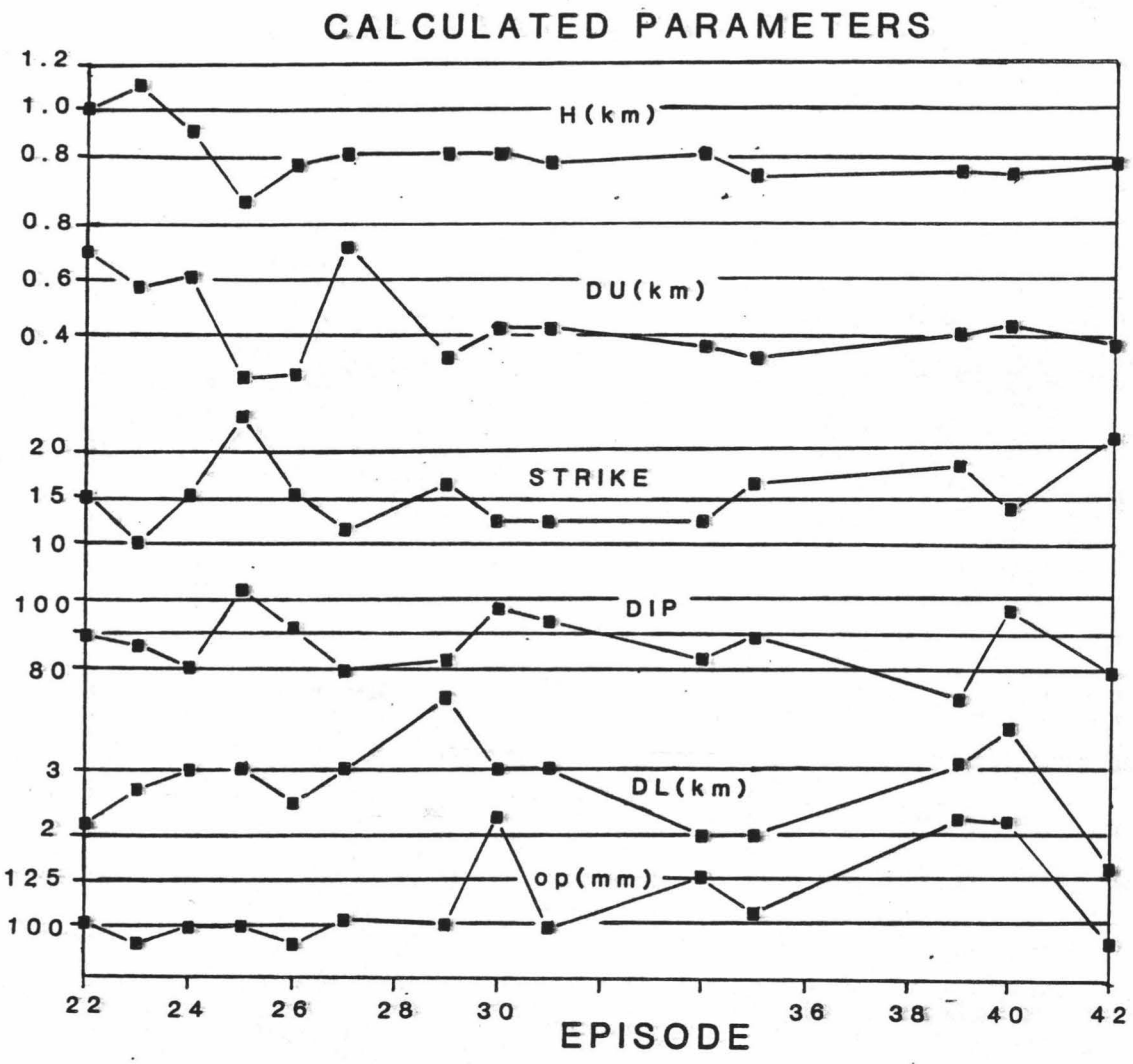

Figure 38. Calculated parameters from DIS3-D for each episode.
H = half length in km
DU = depth to upper surface of dike
DL = depth to lower surface of dike
op = amount of dilation during repose period.

PRESSURES

If the host rock surrounding the magma reservoir behaves elastically, then surface displacements above the chamber are directly related to pressures within it. Decker et al., (1983) used a relationship from Epp et al., (1983) that correlates summit deflations and elevation of eruptive vents to estimate a pressure change of about 0.085 MPa per microradian of inflation/deflation. During the 1983-1987 eruption episodes at Kilauea tilt changes of about 6-19 microradians were common, corresponding to pressure changes of 0.5 to 1.6 MPa.

Pollard et al., (1983) showed that dike thickness can be calculated if the elastic parameters (Poisson's ratio and shear modulus) of the host rock, the half height of the dike and the pressure within the dike are known. The thickness at the center of the dike is given by

$$t=Pa(1-v)/u \qquad (4.1)$$

where P is the pressure at the center of the dike, a is the half height of the dike, v is Poisson's ratio and u is the shear modulus. Rearranging this equation to solve for P results in

$$P=tu/a(1-v). \qquad (4.2)$$

Replacing t with op (the amount of dike opening during the repose period predicted by DIS3D) and P with delP, then we can calculate the change in pressure at the dike center due to the accumulation of magma and resulting deformation during the repose period from the equation

$$delP=opu/a(1-v). \qquad (4.3)$$

DIS3D assumes a constant opening across the entire dike. Therefore, these values represent average pressure changes at the center of the dike near the eruption site and vary from 0.2 to 0.61 MPa.

Figures 39a-d compare various derived KMM-EDM line values to various eruption values. To reduce the noise and hence the scatter of the plots only the better than moderately documented episodes are used in these figures. The KMM-EDM line values used in Figures 39a-d include total line-length extension, calculated eruption-site pressures and change in site-volume due to the growth (expansion) of the dike. Where change in site-volume is calculated by:

$$\text{delsite-vol} = (\text{op} \times 2H \times (DL-DU)). \qquad (4.4)$$

Some of the eruption values used include episode number, volume of lava erupted and summit pressures (inflation prior to eruption).

Figure 39a plots change in site-volume against episode number. The average change in site-volume is about 450,000 cubic meters. However, the standard deviation is high and a saw-tooth pattern is shown here. Although there is a large variation in change in site-volumes, there is no systematic variation with time. The largest the local storage system had expanded was prior to episode 30 (almost a million cubic meters) whereas the smallest was for episode 42 (only about 0.15 million cubic meters). The large change in site volume for episode 30 was followed by a relatively small change in site-volume for episode 31. The lavas of these episodes are anomalous with respect to their major-element composition. Unlike the majority of episodes following 10, the MgO content for the lavas of these episodes displayed a systematic increase with

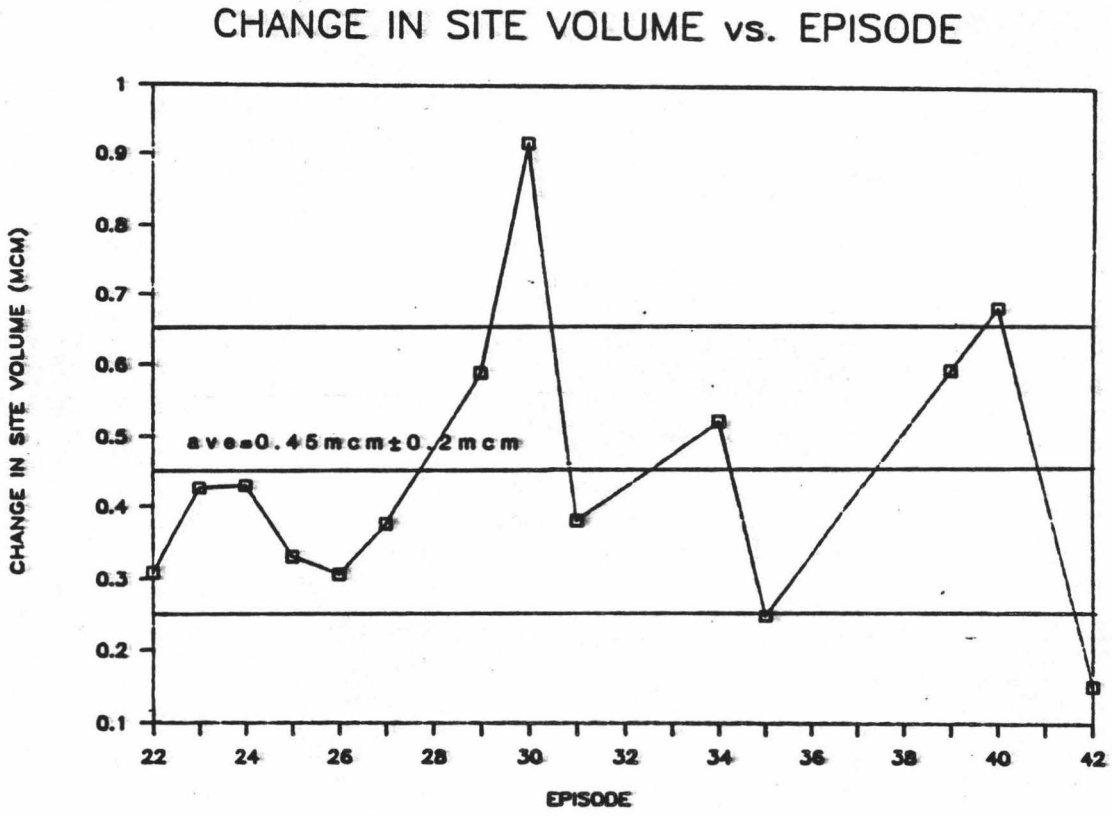

Figure 39a. Change in site volume versus episode number.

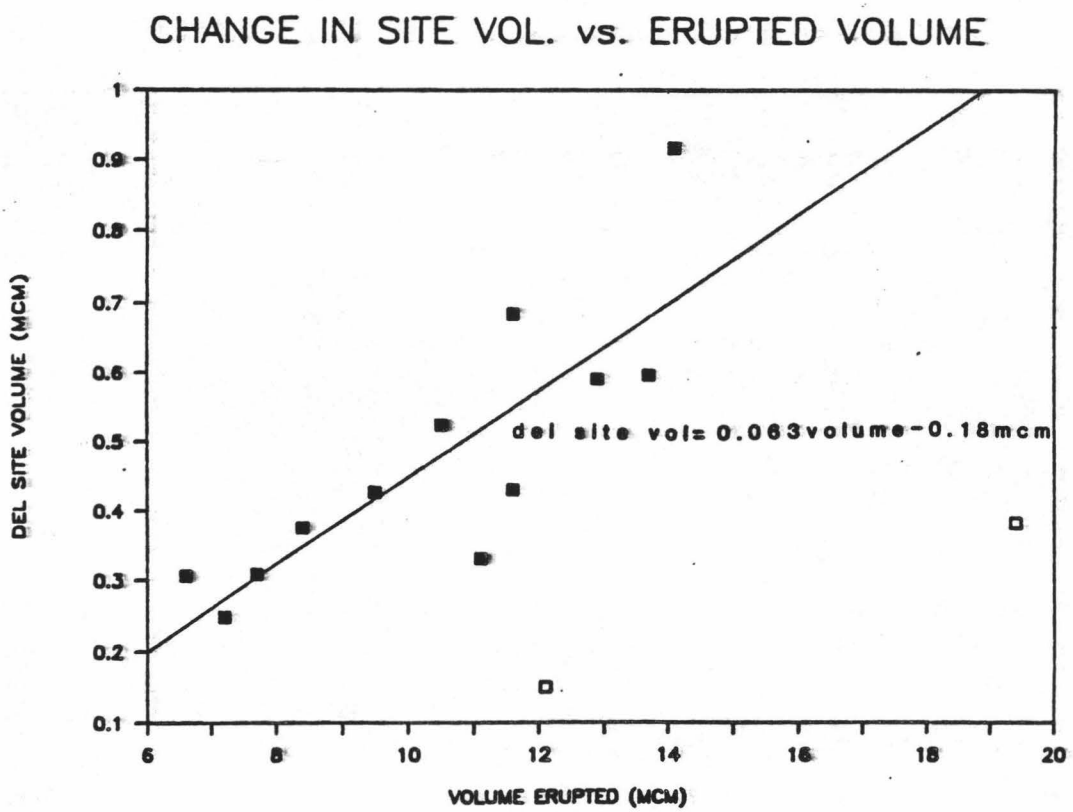

Figure 39b. Change in site-volume plotted against volume of erupted lava. Open boxes indicate values were not used in regression equation.

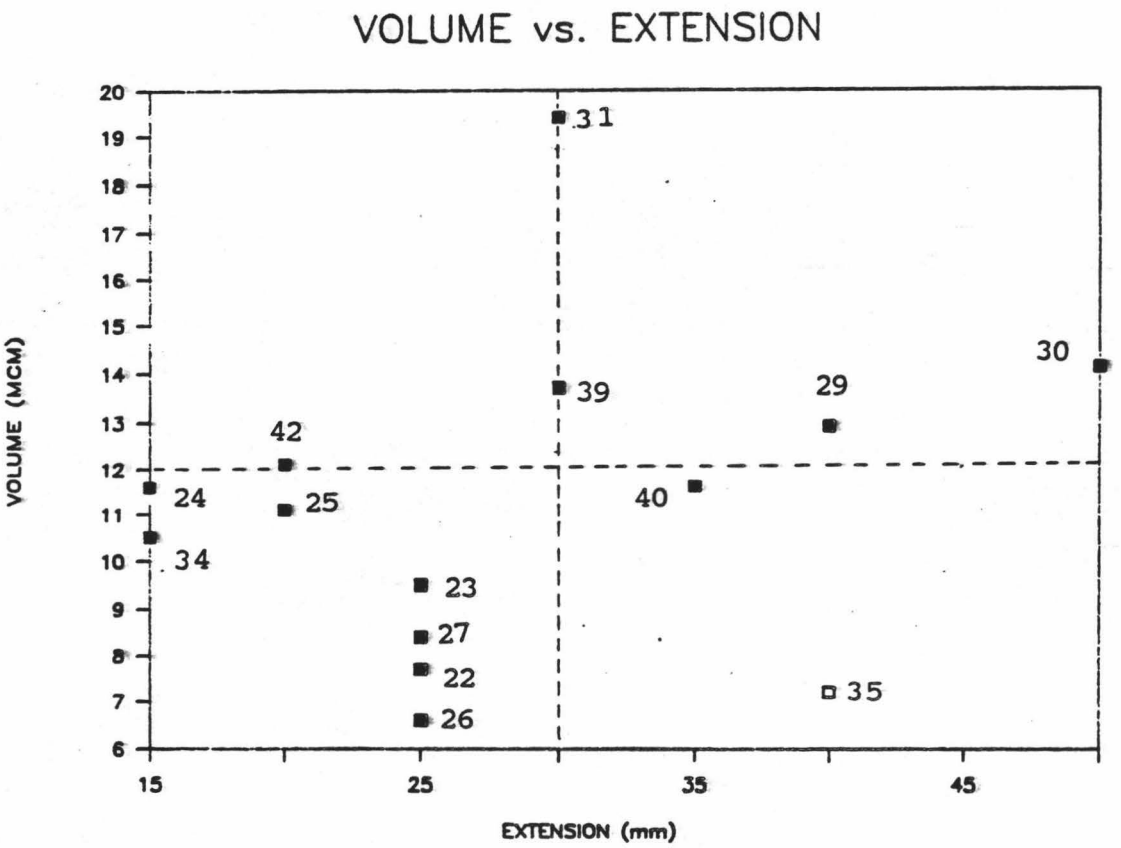

Figure 39c. Line-length extension to the nearest 5 milimeters versus volume of lava erupted. Open box indicates episode that does not fit this model.

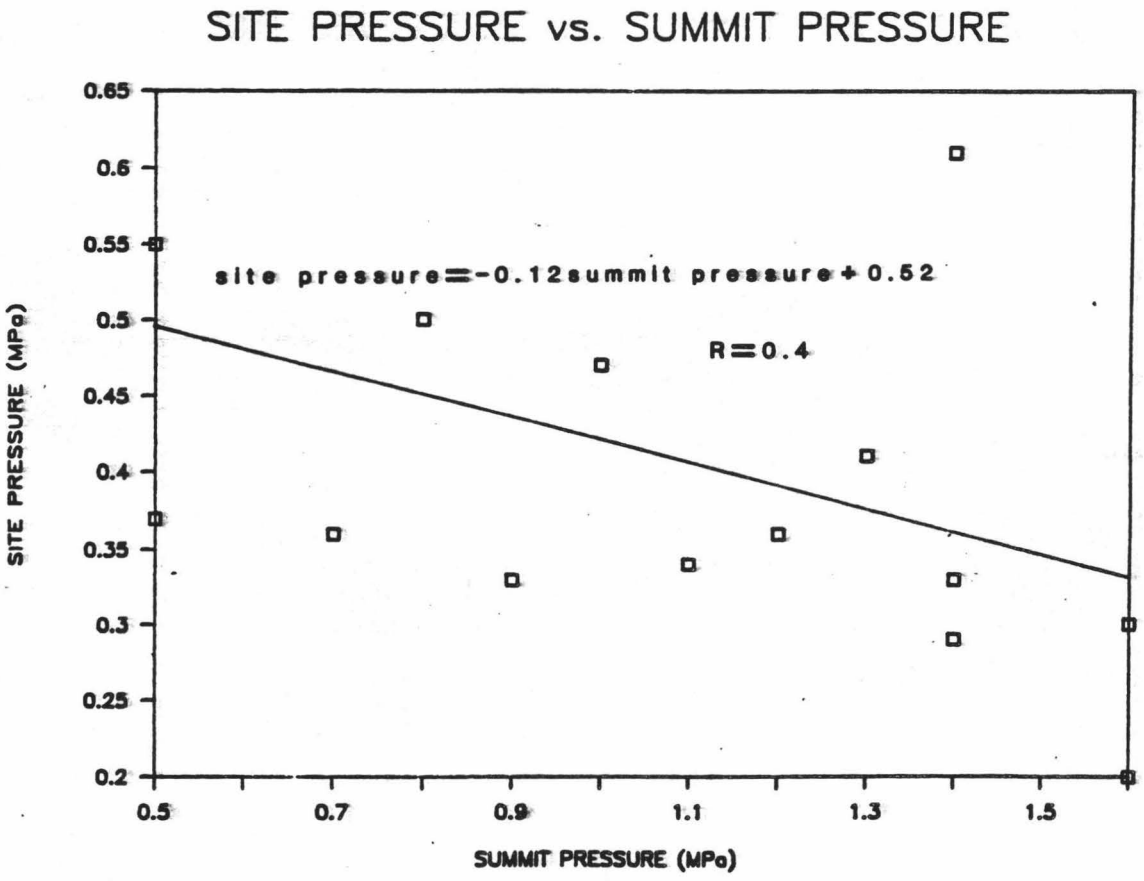

Figure 39d. Change in site-pressure against summit pressure.

time (Garcia et al., 1985) and lavas with some of the highest MgO content were erupted. An increase in storage capacity near the eruption-site may have played a role in this chemical pattern as the increase in stored magma probably represented the addition of a more summit-type magma with a higher MgO composition (closer to a summit-type compostion). The source of this magma was presumably from farther uprift and addition of this more mafic magma apparently affected both episodes 30 and 31.

Since the average repose length was about 24 days, a site-change in volume of 0.45 mcm (Figure 39a) implies that the average rate of intrusion into the local reservoir area was about 0.2 m^3/s. This slow rate can be considered leakage (e.g. Dzurisin et al., 1984).

The change in site-volume for the better than moderately documented episodes is plotted against volume of erupted lava in Figure 39b. In general, there is a good correlation between the change in site-volume and erupted volume. This suggests that the volume of magma stored at the near-vent storage system is a partial measure of the volume of the lava that will be subsequently erupted. Points on the left side of the field indicated a high amount of erupted material for the amount of magma at the local storage site (episodes 31 and 42). This may be related to chemical variation seen in episode 31.

When extension and lava volume are plotted against each other, two fields emerge (Figure 39c). This plot can be divided into two sections at the 30 mm of extension boundary. Episodes that have total line-length extensions of less than 30 mm are generally lower

volume eruptions (less than 12 million cubic meters). Those that have line-length extensions of greater than 30 mm are generally high-volume eruptions (greater than 12 mcm). Episode 35 is an outlier in this plot.

In Figure 39d, change in site-pressure is plotted against summit pressure. This figure indicates an interesting inverse relationship between the two values. However, this correlation is only fair with a correlation of about 0.4. This relationship was not expected and is hard to explain. However, the inflation is taken as the entire inflation during the repose period, whereas the ground deformation results often do not span the entire repose length. A better correlation may have resulted if the amount of summit inflation was measured for only the time span that the ground deformation was measured.

Table 16. Calculated dike pressures, summit pressures and del-site volumes. Also, measured lava volumes and line length extensions to the nearest 5 milimeters.

EPISODE	DIKE PRESS /(MPa)	SUMMIT PRESS /(MPa)	DEL SITE-VOLUME /(cubic meters)	VOLUME /(mcm)	EXTENSION /(mm)
22	0.55	0.5	309,000	7.7	25
23	0.34	1.1	426,400	9.5	25
24	0.33	0.9	430,000	11.6	15
25	0.29	1.4	330,600	11.1	20
26	0.33	1.4	306,400	6.6	25
27	0.36	0.7	375,800	8.4	25
29	0.20	1.6	588,800	12.9	40
30	0.36	1.2	916,400	14.1	50
31	0.30	1.6	380,400	19.4	30
34	0.37	0.5	523,400	10.5	15
35	0.50	0.8	248,400	7.2	40
39	0.47	1.0	593,800	13.7	30
40	0.41	1.3	683,300	11.6	35
42	0.61	1.4	150,100	12.1	20
Average	0.38	1.1	450,000	11.2	28.2
Std Dev.	+0.11	+0.4	+200,000	+3.4	+10.0

MAUNA ULU TRENDS

While the near-vent KMM EDM deformation patterns indicated an elastic response to the addition and removal of magma, the deformation network near Mauna Ulu indicated inelastic deformation. This can be seen as the cumulative line-length changes since July 16 indicate that the targets on both sides of the instrument have gradually been displaced relatively southward by as much as 7 cm (Figure 40). Three explanations of this deformation trend follow. 1) The deformation may suggest an inelastic deformation zone caused by the repeated intrusion, storage and solidification of magma just south of the instrument site displacing all the targets southward relative to the instrument station. This is a possible explanation as the cumulative line lengths for the outer-most targets for each side of the instrument are nearly mirror images of each other (Figure 40). 2) Another possible explanation (although unlikely) to the deformation trend is a simple readjustment (settling) of the instrument site. However, visual examination of the instrument site suggests a very stable platform. Also, if this trend was caused by the gradual readjustment of the instrument site, the line length changes to all the targets would have been the same. This is clearly not the case as the longer lines show more relative displacement than the shorter lines. 3) A third explanation is that a reservoir of unknown geometry, possibly multiple reservoirs with dike-shaped geometries, exists. DIS3D was not able to successfully model a geometry neccessary to account for the observed deformation.

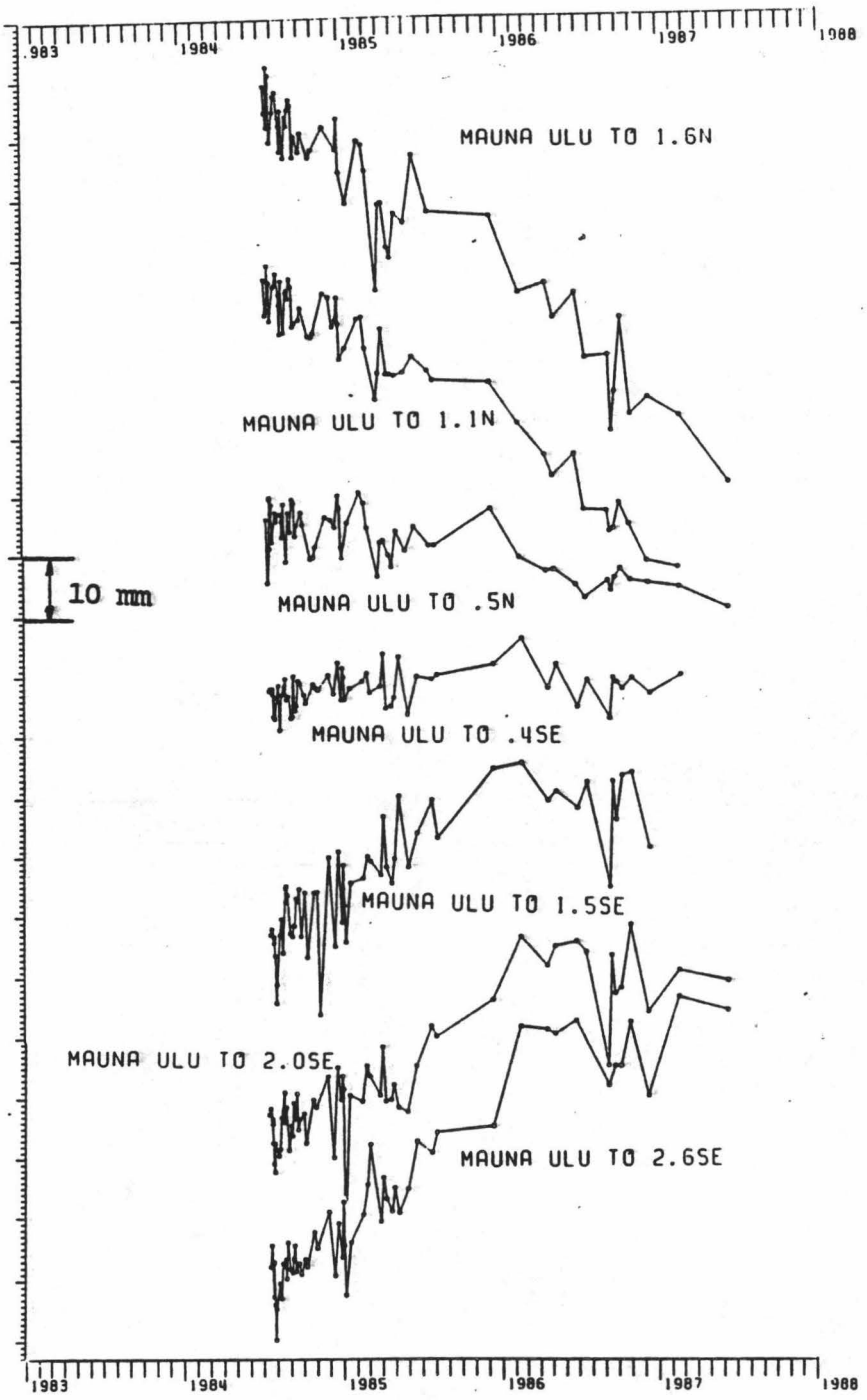

Figure 40. Cummulative line-length changes to each target measured from the Mauna Ulu instrument site. Up is relative extension, down is relative contraction.

There are a number of reasons for the lack of predictable deformation results for the Mauna Ulu surveys. First, the changes in line-length during repose periods were very small (half as large as the KMM line-lenth changes). Second, the ERZ between the caldera and Mauna Ulu is very complex (Klein et al., 1987). Historically, the activity of this section is different in many ways from the part of the rift zone below Mauna Ulu: since 1960, most of the activity in this upper section has been confined to intrusions (75% of the events were intrusive); the rift trends northwest and is therefore oblique to the greatest principal stress (probably complicating the observed deformation patterns); the Koae fault system meets the ERZ near Mauna Ulu; and in the segment above Mauna Ulu intrusions have been as likely to migrate uprift as well as downrift. A complex honeycomb system of magma conduits has been theorized to account for the differences in behavior between the two sections of the rift (Klein et al., 1987). Thirdly, the measurements made on the Mauna Ulu line were less frequent than the measurements at the KMM lines with the probable result that much of the actual surface deformation during the repose periods missed. Fourthly, and maybe most importantly, although the deformation at the Mauna Ulu line initially was elastic in nature, it became inelastic soon after the onset of the experiment. This could be the surface manifestation of solidifying magma injections as previously mentioned. Inelastic deformation requires another set of assumptions and equations not available in DIS3D.

A comparison between Figures 40 and 41 illustrates an important distinction between the two deformation lines. It is apparent that, although the KMM targets had to be replaced on a regular basis, KMM targets experienced elastic recovery. This suggests that the extension-contraction pattern documented at the near-vent deformtion line represents addition and removal of magma. This may not be the case for the Mauna Ulu line. In contrast to the KMM defomation patterns, the Mauna Ulu patterns may suggest that much of the magma entering this location does not leave (possibly solidifying in place). Whatever the cause, the Mauna Ulu line experienced inelastic ground deformation whereas the KMM line did not.

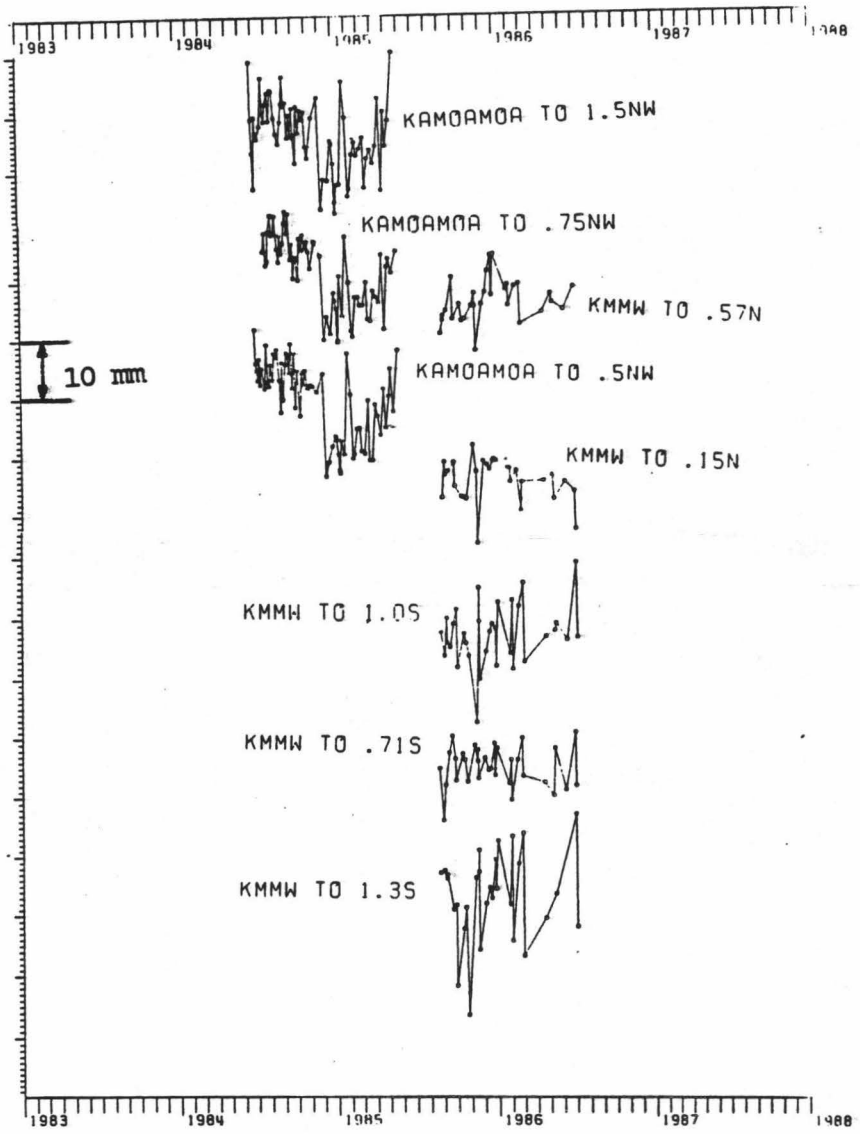

Figure 41. Cummulative line-length changes to selected targets measured from instrument stations on or near Puu Kamoamoa. Up is relative extension, down is relative contraction.

CONCLUSIONS

The average dike geometry was modeled as having a half length of 0.8 km, a DU of just over 400 meters, a DL of 2.9 km, an op of 113 mm, a strike of N65E and a dip of 87. The location of the center of the dike is placed south of KMM by about 200 meters (Figure 42). Magma is calculated to have leaked into the dike at a rate of about 0.2 m^3/s. The average volumetric expansion of this dike during the repose periods was nearly 0.5 mcm. This volume was shown to correlate positively with the volume of erupted lava.

The location and attitude of the modeled dike lies remakably close to the location and attitude of the fissure eruption of episode 35 (Heliker, 1985, personal communication, seen in Figure 42). Here it is assumed that the dike simply migrated upwards to the surface subsequently erupting a curtain of fire.

The minimum dike thickness to prevent freezing during a repose period of 24 days is about 2.0 meters (Wilson et al., in press a). If a dike width of about 2.0 meters is assumed, then the total volume of the near-vent reservoir is about 8 mcm. This represents about 75% of a typical Puu Oo eruption. An assumed dike thickness of 2.0 meters may be too small, as Okamura et al., (in press) have deformation measurements which point to an initial (January 1983) dike thickness of 3.5 meters. If the dike is assumed to have remained thermodynamically stable staying at a width of 3.5 meters over the series of episodic erutions, then a dike with the dimensions stated above would have a volume of magma of about 14 mcm: a volume similar to an average Puu Oo eruption.

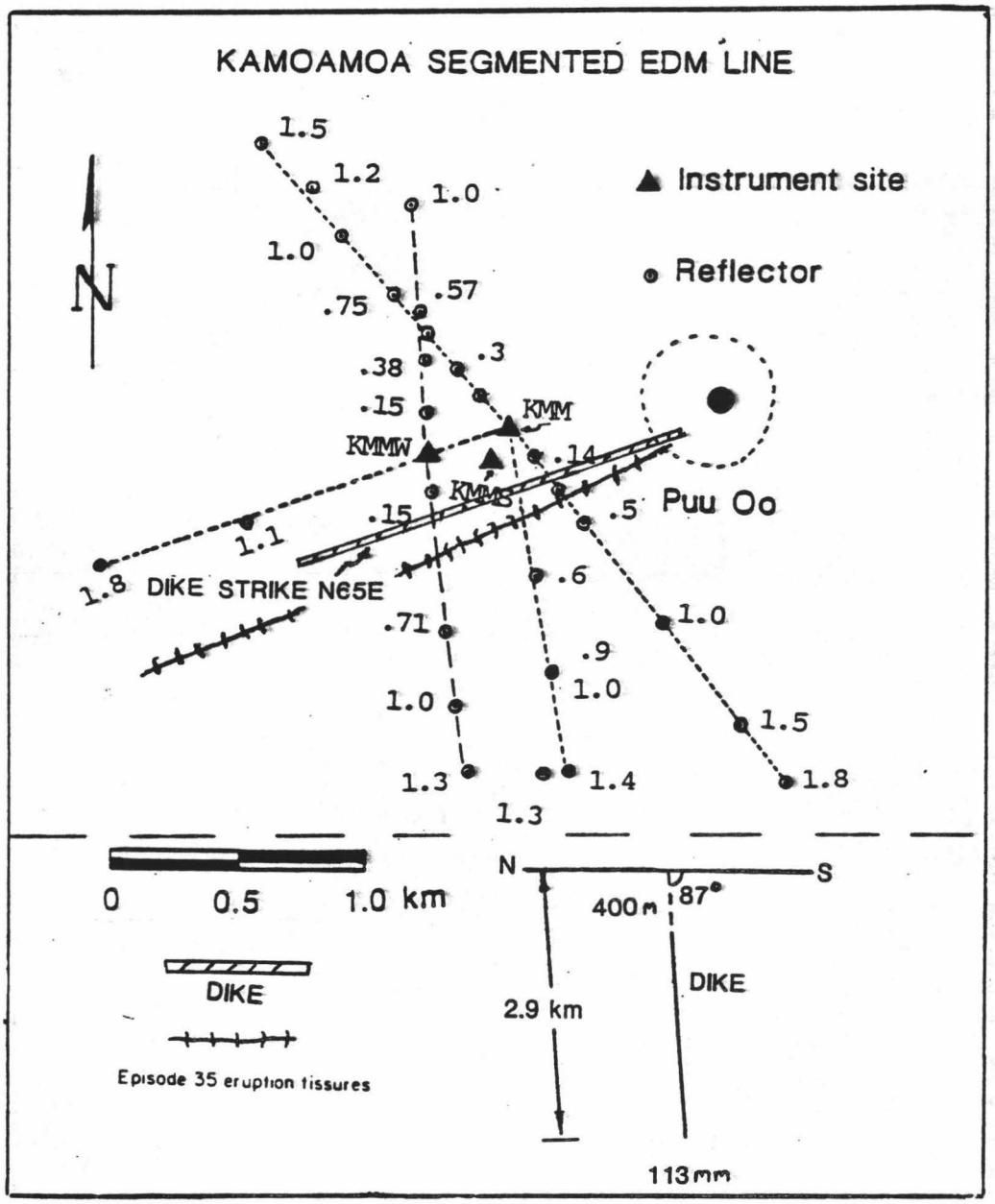

Figure 42. Plan view and cross-section of the dike location as modeled by DIS3D. Also located on map is the position of the rift opening for episode 35.

Deformation studies also indicated that eruption site pressures were less than summit pressures; on the average by about a third. This is important as pressure gradients have been used in combination with fluid dynamic principles to calculated rift zone geometries (Wilson et al., in press a)

The model was also successful in illustrating the inhomogeneous nature of the idealized medium. The inhomogeneous nature of the host rock was shown to be important on the north end of the KMM line near the large ground cracks.

A schematic figure (Figure 43) illustrates the cross-sectional veiw of the modeled near-vent reservoir.

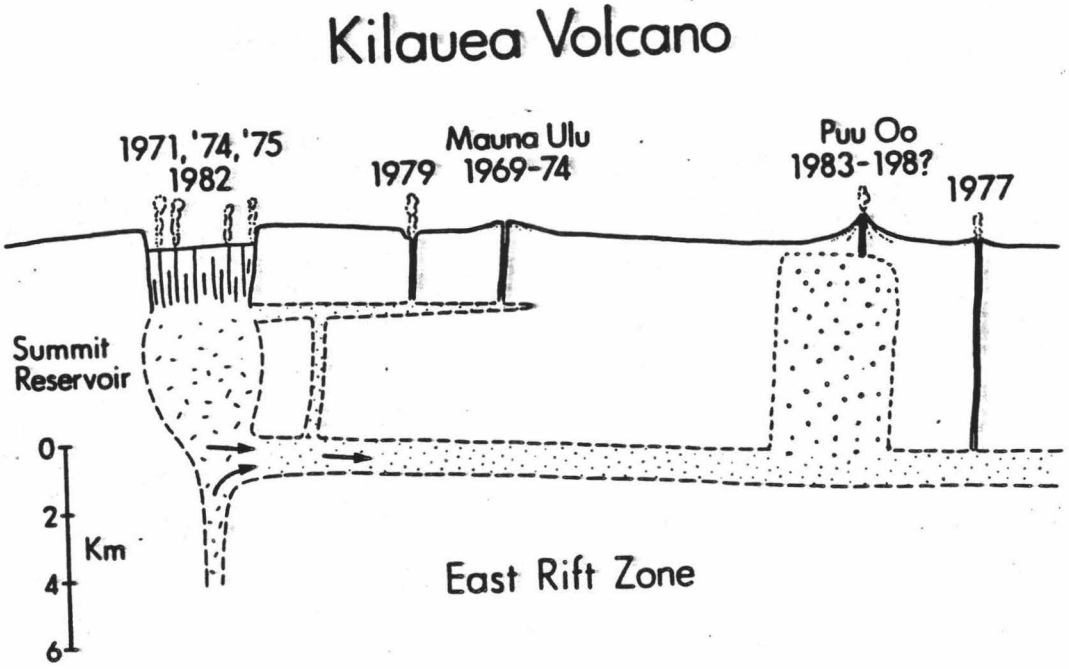

Figure 43. Cross-section of the east rift zone illustrating the location of the near-vent reservoir as modeled by DIS3D.

REFERENCES

Anderberg,M.R., 1973, Cluster analysis for applications: Acedemic Press, Inc., New York, 359 p.

Bijnen, E.J., 1973, Cluster analysis-Survey and evaluation techniques: Tilburg Univ. Press, Groningen, The Netherlands, 112 p.

Clifford, H.T., and Stephenson, W., 1973, An introduction to numerical classification: Academic Press, Inc., New York, 229 p.

Casadevall, T.J., Stokes, J.B., Greenland, L.P., Malinconico, L.L., Casadevall, J.R., and Furukawa, B.T., 1987, SO2 and CO2 emmision rates at Kilauea Volcano, 1979-1984: U.S. Geological Survey Professional Paper 1350, p. 771-780.

Davis, J.C., 1976, Statistics and Data Analysis in Geology, John Wiley and Sons, Inc., New York, 350 p.

Davis, J.C., 1986, Statistics and Data Analysis in Geology, 2nd ed., John Wiley and Sons., Inc., New York, 646 p.

Decker, R.W., Okamura, A.T., and Dvorak, J.G., 1983, Pressure changes in the magma reservoir beneath Kilauea Volcano, Hawaii: EOS (American Geophysical Union Trnasactions), v. 64, p. 901.

Delaney, P.T., and Pollard, D.D., 1982, Solidification of basaltic magma during flow in a dike: American Journal of Science, v. 282, p. 856-885.

Delaney, P.T., and Pollard, D.D., 1981, Deformation of host rocks and flow of magma during growth of minette dikes and breccia-bearing intrusions near Ship Rock, New Mexico: U.S. Geological Survey Professional Paper 1202, 61 p.

Dieterich, J.H., and Decker, R.W., 1975, Finite Element modeling of surface deformation associated with volcanism: Journal of Geophysical Research, v. 80, p. 4094-4102.

Dixon, W.J., and Jennrich, R.I., 1985, Stepwise regression, in BMDP Statistical Software, ed., Dixon, W.J., Univ. of Calif. Press, p 251-263.

Duffield, W.A., Jackson, D.B., and Swanson, D.A., 1976, The shallow, forceful intrusion of magma and related ground deformation at Kilauea Volcano, May 15-16, 1970: Bulletin Volcanologique, v. 39, p. 577-597.

Duffield, W.A., Christiansen, R.L., Koyanagi, R.Y., and Peterson, D.W., 1982, Storage, migration, and eruption of magma at Kilauea Volcano, Hawaii, 1971-1972: Journal of Volcanology and Geothermal Research, v. 13, p. 273-307.

Dvorak, J.J., Okamura, A. T., and Dieterich, J.H., 1983, Analysis of surface deformation data, KIlauea Volcano, Hawaii: October 1966 to September 1970: Journal of Geophysical Research, v.88, p. 9295-9304.

Dvorak, J.J., and Okamura, A.T., 1985, Variations in tilt rate and harmonic tremor during the January-August 1983 east rift eruptions of Kilauea Volcano, Hawaii: Journal of Volcanology and Geothermal Research, v. 25, p.249-258.

Dvorak, J.J., Okamura, A.T., English, T.T., Koyanagi, R.Y., Nalata, J.S., Sako, M.K., Tanigawa, W.R., and Yamashita, K.M., 1986, Mechanical response of the south flank of Kilauea Volcano, Hawaii to intrusive events along the rift zones, Tectonophysics, v. 124,p. 193-209

Dzurisin, D., Koyanagi, R.Y., and English, T.T., 1984, Magma supply and storage at Kilauea Volcano, Hawaii: 1956-1983: Journal of Volcanology and Geothermal Research, v.21, p. 177-206.

Eaton, J.P., 1962, Crustal structure and volcanism in Hawaii, in Macdonald, G.A., and Kuno, H., eds., The crust of the Pacific Basin: American Geophysical Union, Geophysical Monograph Series, v. 6, p. 13-29.

Epp, D., Decker, R.W., and Okamura, A.T., 1983, Relation of summit deformation to east rift zone eruptions of Kilauea Volcano, Hawaii: Geophysical Research Letters, v. 10, p. 493-496.

Erickson, L.L., 1986, A Three Dimensional Dislocation Program with Application to Faulting in the Earth, Master's Thesis, Stanford University, 167 p.

Fiske, R.S., and Jackson, E.D., 1972, Orientation and growth of Hawaiian volcanic rifts: The effect of structure and gravitational stresses: Proceedings of the Royal Society of London, Ser. A, v. 329, p. 299-326.

Fiske, R.S., and Kinoshita, W.R., 1969, Inflation of Kilauea Volcano prior to its 1967-68 eruption: Science, v. 165, p. 341-349.

Garcia, M.O., Byers, C.D., Wolfe, E.W., and Rhodes, J.M., 1984, Chemistry and Mineralogy of lavas from the continuing eruption of Kilauea Volcano, Hawaii: EOS, v. 65, p.1130.

Garcia, M.O., and Wolfe, E.W., in press, Petrology of the lavas from the Puu Oo eruption of Kilauea Volcano, Hawaii: episodes 1-20, in Wolfe, E.W., ed., The Puu Oo eruption of Kilauea Volcano, Hawaii: the first 1 1/2 years: U.S. Geological Survey Professional Paper 1463.

Garcia, M.O., Wolfe, E.W., Ulrich, G.E., Rhodes, J.M., 1985, Petrology of lavas from the Puu Oo eruption of Kilauea Volcano, Hawaii: The 3rd year, EOS v.66, p. 1132-1133.

Greenland, L.P., in press a, Gases from the 1983-84 east rift eruption of Kilauea Volcano, in Wolfe, E.W., ed., The Puu Oo eruption of Kilauea Volcano, Hawaii: the first 1 1/2 years: U.S. Geological Survey Professional Paper 1463.

Greenland, L.P., Okamura, A.T., and Stokes, J.B., in press b, Constraints on the mechanics of eruption of Puu Oo, in Wolfe, E.W., ed., The Puu Oo eruption of Kilauea Volcano, Hawaii: the first 1 1/2 years: U.S. Geological Survey Professional Paper 1463.

Greenland, L.P., Rose, W.I., and Stokes, J.B., 1985, An estimate of gas emmisions and magmatic gas content from Kilauea Volcano: Geochimica et Cosmochimica Acta, v. 49, p. 125-129.

Hartigan, J.A., 1975, Cluster algorithms, John Wiley and Sons., Inc., New York, 351 p.

Hill, D.P., 1969, Crustal structure of the Island of Hawaii from seismic refraction measurements: Bulletin of Seismological Society of America, v. 59, p.101-130.

Jackson, D.B., Swanson, D.A., Koyanagi, R.Y., and Wright, T.L., 1975, The August and October 1968 east rift eruptions of Kilauea Volcano, Hawaii: U.S. Geological Survey Professional Paper 890, 33 p.

Jackson, D.B., in press, Geoelectric observations: September 1982 summit eruption and the first year of the 3 January 1983 east rift zone eruption, Kilauea volcano, Hawaii, in Wolfe, E.W., ed., The Puu Oo eruption of Kilauea Volcano, Hawaii: the first 1 1/2 years: U.S. Geological Survey Professional Paper 1463.

Jardine, N., and Sibson, R., 1971, Mathematical taxonomy: John Wiley and Sons, Ltd., London, 286 p.

Jennrich, R. I., and Sampson, P., 1985, Stepwise Discriminant Analysis, in BMDP Statistical Software, ed., Dixon, W.J., Univ. of Calif. Press, p. 519-537.

Johnson, D.J., 1987, Elastic and inelastic magma storage at Kilauea Volcano, U.S. Geological Professional Paper 1350, p. 1297-1308.

Kinoshita, W.T., 1965, A gravity survey of the Island of Hawaii:Pacific Science, v. 19, p. 339-340.

Klein F.W., 1982, Patterns of historical eruptions at Hawaiian volcanoes: Journal of Volcanology and Geothermal Research, v. 12, p.1-35.

Klein, F.W., Koyanagi, R.Y., Nakata, J.S., and Tanigawa, W.R., 1987, The Seismicity of Kilauea's Magma System: U. S. Geological survey Professional Paper 1350, p. 1019-1185.

Klovan, J.E., and Imbrie, J., 1971, An algorithm and Fortran IV program for large scale Q-mode factor analysis, Journal Inter. Assoc. Mathematical Geol., v. 3 no. 1.

Knudsen, J.G., and Katz, D.L., 1958, Fluid Dynamics and Heat Transfer, McGraw-Hill, New York.

Koyanagi, R.Y., Chouet, B., Aki, K., 1987, Origin of volcanic tremor in Hawaii; Data from the Hawaiian Volcano Observatory 1969-1985: U.S. Geological Survey Professional Paper 1350, p. 1221-1258.

Koyanagi, R.Y., Tanigawa, W.R., and Nakata, J.S., in press, Seismicity associated with the eruption of Kilauea Volcano from January 1983 to July 1984, in Wolfe, E.W., ed.,The Puu Oo eruption of Kilauea Volcano, Hawaii: the first 1 1/2 years: U. S. Geological Professional Paper 1463.

Koyanagi, R.Y., Unger, J.D., Endo, E.T., and Okamura, A.T., 1976, Shallow earthquakes associated with inflation episodes at the summit of Kilauea Volcano, Hawaii: Bulletin Volcanologique, v. 39, p. 621-631.

Macdonald, G.A., and Abbott, A.T., 1970, Volcanoes in the sea: Honolulu, University of Hawaii Press, 441 p.

Maruyama, T., 1964, Statical elastic dislocations in an infinite and semi-infinite medium, Bull. Earthquake Res. Inst., Tokyo Univ. 42, p. 289-368.

Mindlin, R.D., 1936, Force at a point in the interior of a semi-infinite solid, Physics 7, 195-202.

Mogi, K., 1958, Relations between the eruptions of various volcanoes and deformation of the ground surface around them: Bulletin of the Earthquake Research Institute, University of Tokyo, v.36, p. 99-134.

Moore, J.G., 1971, Bathemtry and geology-East Cape of the Island of Hawaii: U.S. Geological Survey Miscellaneous Geological Investigations Map I-677, Scale 1:62,500.

Neal, C.A., Duggan, T.J., Wolfe, E.W., and Brandt, E.L., in press, Lava samples, temperatures, and compositions, Puu Oo eruption of Kilauea Volcano, Hawaii, episodes 1-20, January 3, 1983-June 8, 1984, in Wolfe, E.W., ed., The Puu Oo eruption of Kilauea Volcano, Hawaii: the first 1 1/2 years: U.S. Geological Survey Professional Paper 1463.

Okamura, A.T., Dvorak, J.J., Koyanagi, R.Y., and Tanigawa, W.R., in press, Surface deformation associated with the 1983 Kilauea eruption in Wolfe, E.W., ed., The Puu Oo eruption of Kilauea Volcano, Hawaii: the first 1 1/2 years: U.S. Geological Survey Professional Paper 1463.

Pollard, D.D., Delaney, P.T., Duffield, W.A., Endo, E.T., and Okamura, A.T., 1983, Surface deformation in rift zones: Tectonophysics, v.94, p. 541-584.

Ryan, M.P., Blevins, J.Y.K., Okamura, A.T., and Koyanagi, R.Y., 1983, Magma reservoir subsidence mechanics: Theoretical summary and application to Kilauea Volcano, Hawaii: Journal of Geophysical Research, v. 88, p 4147-4181.

Sneath, P.H.A., and Sokal, R.R., 1973, Numerical taxonomy: W.H. Freeman and Co., San Francisco, 573 p.

Sokal, R.R., and Sneath, P.A., 1963, Principles of Numerical Taxonomy, Freeman and Co., San Francisco, 359 pp.

Sparks, R.S.J., 1978, The dynamics of bubble formation and growth in magmas: A reveiw and analysis, Journal Volcanol. Geotherm. Res., 3, 1-37.

Swanson, D.A., Duffield, W.A., and Fiske, R.S., 1976, Displacement of the south flank of Kilauea Volcano: The result of forceful intrusion of magma into the rift zones: U.S. Geological Survey Professional Paper 963, 39 p.

Swanson, D.A., Duffield, W.A., Jackson, D.B., and Peterson, D.W., 1979, Chronological narative of the 1969-71 Mauna Ulu eruption of Kilauea Volcano, Hawaii: U.S. Geological Survey Professional Paper 1056, 55p.

Tyron, R.C., and Bailey, D.E., 1970, Cluster Analysis: McGraw-Hill, Inc., New York, 347 p.

Vergniolle, S., Jaupart, C., 1986, Two-phase flow and volcanic eruptions: Journal Geophys. Res., v. 91, no. B12, pp. 12,842-12,860.